EXAMINING THE EFFECT OF FUNDAMENTAL PROPERTIES OF CEMENT HYDRATION ON HYDROSTATIC PRESSURE REDUCTION TO BETTER UNDERSTAND STRAY GAS MIGRATION

by

Alexander S. Vuotto III

B.S., University of Pittsburgh, 2014

Submitted to the Graduate Faculty of

Swanson School of Engineering in partial fulfillment

of the requirements for the degree of

Master of Science

University of Pittsburgh

2015

UNIVERSITY OF PITTSBURGH

SWANSON SCHOOL OF ENGINEERING

This thesis was presented

by

Alexander S. Vuotto III

It was defended on

November 24th, 2015

and approved by

John C. Brigham, Ph.D., Assistant Professor, Department of Civil and Environmental Engineering, University of Pittsburgh

Anthony T. Iannacchione, Ph.D., Associate Professor, Department of Civil and Environmental Engineering, University of Pittsburgh

Barbara G. Kutchko, Ph.D., Senior Research Scientist, National Energy Technology Laboratory, U.S. Department of Energy

Thesis Advisor: Julie M. Vandenbossche, Ph.D., Associate Professor, Department of Civil and Environmental Engineering, University of Pittsburgh

EXAMINING THE EFFECT OF FUNDAMENTAL PROPERTIES OF CEMENT HYDRATION ON HYDROSTATIC PRESSURE REDUCTION TO BETTER UNDERSTAND STRAY GAS MIGRATION

Alexander Vuotto, M.S.

University of Pittsburgh, 2015

During wellbore cementing, stray gas migration may occur when a pressure imbalance exists within the hydrating cement slurry, where the pore pressure is less than that of the surrounding formation gas pressure. A fluid column of hydrating cement slurry with appropriate density will provide sufficient hydrostatic pressure to prevent formation gas from invading and migrating through the cemented column. As cement hydration progresses, slurry behavior gradually shifts from that of a liquid to an impermeable solid. This transition is associated with a reduction in hydrostatic pressure, potentially leaving the annulus susceptible to the invasion and migration of untargeted formation gas. The current industry approach relies on measurements of static gel strength of the hydrating cement slurry to define the period of gas migration susceptibility, which is referred to as transition time. The transition time is minimized to reduce gas migration potential; however, many limitations exist with this approach. In order to improve the understanding of gas migration susceptibility, a study was performed to accurately characterize hydrostatic pressure reduction within a cemented annulus using fundamental parameters, such as degree of hydration and capillary porosity. Laboratory tests were conducted using the University of Pittsburgh's wellbore simulation chamber to simulate various depths of interest. By using fundamental parameters, microstructural development and cement material properties may be

predicted at any time and depth along the wellbore and related to the occurrence of gas migration. This study shows that the development of hydration can be predicted as a function of the curing conditions, the mixture design, and the cement composition. Hydration can also be directly linked to strength and constitutive properties of the hydrating cement slurry.

TABLE OF CONTENTS

LIST OF TABLES

LIST OF FIGURES

NOMENCLATURE

Symbol	Explanation
ACF	age conversion factor
API	American Petroleum Institute
ASTM	American Society for Testing and Materials
BWOC	by weight of cement
CCRL	Cement and Concrete Reference Laboratory
C_2S	dicalcium silicate
C_3A	tricalcium aluminate
C_3S	tricalcium silicate
C_4AF	tetracalicium alumino-ferrite
$CaCl_2$	calcium chloride
$CaCl_2$•2H2O	calcium chloride dihydrate
CH	calcium hydroxide
CSH	calcium silicate hydrate
CHP	critical hydration period
CSGS	critical static gel strength
DoH	degree of hydration
E or E_a	activation energy

gMat	grams of material
GU	general use
J	joule
K	Kelvin
mW	milliwatts
NIST	National Institute of Standards and Technology
OBP	overburden pressure
OPC	ordinary Portland cement
OSGS	optimal static gel strength
OWC	oilwell cement
PA DEP	Pennsylvania Department of Environmental Protection
$P_c(\alpha)$	capillary porosity at degree of hydration of α
SCM	supplementary cementitious materials
SGS	static gel strength
TT	transition time
w/c ratio	water-to-cement ratio
WSC	wellbore simulation chamber
VCCTL	Virtual Cement and Concrete Testing Laboratory
α	degree of hydration

ACKNOWLEDGEMENTS

I would like to express my sincere gratitude to my research supervisor, Dr. Julie M. Vandenbossche, for her support, guidance, and motivation throughout my time as both an undergraduate and graduate student at the University of Pittsburgh. I am extremely appreciative of her commitment and belief in me as I have progressed through my academic career. If not for her, I would not be the student that I am today. I would also like to thank the other faculty and professional members serving on my defense committee: Dr. John C. Brigham, Dr. Anthony T. Iannacchione, and Dr. Barbara G. Kutchko from NETL, Department of Energy. I have grown as both a student and a person in large part to the help and inspiration I have received from all of these influential people.

I would like to thank my entire family, especially my parents, for their consistent love, support, encouragement, and understanding throughout not only my academic career, but my entire life. If not for them, I would not be where I am today as a student, and more importantly, as a person.

I would like to acknowledge Mr. Charles C. Hager for his advice and assistance in the laboratory. I would like to extend a special thanks to Dr. Zichang Li for his constant help and guidance throughout my work on this project. I also owe a great deal of credit and thanks to my other fellow graduate students, Mr. Matthew J. Grasinger, Mr. Kevin Alland, Mr. Steven Sachs,

Mr. John DeSantis, Ms. Nicole Dufalla, and Mr. Nathan D. Bech. My experience as a graduate student would not have been nearly as enjoyable without these individuals.

I would like to extend special thanks to Cemex USA for supplying material to allow me to finish the experimental portion of my project, Calfrac Well Services Corp. for conducting SGS testing, and CTL for conducting isothermal calorimetry testing. I would also like to thank Shell, Halliburton, Schlumberger, Lafarge, and U.S. Steel for their insightful meetings and generous donation of materials.

Additionally, I owe thanks to the entire Department of Civil and Environmental Engineering at the University of Pittsburgh, including faculty, staff, technicians, and secretaries, who contributed directly or indirectly to the completion of this work and my overall education.

Finally, I am extremely grateful for the financial support provided by the Department of Energy (NETL Regional University Alliance) for this project. I would also like to extend thanks to Mr. Seth Pelepko from the Pennsylvania Department of Environmental Protection.

I WOULD LIKE TO DEDICATE THIS THESIS TO MY FAMILY FOR ALL OF THEIR LOVE AND SUPPORT.

1.0 INTRODUCTION

1.1 BACKGROUND AND MOTIVATION

Stray gas migration is a well-recognized problem within the oil and gas industry and has been an issue for many years (Dusseault et al. 2014; Komex International 2002; Al-buraik et al. 1998). Not to be confused with traditional gas production, stray gas migration refers to the invasion of gas from other reservoirs outside of the targeted production zone (i.e. shale). In the northern tier of Pennsylvania, these non-target gas-bearing zones are often highly-permeable and shallow in depth when compared to production-level source rock. Stray gas migration is an important problem to consider for industry, as it may lead to detrimental effects on wellbore integrity, potential contamination of groundwater aquifers and drinking wells.

In order for gas migration to occur within the cemented annulus of a given borehole, a pressure imbalance must exist, in that, the cement slurry pore pressure must be less than that of the surrounding formation gas pressure (Carter and Slagle, 1960). Immediately after cement placement is completed, the hydrating slurry behavior is analogous to that of a pure fluid, where hydrostatic pressure is capable of being transmitted within the cemented annulus. Depending on the slurry mixture design density, a fully-fluid cemented annulus will provide sufficient pressure to prevent surrounding formation gas from invading and migrating through the cemented column (Mueller, 2002; Sabins et al., 1982). Due to the nature of cement hydration, slurry behavior

gradually shifts from that of a liquid to a solid. Moreover, the slurry acts as a two-phase material (i.e. a solid network of hydration products and pore fluid) until the cement slurry reaches a fully-solidified state as an impermeable barrier (Bonett & Pafitis, 1996). At this stage, hydrostatic pressure is no longer able to be transmitted within the cemented annulus, which results in a reduction of hydrostatic pressure. Therefore, for the purpose of this study, hydrostatic pressure reduction is considered to be the primary mechanism of gas migration and a critical design consideration for well completion operations. In order to understand and evaluate the potential for gas migration, it is important to be able to characterize the evolution of hydrostatic pressure and corresponding material properties as the cement slurry hydrates within a given borehole.

Various methods to characterize wellbore hydrostatic pressure reduction during cement slurry hydration have been proposed and reported in literature (Zhou & Wojtanowicz, 2011). Among them, the classic shear stress theory is the most-widely accepted method to explain the mechanism of cement column hydrostatic pressure reduction (Sutton et al., 1984a, 1984b). This theory assumes the reduction in hydrostatic pressure is counteracted by the development of wall shear stress (WSS). WSS provides support to the annular column, alleviating the weight of the overlying cement column within the borehole. The removal of material, primarily through fluid loss into the adjacent formation and cement slurry shrinkage, results in a strain that counteracts the hydrostatic pressure (Bonett & Pafitis, 1996). It is important to note that this theory assumes WSS to be equivalent to the static gel strength (SGS) of hydrating cement slurry and proportional to the hydrostatic pressure reduction within the cemented annulus. However, experimental results (Haijin et al., 2012) have shown that the relationship between SGS and hydrostatic pressure reduction is non-linear, suggesting that classic shear stress theory is not appropriate.

Gas well drilling practices require adequate slurry density so that the initial cement slurry hydrostatic pressure is greater than the surrounding formation gas pressure. This is true for the entire length of wellbore exposed to cementing operations. When adequate slurry density is achieved, gas migration from the adjacent formation into and through the cemented annulus is prevented. However, in areas of excessive formation gas pressures, the hydrating cement slurry pressure (see above discussion) can be reduced enough to allow for gas migration occurrence. The time at which hydrostatic pressure decreases below the surrounding formation gas pressure is defined in terms of SGS of the cement slurry and is referred to as the critical static gel strength (CSGS). The CSGS is the strength at which the hydrating cement slurry becomes susceptible to the potential gas migration due to hydrostatic pressure reduction. Assuming sufficient borehole information is available, the CSGS should be determined experimentally; otherwise, a constant value of 100lb/100ft^2 is assumed (American Petroleum Institute, 2010). The API standards imply that the potential for gas migration is negligible once the cement slurry achieves sufficient strength and rigidity. The upper bound of this SGS range (500lb/100ft^2) has been adopted by industry and is referred to as the optimum static gel strength (OSGS). Experimental results indicate that gas cannot freely percolate through cement when the SGS ranges from 250lb/100ft^2 to 500lb/100ft^2 (American Petroleum Institute, 2010). The time period defined by the bounds of CSGS and OSGS is referred to as the transition time (TT) or critical hydration period (CHP) (Mueller, 2002; Sabins et al., 1982). As stated above, if insufficient information is available, CSGS and OSGS are assumed to be 100lb/100ft^2 and 500lb/100ft^2, respectively. These criteria are used for defining the TT for all slurry mixture designs and downhole conditions. Additionally, no standardized procedure or devices are currently available for measuring SGS accurately and consistently (Belrute & Cheung, 1990).

This work will show that it is not appropriate to define the SGS criteria as one set of values, especially since all slurries do not exhibit the same behavior at a given SGS, nor are the downhole conditions the same for all scenarios. Regardless of the validity of the approach, it is common practice within industry to minimize the TT in order to mitigate, if not prevent, the occurrence of gas migration. Although, in theory, this method of gas migration mitigation may limit the time in which it is possible for gas migration, it does not eliminate the potential for gas migration (Belrute & Cheung, 1990). As evidenced by the limitations of SGS and the classic shear stress theory in characterizing the potential for gas migration, a better means to characterize the microstructural development of the cement matrix is needed.

1.2 RESEARCH OBJECTIVES AND SCOPE

This study investigates a new approach, replacing SGS with a fundamental property or set of properties that are better suited for characterizing the hydrostatic pressure reduction of hydrating cement slurry. In general, using this fundamental parameter, material properties may be predicted at any given time or depth along the wellbore. Using this prediction and known borehole conditions, a better means of quantifying hydrostatic pressure reduction the potential for gas migration is possible. Improvements in the slurry design process and understanding of gas migration mechanisms may lead to environmental benefits within the industry, such as prevention of groundwater aquifer contamination.

The specific aims of this study are provided below:

(1) Evaluate standard SGS criteria in accurately characterizing hydrostatic pressure reduction, and, in turn, gas migration potential;

(2) Evaluate the applicability and accuracy of the degree of hydration prediction model, developed by Poole, for Class A oilwell cement (OWC);

(3) Evaluate methods for determining activation energy of a given cement so an accurate prediction of hydration development at various curing temperatures can be achieved;

(4) Relate fundamental properties (i.e. degree of hydration, capillary porosity, etc.) to bulk slurry properties (i.e. hydrostatic pressure loss) relevant in typical downhole conditions;

(5) Perform a Virtual Cement and Concrete Testing Laboratory (VCCTL) simulation on a typical cement slurry design used for surface or intermediate casing cementing. Obtain representative material properties (i.e. DoH, capillary porosity, etc.) and compare the results to predictions and models found in literature;

1.3 ORGANIZATION OF THESIS

This thesis has been prepared according to the guidelines specified by the Office of the Provost at the University of Pittsburgh for an integrated-article (or manuscript) format. It has been divided into five chapters, which are individually explained below. The references are compiled in the bibliography section at the end of the thesis.

In Chapter 2, an overview of all necessary background information, terminology, equipment, and concepts related to cement hydration is presented. The computational approach for predicting hydration development is also presented. Previously developed prediction models

and formulations used for characterizing cement hydration are presented. Additionally, software utilized for predicting and characterizing the cement hydration process, namely, Virtual Cement and Concrete Testing Laboratory (VCCTL), is introduced.

In Chapter 3, a brief description of the components and capabilities of the University of Pittsburgh's wellbore simulation chamber (WSC) is presented. The suitability of this equipment for the purpose of this study is discussed and typical results that may be obtained from WSC pressure testing included. This chapter represents a brief summary of the detailed WSC development from the work by (Li, 2015).

In Chapter 4, a comprehensive review of the experimental testing and data evaluation methods is presented. More specifically, the methodology used to analyze and evaluate isothermal calorimetry, WSC pressure testing, and SGS testing data is discussed. SGS criteria are evaluated using experimental data and various fundamental parameters are used to characterize hydrostatic pressure reduction. Conclusions are then drawn from the experimental results and the concepts presented in Chapter 2.

In Chapter 5, a summary of the findings is provided. From this summary, primary conclusions from this study are presented. Recommendations for future work and improvements on existing research are also suggested.

2.0 BACKGROUND INFORMATION

Hydrostatic pressure reduction within a given cemented annulus is an important consideration when evaluating the potential for gas migration occurrence. This research relates the fundamental properties (i.e. degree of hydration, capillary porosity, etc.) to bulk slurry properties (i.e. hydrostatic pressure loss) relevant in typical downhole conditions. To that end, this chapter presents the necessary background information on the overall cement hydration process, equipment necessary for this research, and the technical basis for predicting and modeling hydration development.

2.1 CEMENT HYDRATION PROCESS

Cement hydration is a process consisting of a set of exothermic reactions of individual cement compounds with water, each of which is assumed to occur independently of one another. This assumption is not entirely correct since interactions between hydrating compounds do exist and can affect hydration behavior (Mindess et al. 2003). For the purpose of this work, it is assumed that cement hydration reactions occur independently.

2.1.1 Cement composition and chemistry

Cement hydration can be evaluated in terms of its individual pure compounds that comprise the overall cement clinker. An understanding of cement composition can be used to determine the physical and chemical characteristics of the mass as hydration progresses. Portland cement is comprised of four primary compounds: tricalcium silicate (C_3S), dicalcium silicate (C_2S), tricalcium aluminate (C_3A), and tetracalcium aluminoferrite (C_4AF) (Mindess et al. 2003). Table 2.1 summarizes these primary cement compounds and typical proportioning of each for a Type I cement, which is used in experimental testing as a part of this work. It is important to note that the "weight percent" column provided in Table 2.1 represents typical values for Ordinary Portland cement (OPC) and may vary depending on the type or class of cement of interest (i.e. Type I OPC or general use (GU) cement, Class A oilwell cement (OWC), etc.). It should also be recognized that the weight percent values do not add up to 100%, with the remaining amount being accounted for by impurities.

Table 2.1. Typical composition of ordinary Portland cement (Mindess et al. 2003).

Chemical Name	Chemical Formula	Shorthand Notation	Weight Percent
Tricalcium silicate	$3CaO{\bullet}SiO_2$	C_3S	55
Dicalcium silicate	$2CaO{\bullet}SiO_2$	C_2S	18
Tricalcium aluminate	$3CaO{\bullet}Al_2O_3$	C_3A	10
Tetracalcium aluminoferrite	$4CaO{\bullet}Al_2O_3{\bullet}Fe_2O_3$	C_4AF	8
Calcium sulfate dihydrate (gypsum)	$CaSO_4{\bullet}2H_2O$	$C\bar{S}H_2$	6

While the hydration process is often characterized by individual cement compound hydration reactions, its chemical composition is commonly reported in terms of oxides (i.e. CaO, SiO_2, etc.). The direct determination of primary individual cement compounds (i.e. C_2S, C_3S, C_3A, and C_4AF) is a complex process that requires both expensive equipment and well-trained, competent staff (Mindess et al. 2003). In comparison, an oxide analysis is typically performed by standard methods (i.e. X-ray fluorescence spectroscopy) and is much more common and easier to determine (Geiker et al. 1990). A shorthand notation of oxide reporting that is universally accepted for describing general-purpose Portland cement has been developed (see Table 2.2). Once an oxide analysis has been performed, indirect determination of cement composition is possible using ideal compound stoichiometries through the Bogue equations. ASTM C150 (2014b) provides the procedure and relevant equations needed to indirectly determine the cement composition using the Bogue equations.

Table 2.2. Typical oxide composition of a Portland cement (Mindess et al. 2003).

Oxide	Shorthand Notation	Common Name
CaO	C	Lime
SiO_2	S	Silica
Al_2O_3	A	Alumina
Fe_2O_3	F	Ferric oxide
MgO	M	Magnesia
K_20	K	Alkalis
Na_2O	N	
SO_3	$\bar{S}$	Sulfur trioxide
H_20	H	water

2.1.1.1 Oilwell cement (Class A)

Exposure conditions and requirements of oilwell cement (OWC) will significantly differ from that of OPC or GU cement typically used in the construction industry. OWC used to encase gas wells is subjected to a wide range of temperature and pressure conditions along the depth and/or length of the wellbore. For these reasons, specifications were created and reported by the American Petroleum Institute (API) to define the different types of OWC available. API currently provides specifications covering all classes of OWC, designated Classes A through H (American Petroleum Institute, 2005); however, the work presented herein will focus on Class A OWC. The petroleum industry commonly uses Class A OWC for surface and intermediate casing strings. These are the wellbore sections where stray gas migration is most prevalent (PA DEP 2009). Table 2.3 illustrates typical compositions (in terms of pure compounds) and fineness for the various API cement classes. It also demonstrates that Class A OWC is similar to Type I OPC in terms of composition and fineness.

Table 2.3. Typical composition and properties of API classes of cement (SPE International, 2015).

API Class	Compounds, %				Wagner Fineness, cm3/g
	C_3S	C_2S	C_3A	C_4AF	
A	52	24	8+	8	1,500 to 1,900
B	47	32	5-	12	1,500 to 1,900
C	58	16	8	8	2,000 to 2,800
G & H	50	30	6	12	1,400 to 1,700

2.1.2 Hydration reactions

Of the four primary cement clinker compounds, both forms of calcium silicate (C_3S and C_2S) account for approximately 72-76% of a typical Portland cement and are primarily responsible for its cementitious qualities (Schindler, 2004). Cement hardening, or the development of cementitious qualities, is caused by chemical reactions between cement clinker compounds and water, as seen in Equations (2.1) and (2.2) (Mindess et al. 2003). The hydration reactions of both calcium silicate compounds are very similar and only vary in the stoichiometry of the individual reactions.

$$2C_3S + 11H \rightarrow C_3S_2H_8 + 3CH \quad (2.1)$$

$$2C_2S + 9H \rightarrow C_3S_2H_8 + CH \quad (2.2)$$

As seen from Equations (2.1) and (2.2), both hydration reactions yield two primary hydration products, calcium silicate hydrate (C-S-H) and calcium hydroxide (CH). The principal hydration product, calcium silicate hydrate, accounts for approximately 50 to 60% of the volume of hydrated paste and can be described as a poorly crystalline material with a highly variable composition that is dependent upon the water content (Schindler, 2004). This principal hydration product is the primary controlling factor for strength development and durability of the hydrating paste. For the purpose of this research, it is assumed that the variability in the composition of CSH will not significantly affect the overall hydration process or microstructural development. On the other hand, calcium hydroxide ($Ca(OH)_2$) is a well-crystallized material with a definite stoichiometry. Additionally, calcium hydroxide is less dense and relatively weak in comparison with C-S-H, and may also become unstable when exposed to acids (Schindler, 2004).

In addition to the hydration of both forms of calcium silicate, the hydration of tricalcium aluminate is primarily responsible for high early heat evolution. The hydration reaction of tricalcium aluminate is given as follows:

$$C_3A + 3C\bar{S}H_2 + 26H \rightarrow C_6A\bar{S}_3H_{32} \quad (2.3)$$

As seen from Equation (2.3) above, a different hydration product is formed, namely, ettringite. This hydration product varies significantly from the aforementioned hydration products. It is important to understand these differences, as they will play an important role in this research. Table 2.4 provides a brief comparison between the primary hydration products.

Table 2.4. Summary of hydration products of Portland cement (Mindess et al. 2003).

Compound	**Specific Gravity**	**Crystallinity**	**Morphology**	**Typical dimensions**
CSH	2.3 - 2.6	Very poor	Spines; Unresolved morphology	1 x 0.1 μm
CH	2.24	Very good	Nonporous, striated	0.01 - 0.1 mm
Ettringite ($C_6A\bar{S}_3H_{32}$)	~1.75	Good	Long, slender, prismatic needles	10 x 0.5 μm
Monosulfo-aluminate	1.95	Fair - good	Thin, hexagonal plates	1 x 1 x 0.1 μm

2.1.3 Hydration kinetics

The hydration development and behavior is directly dependent upon the composition and fineness of the cement, among other factors. The differences in hydration development between individual cement compounds are illustrated in Figure 2.1.

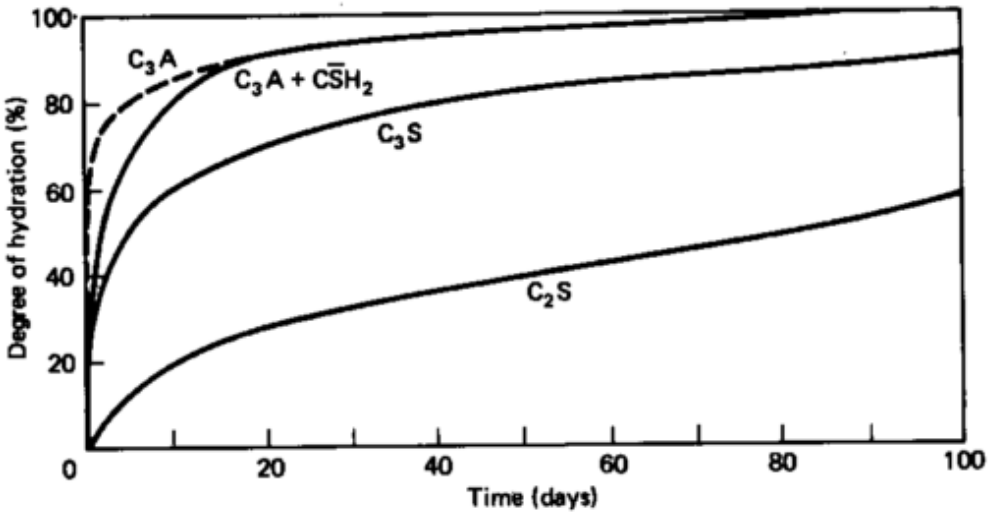

Figure 2.1. DoH development for individual cement compounds (Mindess et al. 2003).

From Figure 2.1 above, it can be seen that the hydration kinetics significantly vary between the primary individual cement compounds. C_3A exhibits the fastest hydration reaction rate among the individual cement compounds, followed by C_3S, C_4AF, and C_2S. It should be noted that individual compounds will not hydrate at equivalent rates, as differences in fineness and clinker cooling rate affect the reactivity. As a result of this hydration variability between different compounds, the degree of hydration of the overall cement slurry is considered to be an "apparent" or "effective" property, as it is a singular reported value that is affected by the individual contributions of each compound or phase. This type of property or characteristic will

appear at various points throughout this work, as it is commonly associated with composite materials, such as Portland cement. The hydration process of a typical cementitious mixture can be characterized by five different heat development stages. Figure 2.2 provides a graphical representation of these stages.

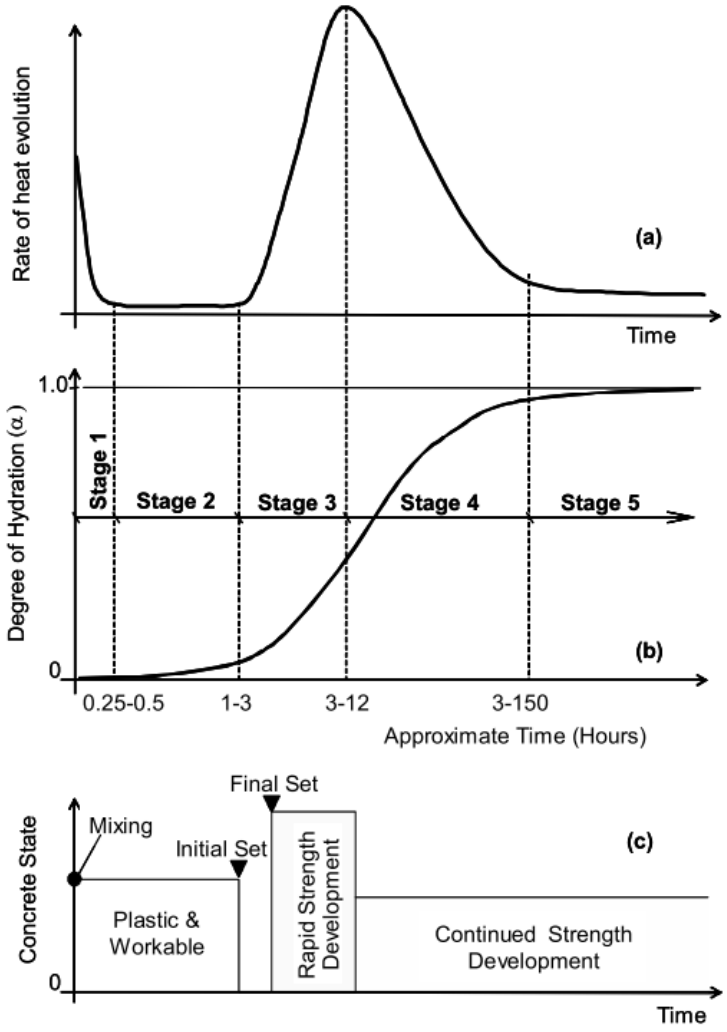

Figure 2.2. Stages during the hydration process (Byfors, 1980).

Heat evolution is considered to be proportional to the rate of the hydration reaction, which means that heat flow data may be used to characterize the hydration behavior of a cementitious mixture. Although all five hydration stages occur for complete hydration, this work

will primarily focus on the first three hydration stages, as the hydrostatic pressure reduction of the cemented annulus typically occurs during these stages. Stage 1 of hydration can be described as initial hydrolysis, where the calcium and hydroxide ions are released from the surface of cement clinker grains resulting in an initial peak in hydration and heat evolution rate. Stage 2 of hydration can be described as the induction or dormant period, where hydration rate decreases as initial hydration products formed in Stage 1 mitigate the contact between unhydrated cement clinker and free water. Once calcium and hydroxide ion concentrations reach a critical value, calcium hydroxide (CH) and calcium silicate hydrate (CSH) hydration products begin to rapidly form resulting in another peak in hydration and heat evolution rate.

2.1.4 Degree of hydration

The progress or development of cement hydration can be quantified by the property of degree of hydration (DoH). During this process, the DoH is defined as the volume fraction of Portland cement (including interground gypsum) that has reacted (hydrated) with water. This property theoretically ranges from 0 to 1, with 1 indicating complete hydration (Schindler et al. 2002). However, in reality, not all of the cementitious material hydrates, and complete hydration (DoH = 1.0) may never be reached. Research conducted by Mills (1966) on the hydration of various cementitious materials suggested that “in most, if not all, cement paste hydration stops before the cement is totally consumed” (Schindler et al. 2002). Figure 2.3 illustrates a physical representation of a simplified cement microstructure as hydration progresses. Additionally, Figure 2.3 corresponds with the hydration kinetics stages listed in the previous section.

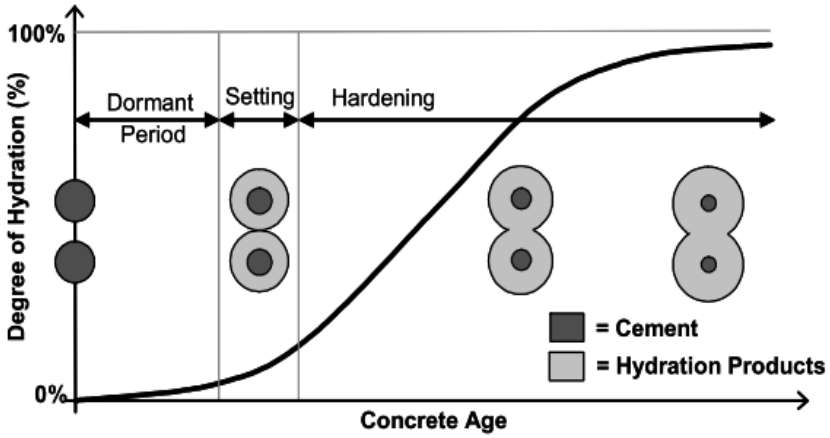

Figure 2.3. Physical meaning of DoH development (Schindler, 2004).

As stated previously, due to the nature of cement composition and the different reaction rates and hydration products of individual clinker phases and their interactions (see Table 2.5), it is generally accepted that the DoH of cement is considered to be an overall approximation or "apparent" property (Lin & Meyer, 2009). Figure 2.4 represents a slightly more detailed illustration of the microstructural development as hydration progresses.

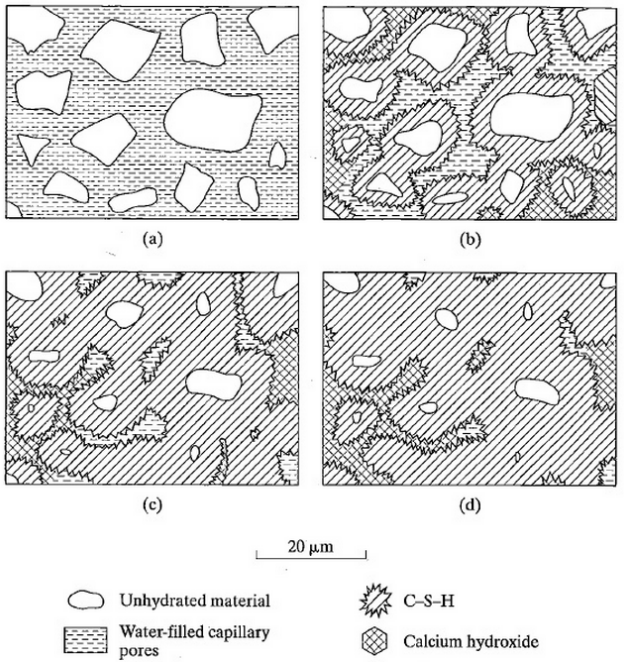

Figure 2.4. Schematic of microstructural development as hydration progresses (Mindess et al. 2003).

Accurate measurement or calculation of DoH may be difficult given the complex microstructure formed. DoH can be calculated using different methods, each having advantages and disadvantages. Direct analysis, otherwise known as visual inspection, is the most accurate and reliable method. No empirical relationships, correlations, or approximations are required for this method. In theory, this method may provide the most fundamental and accurate characterization of hydration development; however, it is time-consuming and difficult to obtain precise measurements. Additionally, a visual analysis may only be performed on a sample where hydration has ceased, as it is incapable of continuously measuring or recording hydration development as the microstructure evolves over time.

Alternatively, heat evolution of a given sample may be used to calculate DoH. This alternative method will be utilized for the purpose of this work. The DoH is a measure of the

quantity of hydration products formed and may, therefore, be linked to the heat of hydration development (Schindler et al., 2002). DoH is calculated using the following Equation (2.4) (Kada-Benameur et al. 2000; Poole, 2007; Schindler et al., 2002; Schindler & Folliard, 2005):

$$\alpha = DoH = \frac{H(t)}{H_{ult}} \tag{2.4}$$

where, $H(t)$ = heat evolved from time 0 to time t (J/gMat);

H_{ult} = total heat available for reaction (J/gram), which can be calculated as follows:

$$H_{ult} = H_{cem} \cdot p_{cem} + 461 \cdot p_{slag} + h_{FA} \cdot p_{FA} \tag{2.5}$$

where, p_{slag} = slag weight ratio in terms of the total cementitious content;

p_{FA} = fly ash weight ratio in terms of the total cementitious content;

h_{FA} = heat of hydration of fly ash;

p_{cem} = cement weight ratio in terms of the total cementitious content;

H_{cem} = heat of hydration of the cement (J/gram) at complete hydration, which can be calculated as follows (Schindler & Folliard, 2005):

$$\begin{aligned} H_{cem} = {} & 500 \cdot p_{C_3S} + 260 \cdot p_{C_2S} + 866 \cdot p_{C_3A} + 420 \cdot p_{C_4AF} \\ & + 624 \cdot p_{SO_3} + 1186 \cdot p_{FreeCa} + 850 \cdot p_{MgO} \end{aligned} \tag{2.6}$$

Equation (2.6) was developed by investigating the heat of hydration of individual cement clinker compounds (Schindler & Folliard, 2005). According to the assumption provided in Section 2.1, hydration reactions of individual cement clinker compounds occur independently of

one another; therefore, this equation is a summation of the representative heat of hydration of each cement clinker compound (Table 2.5). As seen in Table 2.5, the heat of hydration of individual cement compounds, reported by Bogue, corresponds with Equation (2.6).

Table 2.5. Heat of hydration of individual cement components (Schindler et al. 2002).

Component	Heat of hydration (J/g)			
	Mindess and Young (1981)	SHRP-C-321 (1993)	Bogue (1947)	Kishi and Maekawa (1995)
C_3S	490	500	500	502
C_2S	225	256	260	260
C_3A	1160	721	866	865
C_4AF	375	302	420	419
Free Lime	-	-	1165	-
MgO	-	-	850	-
SO_3	-	-	624	-

2.1.5 Microstructural development

DoH is a useful and fundamental property that characterizes the evolution of physical and chemical properties of a given cement slurry. However, to fully understand the process of microstructural development, additional information is needed. For example, w/c ratio affects the physical properties of cement slurry. Figure 2.5 illustrates two different slurry samples, each with a random distribution of cement particles. As seen by comparison, Figure 2.5a represents a

slurry sample with a lower w/c ratio; whereas, Figure 2.5b represents a slurry with a higher w/c ratio.

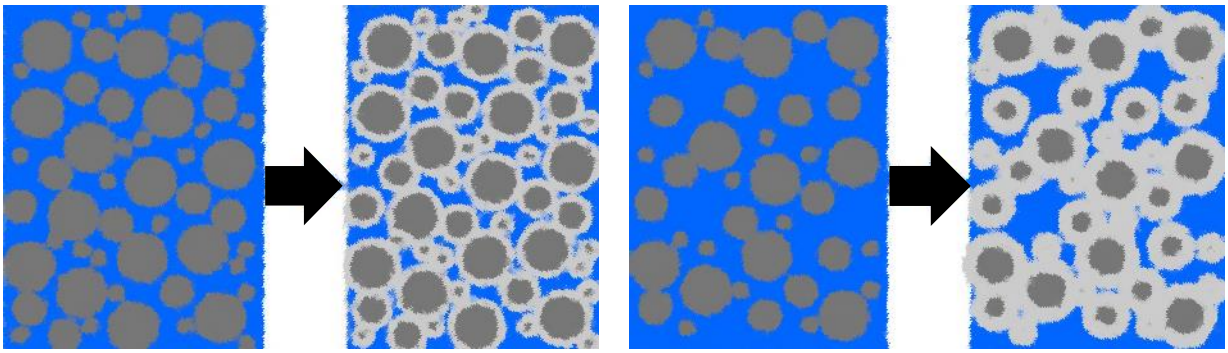

(a) Low w/c ratio (b) High w/c ratio

Figure 2.5. Effect of w/c ratio on cement matrix development (Zhang et al., 2010).

As cement hydrates, the volumetric fraction of solids (hydration products) increases. This development results in an increase of connectivity or percolation of solid microstructure, irrespective of the w/c ratio. Unfortunately, DoH in itself is not capable of completely describing the evolution of this solid microstructure. For example, when the w/c ratio is relatively high (Figure 2.5b), the cement particles are suspended in water with little contact between surrounding particles. As the distance between particles increases, the interaction between particles decreases and a high fluidity (i.e. low solid microstructure connectivity) is observed. When considering both scenarios illustrated in Figure 2.5, the sample with a high w/c ratio must form more hydration products (i.e. a higher DoH) to achieve a similar level of microstructural development. In other words, an equivalent DoH between both samples will result in a different level of solid microstructure connectivity, and therefore, will exhibit different behavior and physical properties. As will be seen later in this work, the characterization of microstructural development will be related to the bulk properties of the slurry (i.e. hydrostatic pressure drop).

2.2 ISOTHERMAL CALORIMETRY

Isothermal calorimetry is a commonly used method for quantifying the amount and rate of heat evolution for a given sample and has been used to characterize cement hydration. As evidenced by its name, isothermal calorimetry essentially measures the amount of heat to be removed from the system (exothermic reaction) in order to maintain a single, specified reaction temperature of the given sample. In this technology, it is assumed that all of the heat generated from the reaction is transferred to the environment. This method of hydration characterization relies heavily on the principles of heat transfer, in that heat generated via physical or chemical reactions will be transferred to its surroundings at a rate proportional to the difference in temperature (Robbins, 2007).

This study used the TAM Air isothermal calorimeter. This calorimeter is a commercially available, eight-channel unit with an operating range of 5 to 90°C (TA Instruments, 2014). The calorimeter consists of eight individual channels that are housed inside an insulated environment, allowing for a maximum of eight different samples to be tested simultaneously at a given isothermal testing temperature. A diagram of the configuration of one of the eight channels can be found in Figure 2.6.

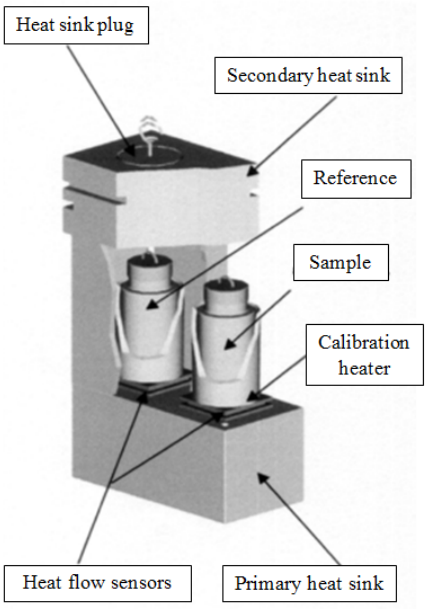

Figure 2.6. Cutaway diagram of single channel in TAM Air calorimeter (AB, 2004).

Each calorimetric channel is arranged in a twin configuration. In this configuration, each channel contains an ampoule that houses the material being characterized while the other chamber contains a reference ampoule that holds an inert material with a thermal capacity similar to that of the sample. The size of the sample chambers allows for ampoules of up to 24 mL, although the reactivity of the system will limit the actual useable sample size. In order to determine the heat produced, the heat flux between the sample and a reference ampoule is measured, which creates a voltage signal proportional to the heat flow. By examining a given material at a constant, specified temperature, a testing variable (i.e. reaction/testing temperature) is removed.

Isothermal calorimetry is preferred for this study because it directly measures the cumulative heat and rate of hydration. Also, unlike direct analysis, isothermal calorimetry is capable of measuring and recording heat evolution (hydration) continuously over time instead of

discrete measurements from visual inspection. Due to the nature of cement composition, the heat evolution measured is an approximation of the combined effects of each constituent.

2.3 THE MATURITY METHOD

The previous sections provide information on the measurement of hydration and the underlying concepts and factors that affect the observed hydration evolution of a given cementitious mixture. The following section provides the background information necessary to understand the relationship between time, heat and hydration.

The maturity method, which is also referred to as the equivalent age maturity concept, is an approach for accounting for the combined effects of time and temperature on concrete mechanical properties (i.e. strength) and/or the development of hydration and microstructure (Schindler et al. 2002). Employment of the maturity method makes it possible to normalize the evolution of hydration and microstructural development between various conditions (i.e. temperature, mixture design, etc.). The history and technical basis of the maturity concept is discussed below to understand the process used to select the appropriate maturity function (and corresponding activation energy, if applicable) for this study. Although none of the maturity methods discussed in the following section are able to consider available moisture, moisture can have a significant effect on hydration and strength development if it is limited. Therefore, for the purposes of this research, it is assumed that adequate moisture is available for hydration.

ASTM C1074 “Standard Practice for Estimating Concrete Strength by the Maturity Method,” defines the maturity method as “a technique for estimating concrete strength that is based on the assumption that samples of a given concrete mixture attain equal strengths if they

attain equal values of the maturity index." The maturity index is expressed as either a temperature-time factor or equivalent age at a specified temperature, depending on which traditional maturity function is being considered. Section 2.3.1 explains the difference between two traditional maturity formulations, namely, the Nurse-Saul and Arrhenius formulations.

Similarly, the general term "maturity" is defined as "the extent of the development of a property of a cementitious mixture." This definition is followed by a brief discussion, which explains that this term is typically used in describing the extent of relative strength development; however, it may also be applied to the evolution of other properties that are dependent on the chemical reactions that occur in a cementitious mixture. The development of hydration or microstructure is directly related to the chemical reactions associated with hydration of cementitious materials; therefore, the concept of maturity may be applied to hydration, as well.

2.3.1 Technical basis for maturity formulations

ASTM C1074 is considered to be the current standard specification for application of the maturity method. Within this specification, two traditional maturity functions are explained and compared. A more comprehensive review of the maturity method and its applications may be found in work by Malhotra (Malhotra & Carino, 2004).

The first traditional maturity function, referred to as the Nurse-Saul formulation, defines the maturity index in terms of a temperature-time factor. This maturity formulation dates back to the early 1950s when research was being conducted on accelerated curing methods, namely electric and low-pressure steam curing of concrete. The temperature-time factor is defined by the following expression (Kjellsen & Detwiler, 1993; Malhotra & Carino, 2004; Mindess et al., 2003):

$$M = \int_0^t (T - T_0)dt \approx \sum_0^t (T_{ave} - T_0)\Delta t \qquad (2.7)$$

where, M = Maturity Index (Temperature-Time Factor) at age t;

T = Temperature of the cement at age t;

T_0 = Datum temperature;

T_{ave} = Average temperature of the cement during time interval during time interval Δt.

A graphical representation of the temperature-time factor can be seen below in Figure 2.7. It should be noted that the datum temperature, which is defined as the lowest temperature at which strength gain is possible, is a function of cement composition and curing conditions (Saul 1951). ASTM C1074 recommends that 0ºC be used as the datum temperature for the case of neat Type I cement (without the use of admixtures).

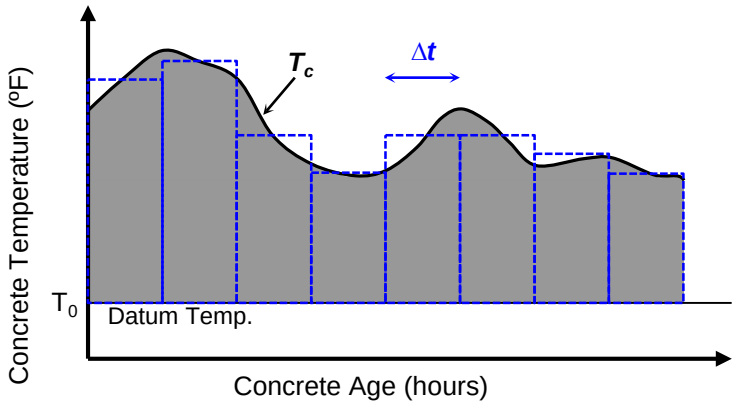

Figure 2.7. Temperature-time history for Nurse-Saul maturity formulation (Carino & Lew, 2001).

Although the Nurse-Saul maturity formulation utilizes the temperature-time factor to express the maturity index, it is also possible to derive an expression for equivalent age using this formulation. Equivalent age represents the duration of a curing period at a given or assumed reference temperature that results in the same maturity as the actual curing period at non-standard/reference temperatures. From this definition of equivalent age, the Nurse-Saul maturity function may also be expressed as follows:

$$t_e(T_r) = \frac{\sum(T - T_0)}{(T_r - T_0)} * \Delta t \tag{2.8}$$

where, t_e = equivalent age at the reference temperature;

T_r = reference temperature

T = curing temperature

T_0 = datum temperature

Equation (2.8) may also be written in the following alternate form:

$$t_e(T_r) = \sum ACF * \Delta t \tag{2.9}$$

Where,

$$ACF = \frac{(T - T_0)}{(T_r - T_0)} \tag{2.10}$$

From Equation (2.10) above, the ratio ACF is defined as the "age conversion factor." Similar to the concept of equivalent age, this ratio may be used to convert a curing interval Δt to an equivalent curing interval at the standard reference temperature.

In 1956, research conducted by McIntosh suggested that a discrepancy may exist in the determination of the maturity index (temperature-time factor or equivalent age) as a result of

variability in the early-age temperature histories for various specimens. Experimental results from this work showed that specimens of equal maturities (established using the Nurse-Saul maturity function) did not necessarily exhibit equivalent strengths, which is the desired result of the maturity method. For example, specimens cured at low, early-age temperatures exhibited weaker strengths at early maturities and stronger strengths at later maturities than what was predicted from the Nurse-Saul maturity function, and vice versa. In 1962, similar research conducted by Alexander and Taplin confirmed the conclusions of McIntosh and Klieger, in that early-age temperature has a significant effect on strength-maturity relationships of pastes and concretes.

In 1968, Verbeck and Helmuth coined the term “crossover effect” to describe these observations and also provided a qualitative explanation for this behavior. It was suggested that the “crossover effect” occurred for two different reasons associated with early-age hydration of cementitious materials (Malhotra & Carino, 2004). First, Verbeck and Helmuth suggested that rapid strength gain occurs during the early stages of curing, in that high initial temperature may result in a more than proportional increase in hydration rate than that predicted by the traditional Nurse-Saul maturity function, hence the high early strength gain. Second, the nature, orientation, and distribution of hydration products, the latter two of which are affected by early-age curing temperature, have a significant effect on the resulting strength. For example, rapid hydration caused by a high early-age curing temperature results in a non-uniform distribution of hydration products within the pore space of the hardening paste. This non-uniform distribution leads to lower strengths than those predicted from the traditional maturity function. Additionally, high early-age curing temperatures will result in the formation of low permeability “shells” of hydration products around the unhydrated cement grains. This low permeability barrier limits the

diffusive capability required for later-age hydration, which will result in a reduction in ultimate strength. The “crossover effect” is illustrated in Figure 2.8.

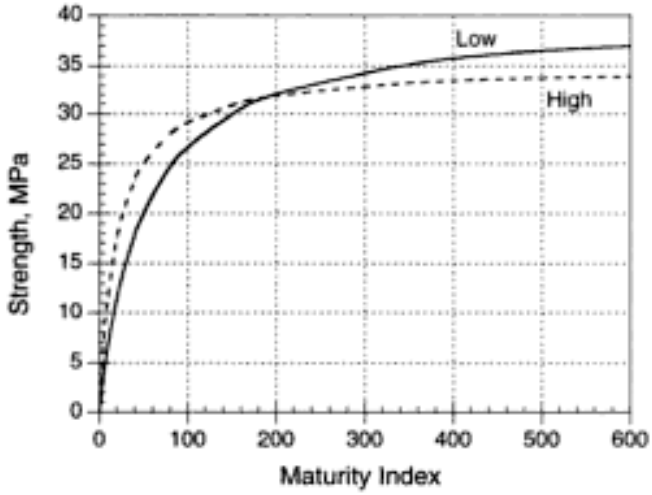

Figure 2.8. The effect of early-age curing temperature on the strength-maturity relationship (Malhotra & Carino, 2004).

Due to the limitation of the Nurse-Saul maturity function in being unable to accurately account for the “crossover effect,” or more specifically, the effect of temperature on early-age hydration behavior, a more robust approach was necessary. In 1960, Copeland et al. suggested that the early-age hydration behavior may be described by the Arrhenius equation, instead of the traditional Nurse-Saul formulation that had been used until this point in time. In 1977, Freiesleben Hansen and Pedersen suggested the following expression for equivalent age based on the Arrhenius equation (Carino & Lew, 2001; Poole, 2007):

$$t_e(T_r) = \sum_{0}^{t} e^{\left(-\frac{E_a}{R}\left(\frac{1}{T_c}-\frac{1}{T_r}\right)\right)} * \Delta t \qquad (2.11)$$

where, $t_e(T_r)$ = equivalent age at the reference curing temperature ($°K$);

T_c = average temperature of concrete during time interval $\Delta t, °K$;

T_r = reference temperature, $°K$;

E_a = activation energy, J/mol.

R = universal gas constant,8.3144 J/(mol*°K);

From Equation (2.11) above, the age conversion factor is defined as an exponential function in terms of absolute temperature. It is important to notice this difference between the Nurse-Saul and Arrhenius equations, as it has a significant effect on the calculation of the maturity index. Figure 2.9 illustrates the difference in the temperature dependence of the age conversion factor as calculated from various maturity formulations.

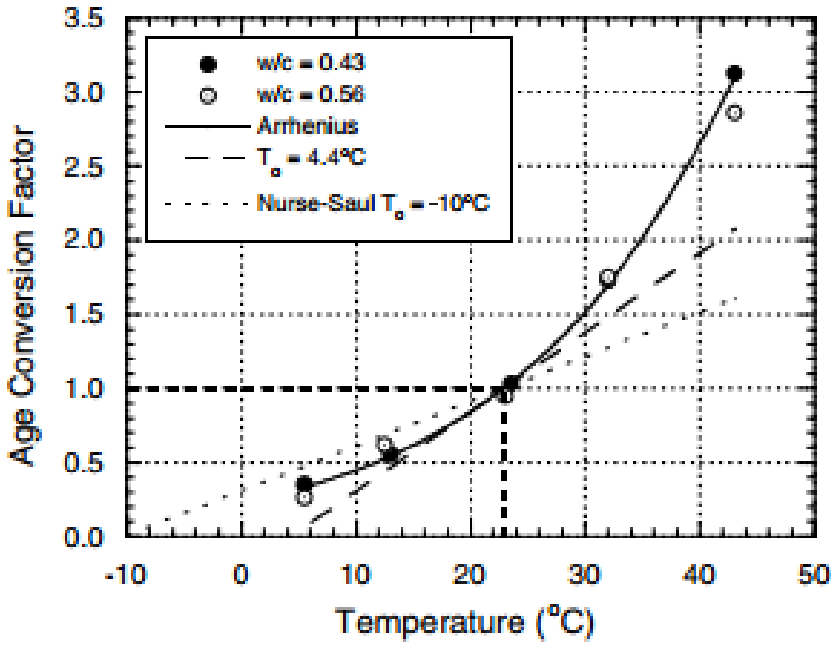

Figure 2.9. Effect of activation energy on the age conversion factor vs. temperature relationship (Malhotra & Carino, 2004).

As evidenced by Figure 2.9 and Equation (2.11), the Nurse-Saul maturity formulation exhibits a linear behavior as a function of curing temperature; whereas, the Arrhenius-based maturity formulation suggested by Freiesleben Hansen and Pedersen (and other formulations) is seen to exhibit a non-linear behavior as a function of curing temperature. This difference is crucial in understanding why the Arrhenius-based maturity formulation is superior to that of the Nurse-Saul function in predicting relative strength gain and hydration development. Research conducted by Byfors and Naik (1980) concluded that the Arrhenius function is well suited for representing the combined effects of time and temperature on strength gain of concrete under a wider range of temperature conditions as compared to the Nurse-Saul function. These conclusions were verified by an investigation conducted by the National Bureau of Standards, where it was concluded that "…a nonlinear function, such as the Arrhenius equation, can better represent the effect of temperature on strength development over wide temperature ranges" (Malhotra & Carino, 2004). Therefore, for this work, the Arrhenius equation is used establish the maturity of a given specimen/sample.

2.3.2 Arrhenius theory

In order to accurately model the hydration behavior of a given cement slurry, it is necessary to characterize the temperature sensitivity of the cementitious materials. The temperature sensitivity of hydration is best described by the Arrhenius equation and the concept of activation energy (Poole 2007). The theory of reaction rates commonly used today originated from the work of Arrhenius (1889), who originally developed Equations (2.12) and (2.13) to account for the influence of temperature on the rate of inversion of sucrose. The exponential relationship is based on collision probabilities, thermodynamics, and statistical mechanics for homogenous gas

and liquid single-phase reactions. This theory states that "…the variation of the specific rate of the reaction with temperature should be expressed by an equation of the form" (Glasstone, Laidler, & Erving, 1941):

$$\ln(k) = \ln(A) - \frac{E}{R * T} \tag{2.12}$$

$$\mathrm{k} = \mathrm{A} * \exp\left(\frac{-E}{R * T}\right) \tag{2.13}$$

where, k = specific rate of reaction,

A = parameter that is independent or varies little with temperature,

E = activation energy (J/mol),

T = Absolute reaction temperature (°K), and

R = Universal gas constant J/(mol K).

The activation energy of a reaction represents the energy that a molecule in the initial state of the process must acquire before it can take part in a reaction. The activation energy (E) in the Arrhenius equation (Equations (2.12) and (2.13)), defines the shape of the age conversion factor as a function of temperature. As stated in Section 2.1, the concept of activation energy and DoH of a cementitious material is considered to be an "apparent" or "experimental" property or characteristic because a single value is used to characterize the overall hydration of cementitious materials, which is comprised of individual cement compounds that hydrate at different rates. Arrhenius' theory does not describe the temperature sensitivity of the hydration of individual chemical reactions, but it is considered to be the best tool available to account for the effect of

temperature on the combined rate of hydration due to all chemical reactions (Poole 2007). Inaccurate characterization of activation energy will lead to errors in models used for estimating the temperature rise, thermal stresses, and mechanical properties of concrete elements (Poole 2007). The further the curing temperature is removed from the reference temperature, the more important the assumed activation energy becomes (Schindler, 2004).

2.4 COMPUTATIONAL APPROACH TO PREDICTING HYDRATION

2.4.1 Hydration prediction model

In addition to being able to measure heat evolution to calculate DoH of a given cementitious mixture, it is also necessary to be able to characterize and predict hydration development, as stated in objective (3) from Chapter 1. Over the years, a number of different models have been developed to predict hydration development of various cementitious materials. A list of available and commonly used hydration models is provided in Table 2.6.

Table 2.6. Hydration-maturity relationships (Schindler et al. 2002).

$$\alpha(t_e) = \exp(-\left[\frac{\tau}{t_e}\right]^{\beta})$$

Where:

$\alpha(t_e)$ = degree of hydration at equivalent age, t_e,

t_e = equivalent age at reference temperature (hrs),

τ = hydration time parameter (hrs), and

β = hydration slope parameter.

References: Freiesleben Hansen and Pedersen (1985), Radjy and Vunic (1994), Kjellsen and Detwiler (1993)

$$\alpha(t_e) = \exp\left[-\lambda_1 \left(\ln\left(1 + {t_e}/{t_1}\right)\right)^{-K_1}\right]$$

Where:

t_e = equivalent age at reference temperature (hrs),

λ_1 = hydration shape parameter,

K_1 = hydration slope parameter, and

t_1 = time parameter (hour).

References: Byfors (1980), Jonasson (1984), and McCullough and Rasmussen (1999)

$$\alpha(t_e) = \frac{t_e}{t_e + {1}/{C}}$$

Where:

t_e = equivalent age at reference temperature (hrs),

C = hydration shape parameter dependent on the particle size distribution and rate constant.

References: Knudsen (1982), referred to as the dispersion model.

Table 2.6 (continued)

$$\alpha(t_e) = 1 - \exp[-\gamma * t_e]$$ Where: t_e = equivalent age at reference temperature (hrs), γ = hydration shape parameter. References: Nakamura et al. (1999)

A number of researchers have suggested that the shape of the hydration (heat evolution) curve for cementitious mixtures can be best described by a three-parameter exponential model, as defined in Equation (2.14) (Pane and Hansen 2002; Schindler and Folliard 2005). This hydration prediction model is the most commonly used mathematical relationship and will be evaluated for the purposes of this study.

$$\alpha(t_e) = \alpha_u * \exp\left(-\left[\frac{\tau}{t_e}\right]^{\beta}\right) \quad (2.14)$$

where, $\alpha(t_e)$ = degree of hydration at equivalent age t_e;

τ = hydration time parameter (hours);

β = hydration shape parameter;

α_{ult} = ultimate degree of hydration.

The parameters of the exponential hydration model (α_u, τ, and β), as seen in Equation (2.14), are used to describe the shape of the heat evolution or hydration kinetics curve. These parameters are used to capture the effects of different mixture constituents (i.e. cement chemistry and composition, admixtures, etc.) on the development of hydration of a cementitious mixture. In this model, α_{ult} corresponds with the cumulative amount of heat that evolves from a

cementitious mixture at complete hydration, τ corresponds with the initiation of the acceleration stage (stage 3) of the hydration curve (see Figure 2.2), and β provides the rate of hydration. Additionally, activation energy is required for accurate calculation of equivalent age (Equation (2.11)).

Poole performed a study to develop empirical relationships for estimating the hydration parameters and activation energy as a function of cement composition, w/c ratio, fineness, and admixtures used. These empirical relationships can be used to determine appropriate input values required for the exponential hydration model (Equation (2.14)). For reference, these hydration parameter expressions are provided below (Equations (2.15), (2.16), and (2.17)). These individual hydration parameter expressions were determined from a multivariate regression model by Poole based on semi-adiabatic calorimetry tests (Poole 2007).

$$\alpha_{ult} = \frac{1.031 \cdot w/c}{0.194 + w/c} + \exp\begin{pmatrix} -0.0885 - 13.7 \cdot p_{C_4AF} \cdot p_{cem} \\ -283 \cdot p_{Na_2Oeq} \cdot p_{cem} - 9.90 \cdot p_{FA} \cdot p_{CaO-FA} \\ -339 \cdot WRRET - 95.4PCHRWR \end{pmatrix} \tag{2.15}$$

$$\tau = \exp\begin{pmatrix} 2.92 - 0.757 \cdot p_{C_3S} \cdot p_{cem} + 98.8 \cdot p_{Na_2O} \cdot p_{cem} + 1.44 \cdot p_{GGBF} \\ +4.12 \cdot p_{FA} \cdot p_{CaO-FA} - 11.4 \cdot ACCL + 98.1 \cdot WRRET \end{pmatrix} \tag{2.16}$$

$$\beta = \exp\begin{pmatrix} -0.464 + 3.41 \cdot p_{C_3A} \cdot p_{cem} - 0.846 \cdot p_{GGBF} + 107 \cdot WRRET \\ +33.8 \cdot LRWR + 15.7 \cdot MRWR + 38.3 \cdot PCHRWR + 8.97 \cdot NHRWR \end{pmatrix} \tag{2.17}$$

where, *LRWR* = ASTM Type A water reducer;

MRWR = mid-range water reducer;

NHRWR = ASTM Type F naphthalene or melamine-based high-range water reducer.

In the case where water reducer/retarder, fly ash, silica fume, or slag admixtures are not used, as is the case for this study, Equations (2.18), (2.19), and (2.20) can be simplified as follows:

$$\alpha_{ult} = \frac{1.031 \cdot w/c}{0.194 + w/c} + \exp\left(-0.0885 - 13.7 \cdot p_{C_4AF} \cdot p_{cem} - 283 \cdot p_{Na_2Oeq} \cdot p_{cem}\right) \quad (2.18)$$

$$\tau = \exp\left(2.92 - 0.757 \cdot p_{C_3S} \cdot p_{cem} + 98.8 \cdot p_{Na_2O} \cdot p_{cem} - 11.4 \cdot ACCL\right) \quad (2.19)$$

$$\beta = \exp\left(-0.464 + 3.41 \cdot p_{C_3A} \cdot p_{cem}\right) \quad (2.20)$$

In addition to the hydration parameter expressions listed above, Poole also conducted a non-linear regression analysis on various isothermal calorimetry tests in order to develop an expression to predict the activation energy as a function of cement composition and admixtures. Similar to the hydration parameter expressions, the prediction of activation energy associated with the hydration of cement types available for this study must be determined. The activation energy prediction model developed by Poole is provided in Equation (2.21).

$$\begin{aligned} E_a = 41{,}230 + 1{,}416{,}000 \cdot \left[\left(p_{C_3A} + p_{C_4AF}\right) \cdot p_{cem} \cdot p_{SO_3} \cdot p_{cem}\right] - 347{,}000 \cdot Na_2O_{eq} \\ - 19.8 \cdot Blaine + 29{,}600 \cdot p_{FA} \cdot p_{CaO-FA} + 16{,}200 \cdot p_{GGBFS} - 51{,}600 \\ \cdot p_{SF} - 3{,}090{,}000 \cdot WRRET - 345{,}000 \cdot ACCL \end{aligned} \quad (2.21)$$

where, p_{cem} = % cement in mixture;

p_{FA} = % fly ash in mixture;

p_{CaO-FA} = % CaO in fly ash;

p_{GGBFS} = % GGBFS in mixture;

p_{SF} = % silica fume in mixture;

Blaine = Blaine fineness of cement;

Na_2O_{eq} = % Na_2O_{eq} in cement (= 0.658 × %K_2O + %Na_2O);

WRRET = ASTM Type A&D water reducer/retarder, % solids per gram of material;

ACCL = ASTM Type C calcium-nitrate based accelerator, % solids per gram of cementitious material.

Table 2.7 presents a summary of the testing parameters and conditions used for developing the hydration parameter relationships and activation energy prediction model in the Poole study. In order to evaluate the feasibility of applying the hydration parameter expressions and activation energy prediction model developed by Poole (see Equations (2.15), (2.16), (2.17), and (2.21)) for the purpose of this study, a statistical comparison of cement compositions used in the Poole study were made with the cements included in this study (Table 2.8).

Table 2.7. Parameters considered in hydration model development (Poole 2007).

Parameter	Range
Curing temperature, ºC	5, 15, 23, 38, and 60
w/c ratio	0.32, 0.4, 0.44, 0.5, 0.55, 0.68
Cement type	9 cements including Types I, 1/II, III, and V
Fly ash (FA), wt% replacement	15 – 55
Blast furnace slag (GGBFS), %	30 – 70
Silica fume (SF), wt% in mixture	5 – 10
ASTM Type C calcium-nitrate based accelerator (ACCL), %BWOC	0.74 – 2.23
Air-entraining admixture (AEA), %BWOC	0.04 – 0.09
ASTM Type A&D water reducer/retarder (WRRET), %BWOC	0.18 – 0.53
ASTM Type A water reducer (LRWR), %BWOC	0.22 – 029

Table 2.7 (continued)

Mid-range water reducer (MRWR), %BWOC	0.34 – 0.74
ASTM Type F naphthalene or melamine-based high-range water reducer (NHRWR)	0.78 – 1.25
Polycarboxylate-based HRWR (PCHRWR)	0.27 – 0.68

Table 2.8. Inference space: cement type comparison

Cement mill test results (ASTM C114)		9 cements (Types I, I/II, III and V)			Class A	Type I	Type II/V
		Range	Average	Std. Dev.			
Silicon Dioxide (SiO_2), %		19.18-21.63	20.36	0.84	21.2	**19.1**	20.41
Aluminum Oxide (Al_2O_3), %		3.88-5.43	4.84	0.55	**3.7**	4.7	4.04
Ferric Oxide (Fe_2O_3), %		2.01-5.29	3.12	1.03	4.0	3.1	3.71
Calcium Oxide (CaO), %		61.45-64.51	63.59	0.98	63.6	62.0	63.07
Magnesium Oxide (MgO), %		0.77-2.64	1.27	0.56	**2.7**	**4.3**	**4.62**
Sulphur Trioxide (SO_3), %		2.38-4.4	3.24	0.69	2.7	3.2	2.85
Alkalies (Na_2O equivalent), %		0.42-0.85	0.56	0.15	**0.37**	0.82	0.53
Loss of Ignition (LOI)		1.2-4.1	2.20	0.85	**1.03**	2.1	1.39
Insoluble Residue, %		0.18-1.43	0.56	0.52	**0.08**	0.31	0.40
Free CaO, %		0.91-4.0	2.29	1.06	**0.42**	1.84	1.14
Base cement phase composition (Bogue calculations)	C_3S, %	49.85-66.54	57.95	5.50	60.0	57.2	61.07
	C_2S, %	7.38-24.41	14.64	5.56	15.9	11.6	12.45
	C_3A, %	1.76-10.99	7.55	3.08	3.0	7.0	4.43
	C_4AF, %	6.12-16.10	9.50	3.13	12.06	9.4	11.29
Blaine (ASTM C204), m_2/kg		350-552	423.7	72.1	362	399	**325**
Total heat available for reaction H_{cem}, J/g		458-530	488.7	23.5	461.1	494.6	**446.6**

Note: Solid underline denotes the value is outside one standard deviation from the average. A dashed underline denotes the value is outside two standard deviations of the average. **Bold** denotes values that are outside of the range of values used.

From Table 2.8, the composition of Class A, Type I, and Type II/V cements used for experimental testing are seen to differ from the cements used in the Poole study by at least one standard deviation in a number of categories. In some cases, the cement composition reported for the three experimental cement types is completely outside of the range used for in the inference space. This observation suggests that the previously developed hydration parameter expressions

may not be suitable for use in predicting hydration development for the cement used in this study. Although all three cement types used for this study show differences when compared to the inference space, the composition of Class A OWC deviates the most from the inference space average. Therefore, it may be concluded that the hydration parameter relationships and activation energy prediction model developed by Poole are least suitable for the Class A OWC.

2.4.1.1 Experimental determination of activation energy

When evaluating the temperature sensitivity of cementitious materials, it is always best to determine activation energy experimentally. ASTM C1074 (2014a) provides a graphical method for calculating the experimental activation energy from heat evolution data that may be obtained from isothermal calorimetry testing. Isothermal calorimetry testing was performed by CTL on Class A OWC for a range of mixture designs. A summary of the mixtures tested and relevant isothermal testing conditions is summarized in Section 4.2.1.1.

According to Glasstone et al. (1941), the activation energy can be experimentally obtained by plotting the natural log of the reaction rate (k) versus the inverse of the reaction temperature. In isothermal calorimetry testing, a heat flux is measured between the sample of interest and a reference ampoule, which creates a voltage signal proportional to the heat flow. The voltage data, reported in terms of millivolts per gram of material (mV/gMat), is then converted to power (heat rate), reported in units of milliwatts per gram of material (mW/gMat). From this power (heat rate) plot as a function of time, activation energy may be determined by multiplying the negative of the slope of the best-fit line by the universal gas constant, R. This interpretation of activation energy is typically used to characterize the reaction rate of cementitious materials at various temperatures (Poole 2007). An example of this plot is provided below in Figure 2.10. Due to the subjectivity in defining the acceleration period (linear portion)

of the heat rate curve, the results of this method often exhibit high variability. A detailed description of this traditional graphical method used for the determination of activation energy is provided in ASTM C1702 (2014).

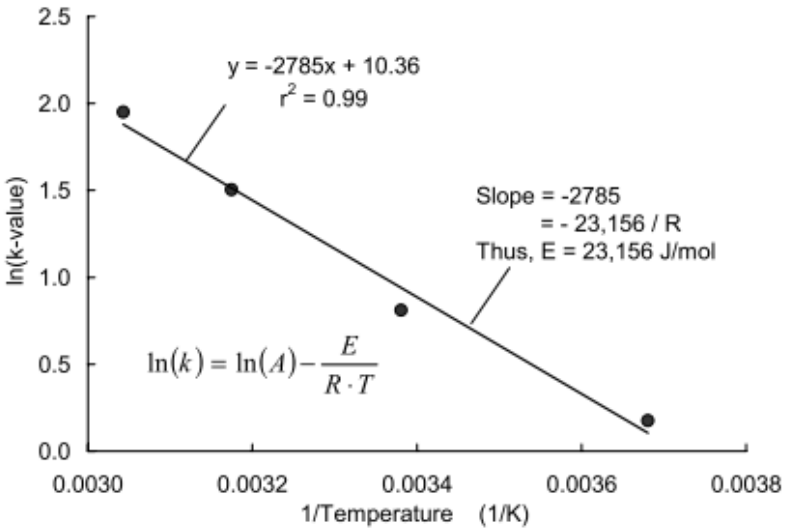

Figure 2.10. Example calculation of activation energy (Schindler et al. 2002).

An alternative graphical method for the determination of activation energy provided by Poole et al. (2007) is also available. Similar to the traditional graphical method presented in ASTM C1074 (2014), this modified method also requires isothermal calorimetry testing at a range of test temperatures for proper evaluation; however, DoH data is utilized in lieu of heat rate evolution data, as is used in the traditional method. DoH results are generated using the energy (cumulative heat) data from isothermal calorimetry testing and the total potential heat evolution based on the given cement composition (Equation (2.6)). At each set of isothermal calorimetry test conditions, the DoH results are fit with the three parameter exponential hydration model (Equation (2.14)) to solve for α_u, τ, and β using a least squares fit. In this study,

the three parameters required for the hydration model at each isothermal test temperature are established (see Table 4.3).

Once all three parameters are defined using a least squares fit, the natural log of the hydration time parameter (ln(τ)) is plotted as a function of the inverse of the respective isothermal test temperature (1/T(°K)), as seen in Figure 2.11. Three separate data points are provided for each isothermal test temperature, each of which corresponds to a different w/c ratio (see Section 4.2.1.1 for a detailed discussion of the experimental design utilized for isothermal calorimetry testing).

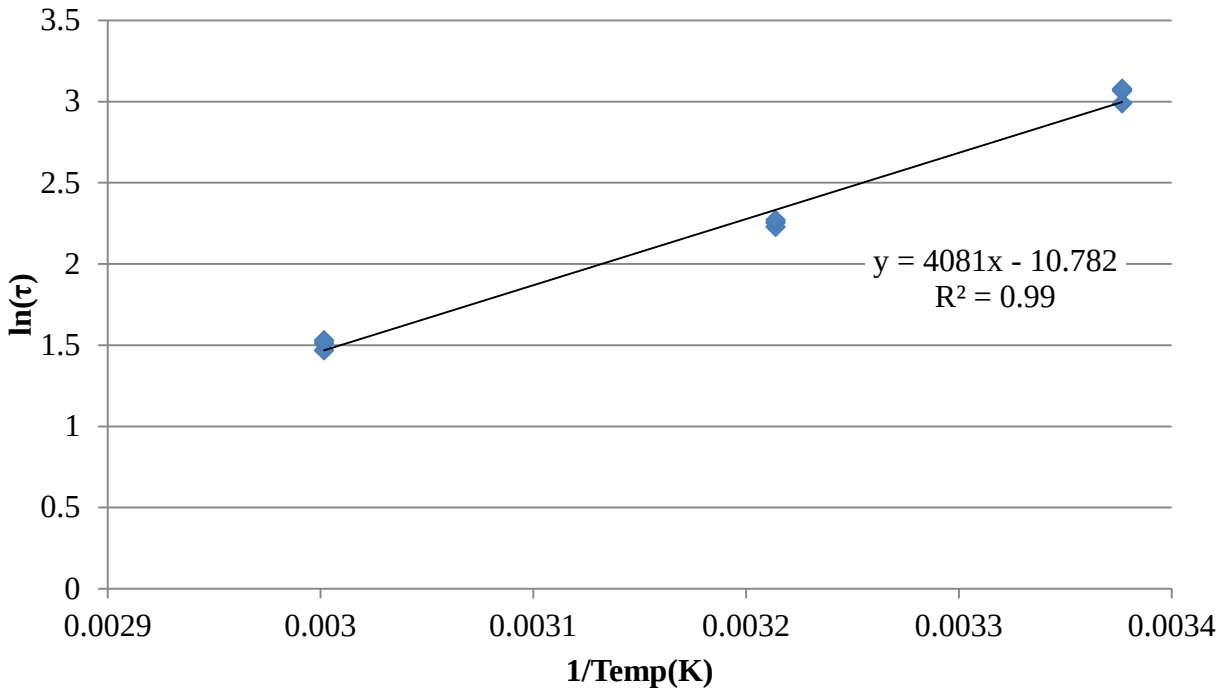

Figure 2.11. Experimental determination of activation energy.

From the results presented in Figure 2.11, activation energy can be determined; however, a discrepancy exists within the procedure provided in the literature. According to Poole,

activation energy is determined by multiplying the slope of the best fit line illustrated in Figure 2.11 ($\ln(\tau)$ vs. $1/T$) by the *negative* of the natural gas constant, R. As seen from Figure 2.11, a direct relationship exists between the hydration time parameter (τ) and inverse temperature ($1/T$); therefore, the slope of the best fit line should be multiplied by the *positive* value of the natural gas constant, R. Additionally, for this modified method of activation energy determination, α_u and β are assumed to be independent of the isothermal test temperature, which generally holds true, as much less variation in these two parameters is observed when the exponential hydration model is fit to the cumulative heat data between the various isothermal test temperatures. Using the results from Figure 2.11, it is determined that 33,929 J/mol is an appropriate value for the experimental activation energy for Class A OWC.

2.4.2 Virtual Cement and Concrete Testing Laboratory (VCCTL)

One of the goals of this study is to relate fundamental properties of cement hydration (i.e. DoH, capillary porosity, etc.) to bulk slurry properties (i.e. hydrostatic pressure loss) relevant in typical borehole conditions. Due to the difficulty in measuring these fundamental properties while a cementitious mixture is being tested within the WSC, it is necessary to estimate these properties as a function of predicted hydration from the sample temperature history. In order to do this, different types of software were evaluated (Stark, 2011). Ultimately, the VCCTL software developed by NIST was selected. This model attempts to simulate cement and concrete hydration and microstructure formation on the elementary (microscopic) level of scale. This is an alternative to the simplified empirical models, which are based on experimental observations of macroscopic phenomena (Bentz, 2005). Assuming the chemical, physical and mechanical characteristics of cement hydration are properly considered, microscopic models are more useful

and accurate than empirical models (Lin & Meyer, 2009). The other advantage is that VCCTL defines the composition of the hydration product at each DoH. This facilitates the ability to identify the role of each type of hydration product on the overall performance of the cement at any given DoH.

2.4.2.1 Underlying concepts of software (Technical Basis)

The VCCTL software utilizes models that are classified as digital-image-based models. These models operate at the microscopic or sub-particle level; each cement particle is represented as a collection of elements (i.e. pixels or voxels). Hydration is simulated by operating on these pixels using a set of cellular-automata-like rules. The random movement of ions is intrinsically modeled, as well as the complete dissolution of the finest cement particles. Properties, such as DoH, percolation, and volume fractions of various cement phases, are easily computable from the three-dimensional hydrated structure. Self-desiccation is simulated by emptying the capillary pores as hydration proceeds. The software operates using hydration cycles or iterations, each of which are based on dissolution, diffusion, and a reaction stages. To obtain the evolution of time as hydration progresses, calibration with experimental data is required. Alternatively, if no experimental data is available, the hydration time is derived from the number of cycles or iterations according to the relation: $t \propto cycles^2$ (Principigallo, Lura, van Breugel, & Levita, 2003).

An understanding of the underlying operating principles of the VCCTL microstructure models will clarify the meaning of some of the parameters and options available within the software. VCCTL models are based on a digital-image representation of a three-dimensional microstructure. In other words, microstructures are mapped onto a regular three-dimensional grid of cubic volume elements, which are referred to as voxels. For cement pastes, each voxel is 1 μm per side; however, for larger scale packings of fine or coarse aggregates, the voxel size depends

on the smallest particle. When a cement paste microstructure is created on this voxel grid, each voxel is occupied by exactly one phase (i.e. C_3S, slag, free water, etc.). To simulate hydration of initial microstructures, rule-based interactions are applied to all of the voxels within the microstructure. The rules are designed to simulate the various chemical reactions (see Section 2.1.2) and mass transport that occur during hydration. As a result, the three-dimensional digital image microstructure is incrementally updated to simulate microstructure development. By using this iterative process, new hydration product phases are introduced, such as CSH, calcium hydroxide, ettringite, and others (Bullard, 2009).

An example of the software interface cement material database is provided in Figure 2.12. It should be noted that the two-dimensional microstructure image is provided to the user to illustrate the distribution and amount of individual cement clinker compounds prior to simulating hydration (Bullard, 2009). A description of the VCCTL cement type and associated cement data files (i.e. volume and surface area fractions of individual cement phases) are also provided.

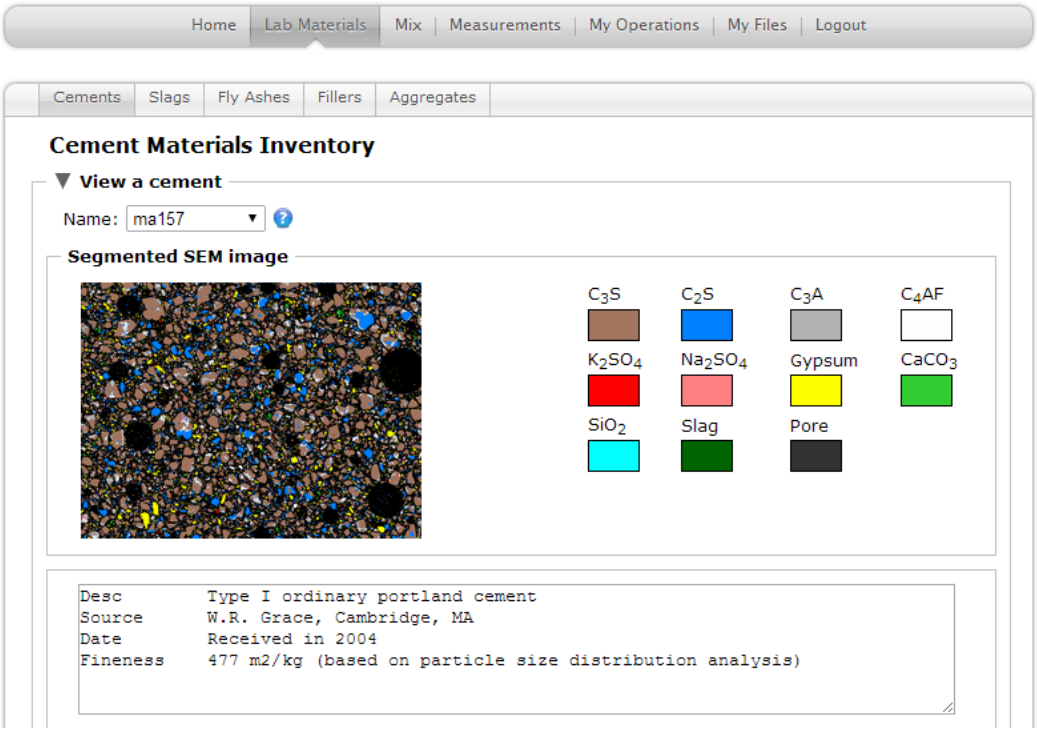

Figure 2.12. VCCTL user interface (Bullard, 2009).

VCCTL contains a database of standard cement types, referred to as Cement and Concrete Reference Laboratory (CCRL). CCRL contains a total of 27 standard cement types, each of which has composition and material property information (i.e. crystalline phase fractions, compressive strength data, etc.). It should be noted that the amount of material property information varies significantly between VCCTL cements included in the CCRL.

3.0 WELLBORE SIMULATION CHAMBER: HYDROSTATIC PRESSURE REDUCTION SIMULATION

A laboratory-scale WSC was previously developed to study the performance of OWC slurries by simulating hydrostatic pressure reduction in the cemented annulus under typical downhole conditions. In addition to the device itself, specific casting and testing protocols are available, which detail the procedures required for proper operation of the equipment. The WSC equipment configuration and monitoring systems allow for accurate characterization of cement hydration throughout the simulation. The following chapter includes a brief description of the components and capabilities of the WSC, a discussion of the suitability of equipment for the purpose of this study, and typical results that may be obtained from pressure testing. This chapter represents a brief summary of the detailed WSC development from the work by (Li, 2015).

3.1 WSC COMPONENTS

3.1.1 Testing equipment and sample

A schematic of the WSC (including a representative formation sample) is presented in Figure 3.1 with photos of the equipment shown in Figure 3.2a and Figure 3.2b. In the order of starting from the central point of the device and moving outward, the WSC is comprised of an inner steel

casing, cemented annulus, surrounding rock formation with upper steel ring attachment, and pressure chamber wall. A piston is used to evenly apply a mechanical load on the slurry surface within the annulus to simulate a hydrostatic pressure at any depth of interest, as a result of the simulated cement column above. Table 3.1 presents the dimensions of the various WSC components. The cylindrical pressure chamber, which holds the prepared formation sample, is certified to be operated at pressures up to 1,500 psi. This operational pressure capacity is significantly above the pressure ranges associated with surface and intermediate casing strings of a typical borehole, where stray gas migration has been identified as most prevalent. Surface casing strings (in the Marcellus play) typically range from 350 to 800 feet deep, and in some cases, up to 3,000 feet (Williams et al., 2012). Therefore, the hydrostatic pressure generated by the cement column can be calculated and typically ranges from 270 to 650 psi, but up to 2,450 psi for a 3,000 feet cement column.

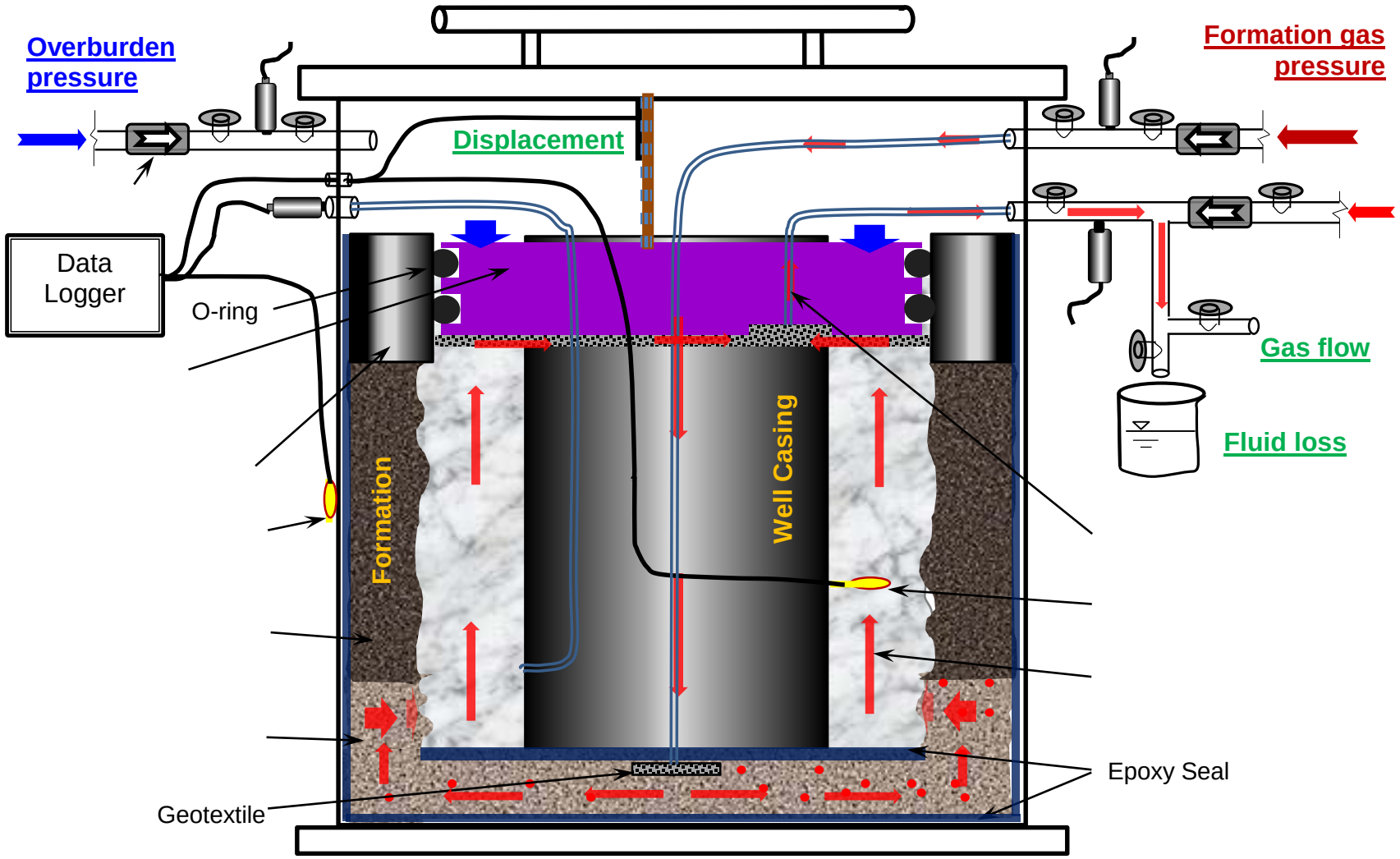

Figure 3.1. Schematic of WSC.

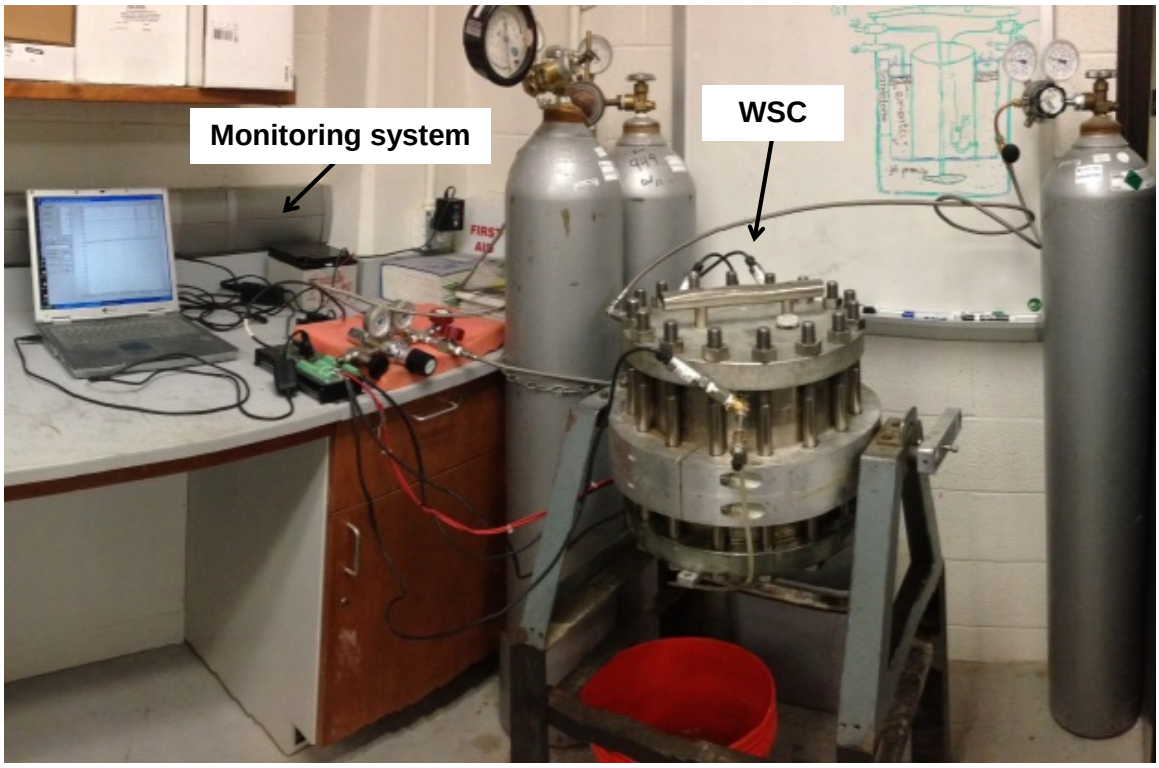

(a) Overview

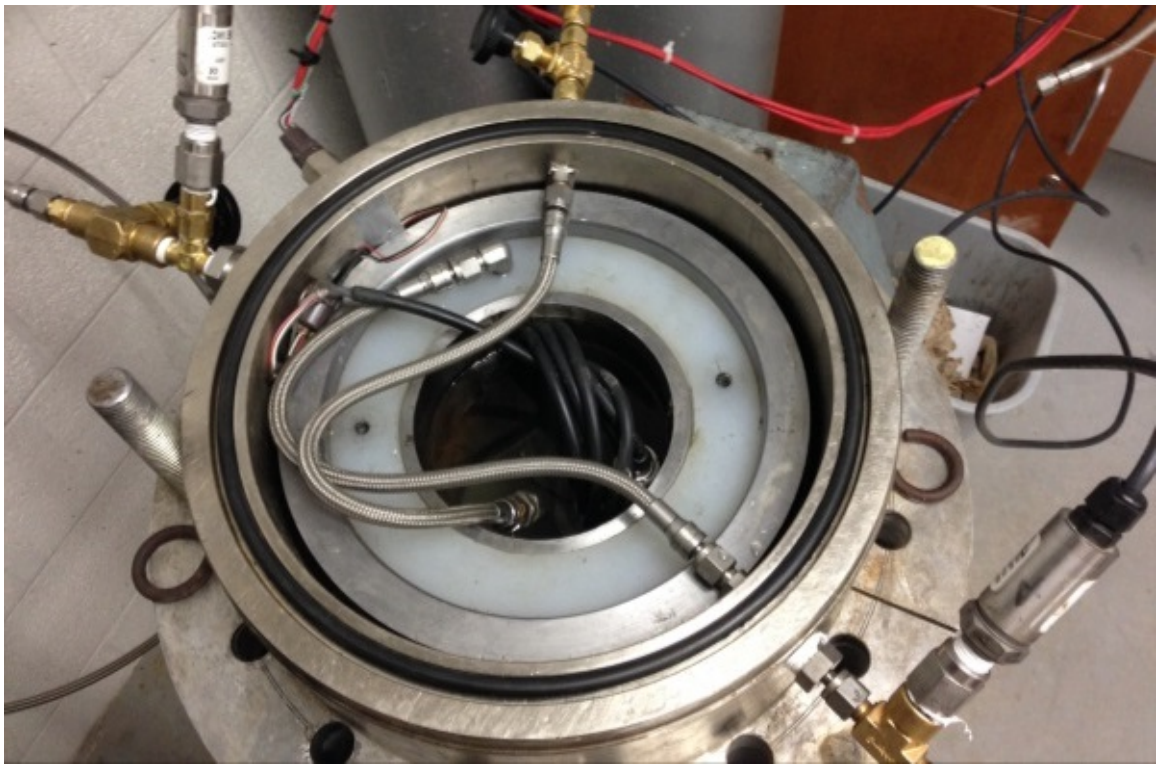

(b) Formation sample and inner assembly configuration

Figure 3.2. Inside view of WSC.

Table 3.1. Dimensions of WSC apparatus.

Category	Parameter	Value
Pressure chamber	Inner diameter	9.75 in
	Inner height	10.0 in
	Maximum working pressure (Safety factor = 3.0)	1,500 psi
Formation sample	Outsider diameter	9.4 in
	Borehole diameter	8.0 in
	Total height	5.0 in
	Thickness of bottom sandstone layer	1.0 in
Upper steel ring	Total height	3.5 in
	Inner diameter	7.95 in
	Outsider diameter	9.5 in
Inner steel casing	Outside diameter	5.5 in
	Length	7.5 in
	Polished section length	3.5 in
	Non-polished section length	4.0 in
Piston	Thickness	2.0 in
	Outsider diameter	7.995 in
	Inner diameter	5.555 in
	Geotextile thickness at bottom of piston	0.25 in
Cement slurry	Column length	5.5 in
	Total volume	146 in^3

3.1.2 Monitoring system

The WSC is equipped with a comprehensive monitoring system that continuously records pressures and temperatures required for data evaluation. The extensive pressure and temperature control/monitoring system is essential for ensuring accurate simulation of typical downhole conditions within chamber. All temperature and pressure measurements are recorded at 20-second time increments. After the cement slurry is externally mixed and placed into the annulus, the variables underlined in Figure 3.1 can be monitored continuously throughout the simulation. It should be noted that the WSC is a versatile piece of equipment and its capabilities extend beyond the scope of this study. Only the following measurements were used for this research:

1.) Slurry temperature

A thermocouple is fixed within the annulus at mid-depth of the formation. The slurry temperature is recorded continuously throughout the simulation. The slurry temperature profile is a critical parameter for characterizing and predicting the hydration of the cement slurry.

2.) Formation/chamber temperature

A thermocouple is installed on the outer surface of the chamber. This temperature represents the environment in which the cement slurry is hydrating within. It is only possible to control or vary this temperature by placing the entire WSC apparatus into a temperature controlled water tub or environmental room.

3.) Slurry pore pressure

A hole is drilled through the inner steel casing at a location of 1.0 in above the bottom surface of the annulus. A pressure transducer is installed at this location to measure the pore pressure within the hydrating slurry column. This pressure measurement is the primary data used for evaluating hydrostatic pressure reduction of the cement slurry.

4.) Applied overburden pressure

Overburden pressure (which is essentially the hydrostatic pressure exerted by the cement column above the point or depth of interest) is simulated using nitrogen gas. As stated previously, in order to ensure even application of this pressure to the top surface of the slurry, a mechanical piston is used. The remaining void space not occupied by the prepared formation sample within the chamber is filled with dye water. This is done for two reasons: 1) to reduce the variability in initial pressure and temperature measurements when first applying the overburden pressure, and 2) to help identify the location at which

communication occurs between the external, pressurized environment and cemented annulus if a test failure occurs. A pressure transducer and regulator are installed outside of the pressure chamber to allow for control of the applied overburden pressure. In the current laboratory setup, a constant overburden pressure is applied throughout the duration of the simulation.

5.) Backflow pressure

A backflow pressure is available and controlled with a check valve. The purpose of this pressure measurement is to provide an outlet for fluid and gas. Also, this pressure measurement provides a check for the slurry pore pressure measurement, as both should have similar readings throughout the duration of the simulation.

3.2 FORMATION PRODUCTION

A technique and accompanying casting protocol has been developed for casting the simulated sandstone formations from a cementitious-based mixture, as shown in Figure 3.3. An easily repeatable procedure is advantageous because any prescribed porosity and permeability representative of in-situ formation conditions can be replicated in a quick and inexpensive manner. It should be noted that WSC pressure testing is capable of simulating hydrostatic pressure reduction using low-permeability formations, as well as investigating for gas migration occurrence using high-permeability formations. For the purpose of this work, hydrostatic pressure reduction using only low-permeability formations is considered. While the inner steel casing of a prepared formation sample may be reused, the simulated cored rock section must be cast for each simulation. The large number of formations required to complete numerous WSC

simulations mandates that the formation casting process be easily repeatable. A detailed casting protocol and formation sample preparation can be found in the WSC development work by (Li, 2015).

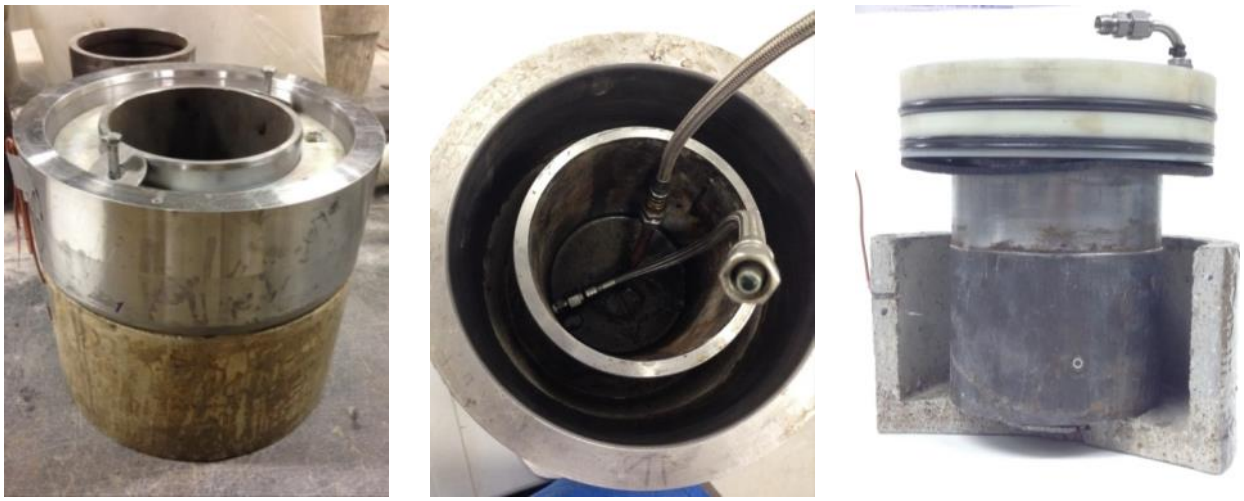

(a) Overview (b) Top view (c) Profile view

Figure 3.3. Formation sample.

3.3 TYPICAL WSC PRESSURE TEST RESULTS

As explained in Section 3.1, the WSC equipment and monitoring system is capable of recording various pressure and temperature measurements throughout the duration of WSC test. Figure 3.4 illustrates a comprehensive plot of results obtained from a WSC test conducted on neat Class A OWC slurry at w/c ratio of 0.46. For this specific WSC test, an overburden pressure of 350psi was applied. It should be noticed that the various pressure and temperature measurements are recorded as a function of time. These results are further evaluated in Chapter 4 and are used to draw useful conclusions about the hydrostatic pressure reduction as a function of fundamental

parameters, such as DoH and capillary porosity. Additionally, Figure 3.5 illustrates a simplified version of the comprehensive WSC test results displayed in Figure 3.4 and will be used to evaluate different fundamental parameters.

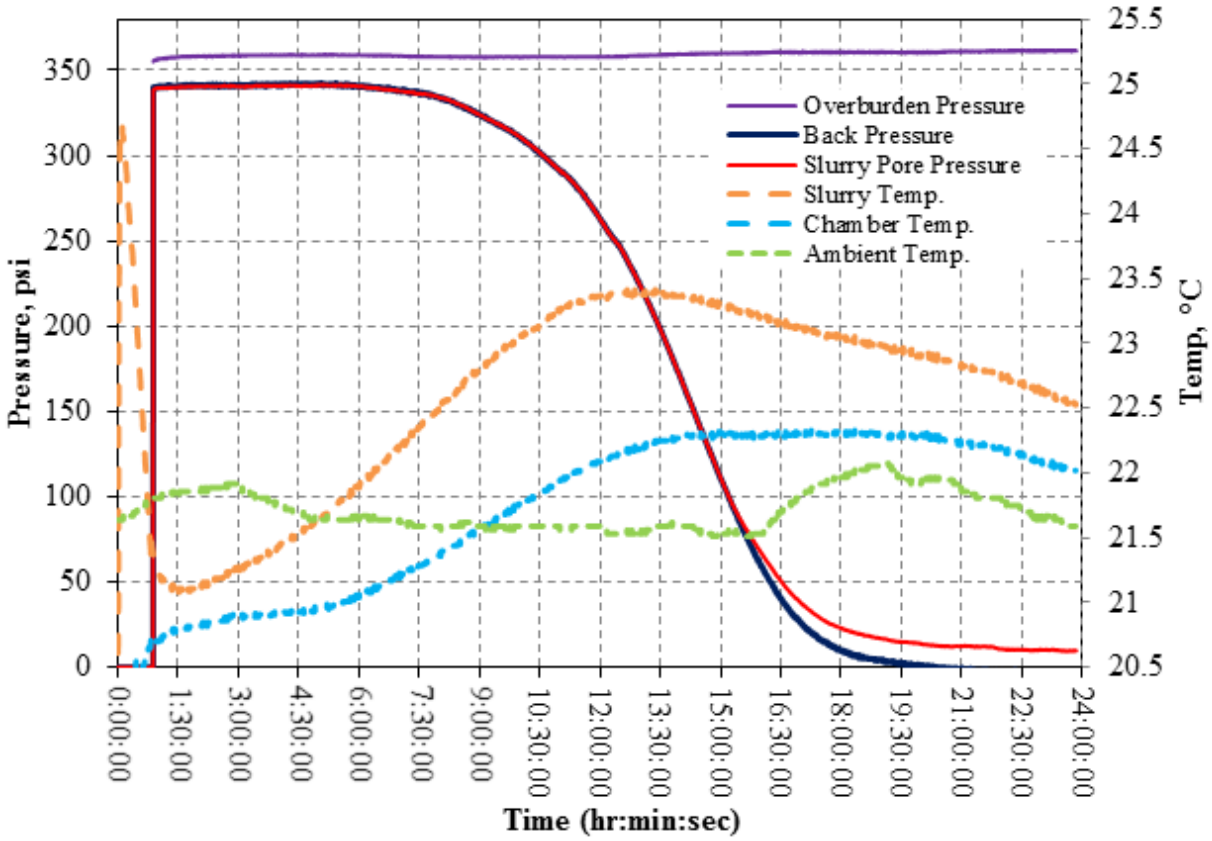

Figure 3.4. Comprehensive WSC test results for Class A OWC.

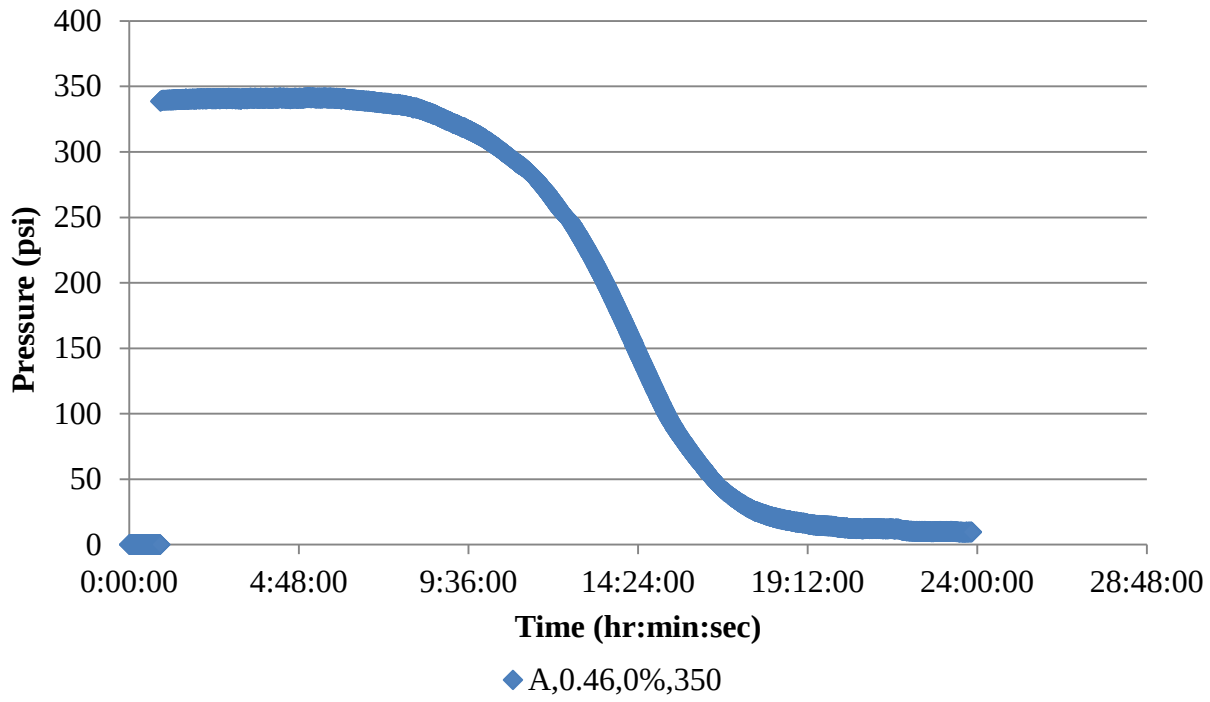

Figure 3.5. Pressure vs. time: neat Class A OWC with 0.46 w/c ratio.

3.4 EVALUATING WSC TEMPERATURE MEASUREMENT ACCURACY

Before the WSC test results (Figure 3.4) can be evaluated using fundamental parameters, it is necessary to assess the accuracy of the thermocouples used to obtain the temperature profile of the hydrating cement. More specifically, it must be determined whether the thermocouple accuracy is adequate or may lead to significant errors in hydration prediction. When initially evaluating the accuracy of the thermocouples used for recording temperature profiles during WSC pressure testing, the "measured" cement temperature was slightly higher than the "true" or actual cement temperature measured directly in the slurry. For WSC testing conducted on Class A OWC at a w/c ratio of 0.46, the maximum temperature difference between the "true" and

"measured" cement temperature over a 24-hour hydration period was found to be approximately 0.5ºC, while occurring at approximately 7 hours after mixing. A sensitivity analysis was performed by calculating the predicted hydration development of the tested cement slurry with a given temperature profile. The exponential hydration prediction model (Equation (2.14)) and corresponding hydration parameter relationships (Equations (2.18), (2.19), and (2.20)) were used for the hydration prediction to ensure that any temperature difference or inaccuracy of the thermocouples would not significantly affect the results. Figure 3.6 presents the DoH prediction results using the temperature profile of Class A OWC slurry during WSC testing.

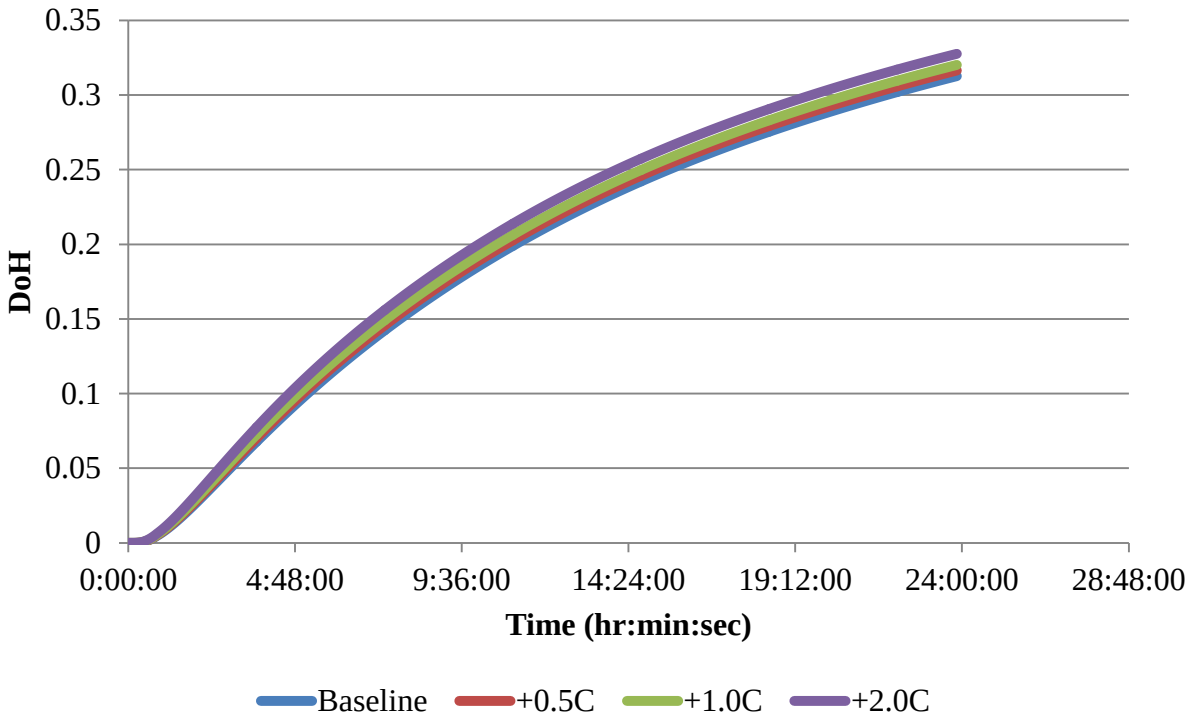

Figure 3.6. Proof of concept: WSC temperature measurement accuracy.

This hydration prediction of the "true" cement temperature history can be considered as the baseline measurement (see the blue line in Figure 3.6). This baseline measurement was then

modified by adding varying levels of temperature shifts or assumed inaccuracies to assess the significance of the temperature effect on the predicted hydration development. As seen in Figure 3.6, the temperature shifts applied to the baseline measurement are as follows: ±0.5, ±1.0 and ±2.0ºF. Assuming a maximum temperature shift or inaccuracy of +0.5ºF, the largest difference between DoH predictions is approximately 1.2%, which occurs at the completion of the WSC test (approximately 24 hours after mixing). It may be concluded that this temperature shift or inaccuracy of 0.5 ºF does not significantly affect the DoH prediction; therefore, the thermocouples used for monitoring temperature profiles during WSC testing are deemed adequate.

4.0 EXPERIMENTAL RESULTS AND DATA EVALUATION TECHNIQUES

The following chapter presents all necessary information associated with the experimental design, test results, and data evaluation techniques utilized. Results obtained from SGS testing, isothermal calorimetry testing, and WSC pressure testing are included. Conclusions regarding these results and how they relate to each other and the objectives of this work are also presented. Various concepts, as introduced in Chapter 2, are also utilized to evaluate and describe the test results obtained.

4.1 SGS EVALUATION

The following section investigates the adequacy of the concept of SGS in describing cement microstructural development, and, in turn, accurately characterizing hydrostatic pressure reduction observed during WSC pressure testing. Table 4.1 presents the conditions at which SGS testing was conducted on neat Class A OWC slurry (no admixtures used). Figure 4.1 presents graphical SGS results (performed by Calfrac Well Services Corp.) for the same Class A OWC that was used for WSC pressure testing (see Figure 3.4 and Figure 3.5 for WSC pressure results). It should be noted that discrete SGS measurements begin at approximately 52 minutes after mixing. This is done intentionally, as that duration of time is representative of typical cement

placement times for surface casing strings. Also, as seen from Figure 4.1, the SGS testing was conducted at a constant temperature of 22.8°C.

Table 4.1. SGS testing conditions and results.

Cement Class/Type	Class A
Additives	None (Neat)
Cement Density	15.6 lb/gal (~0.46 w/c)
Start Time	8/25/14, 8:15AM
Transition Time	1:07:15
Time @ SGS = 100lb/100ft^2	0:28:13
Time @ 200lb/100ft^2	1:01:01
Time @ 300lb/100ft^2	1:16:25
Time @ 400lb/100ft^2	1:26:51
Time @ 500lb/100ft^2	1:35:15

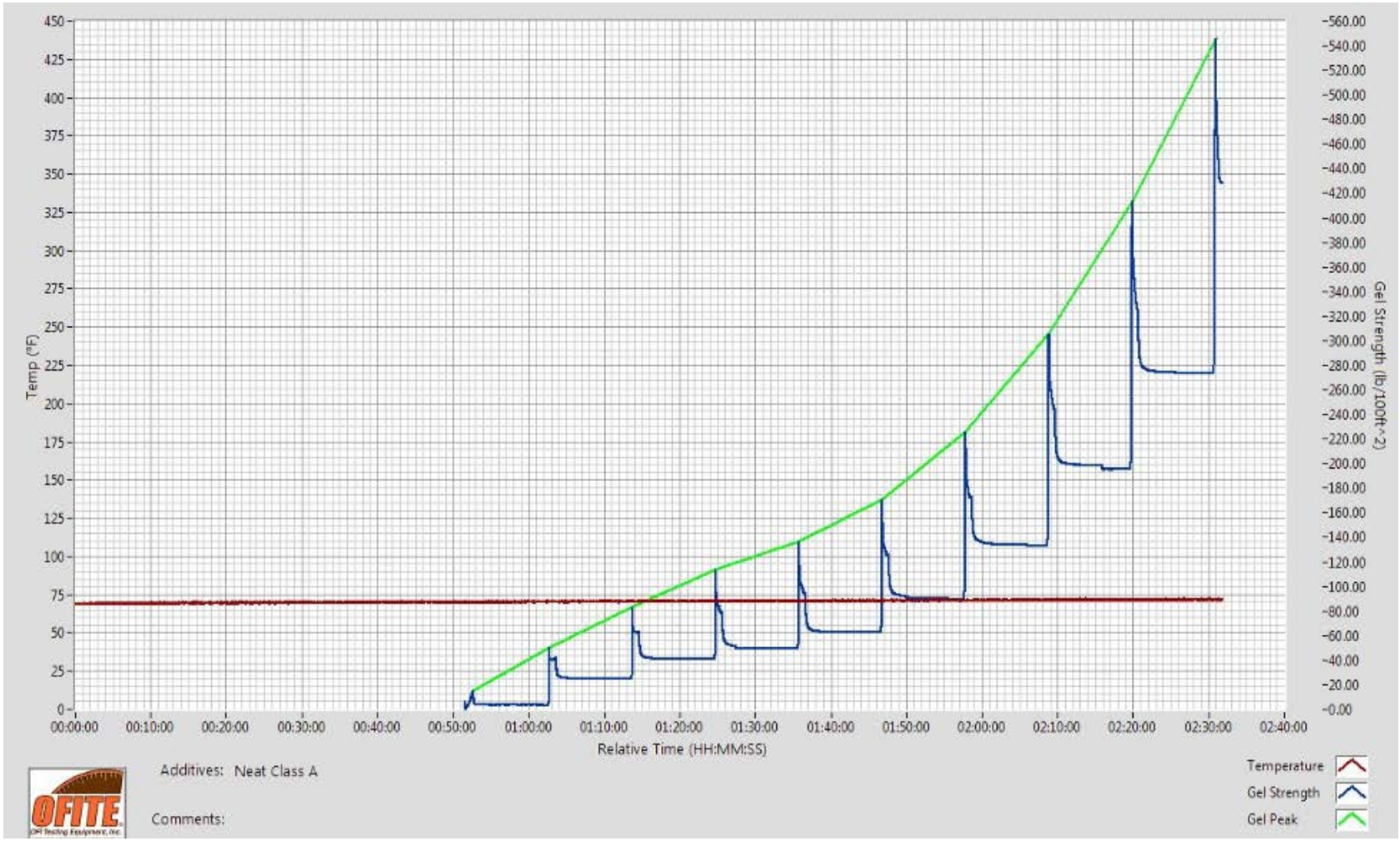

Figure 4.1. SGS results at 22.8°C.

In order to evaluate hydrostatic pressure reduction of Class A OWC during WSC testing as a function of SGS, the concept of equivalent age is necessary (see Section 2.3.1). Given the constant temperature profile of the neat Class A OWC slurry during SGS testing, the results from Figure 4.1 may then be plotted as a function of equivalent age, according to Equation (2.11). From this equation, all required inputs are known except for the activation energy. Due to the fact that SGS testing was conducted on the same Class A OWC used for isothermal calorimetry testing, the experimental activation energy value of 33,929 J/mol is used, as explained in Section 2.4.1.1. Figure 4.2 illustrates the SGS results as a function of equivalent age. In order to evaluate the WSC pressure results (Figure 3.4, Figure 3.5) as a function of SGS, the temperature profile associated with WSC testing must be similarly used to express hydrostatic pressure reduction as a function of equivalent age. Figure 4.3 illustrates the WSC pressure results as a function of equivalent age as defined by Equation (2.11). By combining the results of Figure 4.2 and Figure 4.3, WSC pressure results may be evaluated as a function of SGS. Figure 4.4 illustrates the WSC pressure results of neat Class A OWC slurry as a function of SGS. It should be noted that a limited number of points are plotted in this figure due to the discrete SGS measurements, as seen in Figure 4.1.

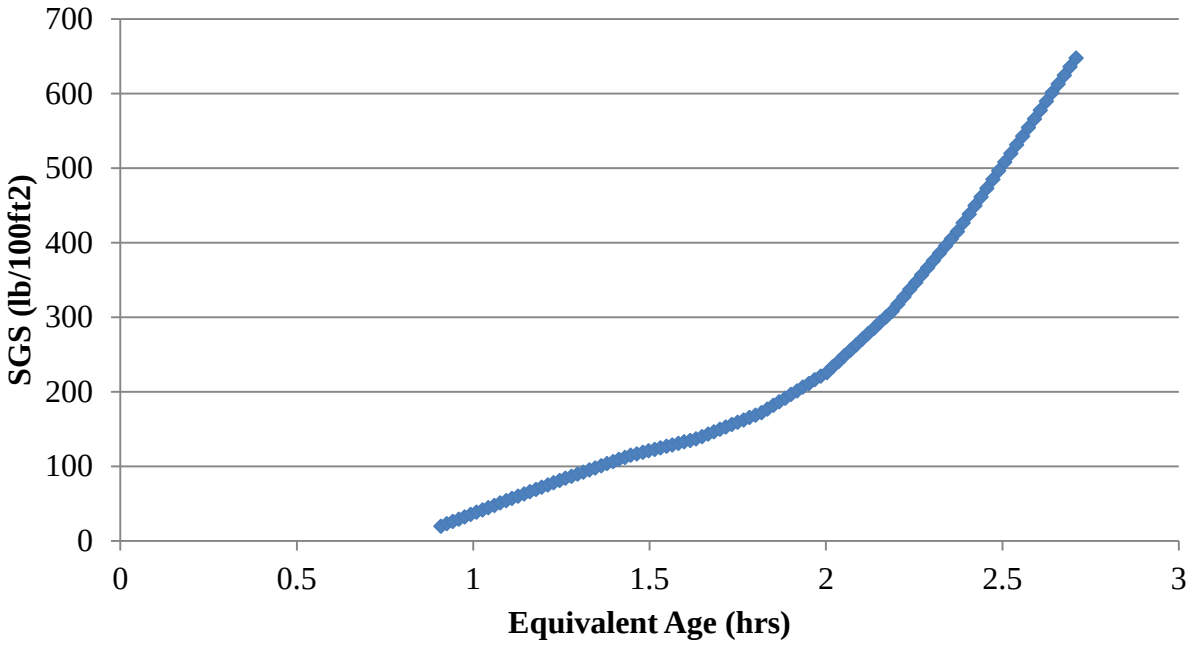

Figure 4.2. SGS vs. equivalent age.

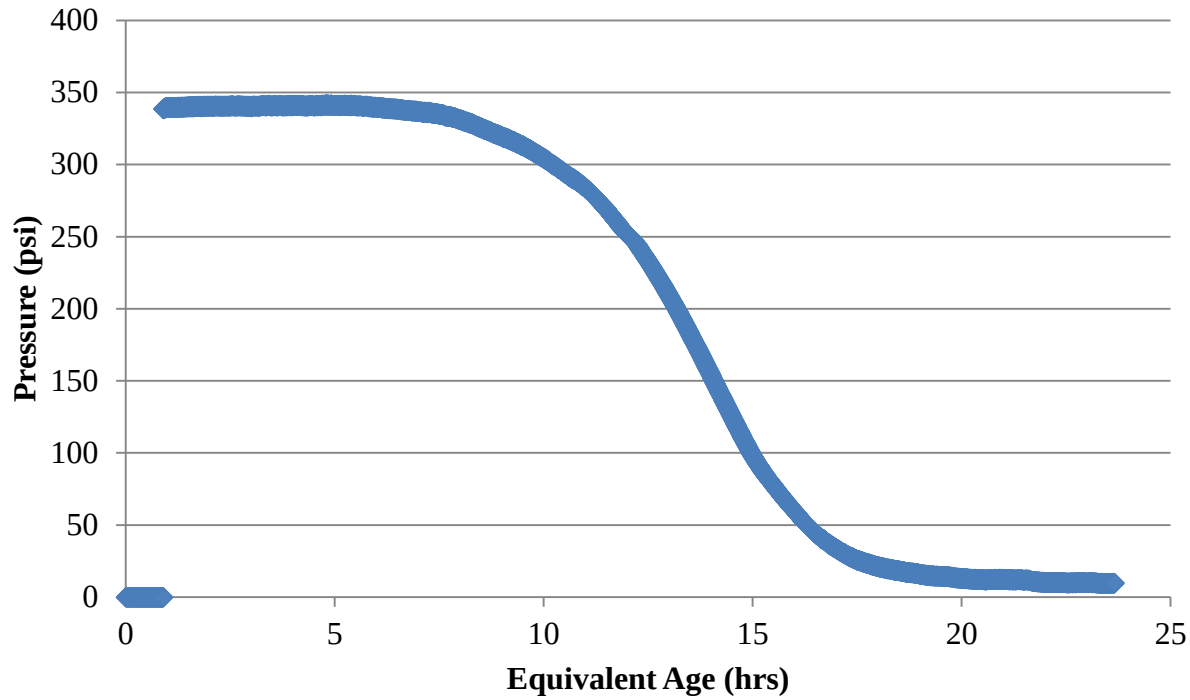

Figure 4.3. Pressure vs. equivalent age.

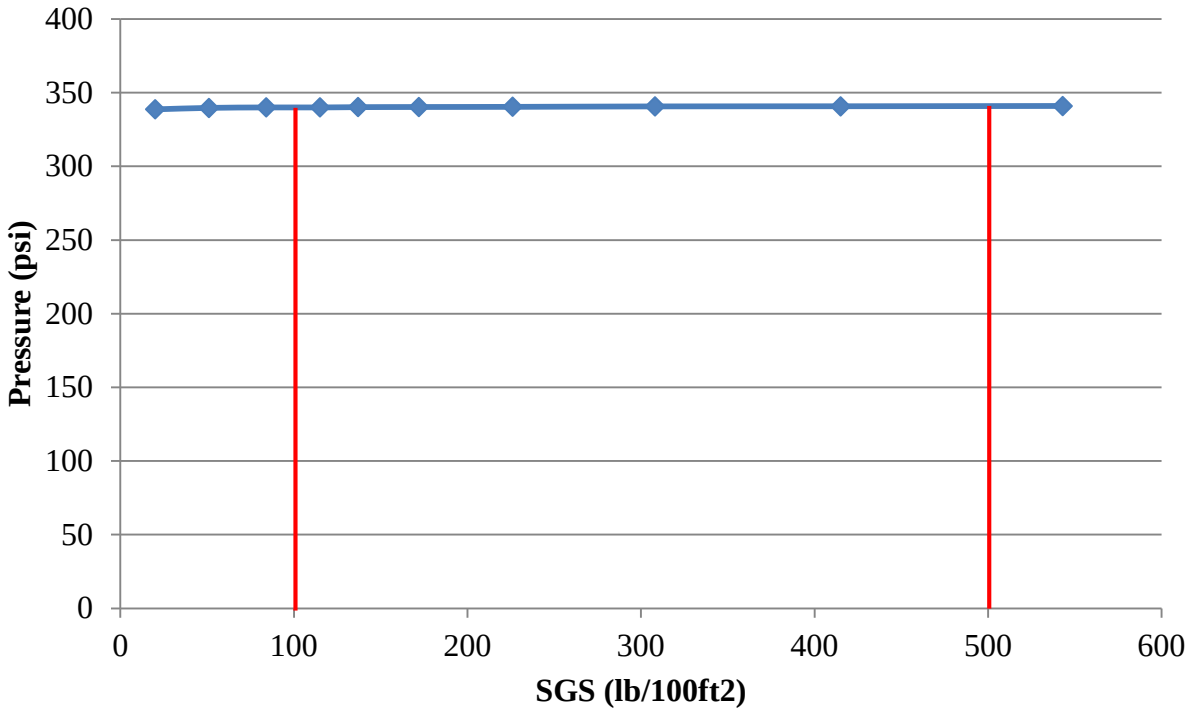

Figure 4.4. Pressure vs. SGS.

As explained in Section 1.1, the industry-accepted SGS criteria for defining the TT, or period of time that the cementitious slurry is most susceptible to stray gas migration, are equal to 100lb/100ft^2 and 500lb/100ft^2. From Figure 4.4, it is obvious that these SGS criteria do not adequately describe the TT of the Class A OWC slurry tested, as initiation of hydrostatic pressure drop has not yet occurred. The results presented in Figure 4.4 verify the initial assertion that SGS alone is incapable of accurately defining the TT, let alone characterizing the potential for stray gas migration.

4.2 DEGREE OF HYDRATION

The following sections introduce the concept of DoH as a fundamental parameter used to characterize the hydrostatic pressure reduction of hydrating cement slurry in the WSC. After determining the inadequacy and limitations of SGS in accurately characterizing cement hydration, this fundamental parameter aims to improve on the currently accepted approach of the oil and gas industry. In this study, DoH will be calculated using the exponential hydration prediction model (Equation (2.14)). The three hydration parameters (α_u, τ, and β) and activation energy must be established for each mixture before this hydration model can be used. These parameters can be determined using empirical relationships or experimental data. Figure 4.5 is a diagram defining the two methods available for implementing the hydration model.

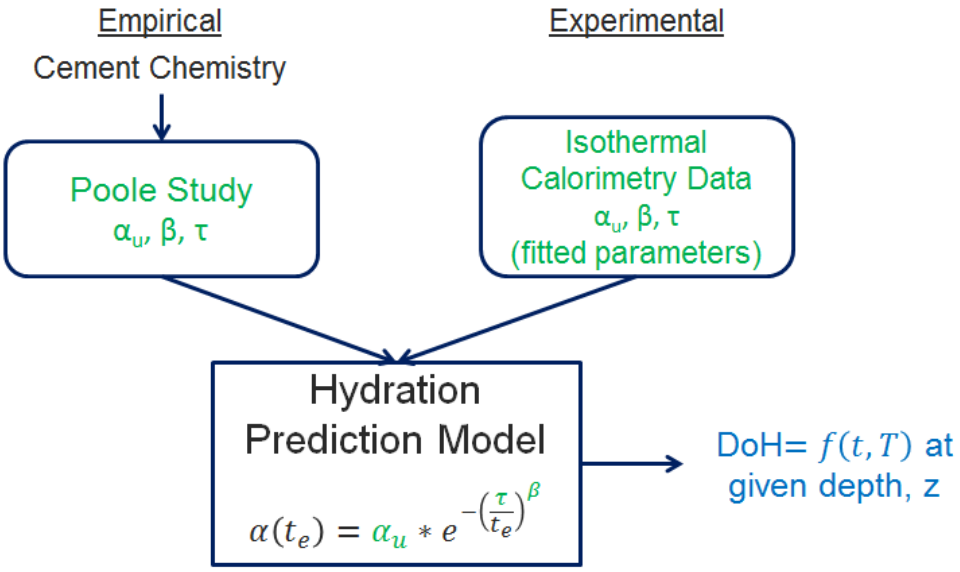

Figure 4.5. Inputs for hydration prediction model.

The first method predicts DoH using the empirical relationships developed by Poole to establish the model parameters (Equations (2.15), (2.16), (2.17), and (2.21)). As discussed in Section 2.4.1, semi-adiabatic calorimetry and isothermal calorimetry testing was performed on a limited number of cement material samples (see Table 2.8). From these test results, empirical relationships were developed and reported as a function of cement composition, admixtures, w/c ratio, and fineness. However, these empirical relationships are only suitable for predicting the DoH of cement slurries with a cement composition and mixture design similar to that used in the development of the database used to develop these prediction equations. Therefore, when analyzing a cement type with a composition not within the inference space, an alternative method for establishing the hydration model inputs is required to achieve an accurate prediction of DoH.

The second or alternative method for predicting the DoH is to establish the hydration model parameters by performing isothermal calorimetry testing on the slurry mixture. For the purpose of this study, isothermal calorimetry testing was conducted on Class A OWC slurries at different temperatures, w/c ratios, and admixture dosages. Section 4.2.1 provides detailed information regarding the experimental design, testing protocol, and data analysis techniques used when performing the isothermal calorimetry testing. At the end of this section, this alternative method of DoH prediction is revisited and described in further detail.

4.2.1 Isothermal calorimetry testing

Calorimetry is the most direct test method to quantify the heat evolution from a cementitious mixture (Poole, 2007). From Table 2.8, it was determined that Class A OWC had the least

similar composition as compared to the composition of the cements used by Poole for the development of the hydration parameter relationships. Therefore, the empirical relationships are deemed to be less suitable for establishing hydration model parameters for Class A OWC used in WSC testing. Isothermal calorimetry testing was performed on Class A OWC to obtain more reliable values for the three hydration parameters and the equivalent age required for defining the DoH as a function of time. The following sections present the experimental design, test protocol, and data analysis/evaluation techniques regarding isothermal calorimetry testing and results.

4.2.1.1 Experimental design

Isothermal calorimetry testing was performed by CTL on various cementitious pastes at different levels of temperature, w/c ratio, and admixture (accelerator) dosage using an eight channel isothermal conduction calorimeter. Table 4.2 presents a test matrix that summarizes the isothermal calorimetry test parameters considered (i.e. w/c ratio, isothermal testing temperature, and admixture dosage level). The eight isothermal test conditions identified in Table 4.2 were performed at each of the four specified isothermal test temperatures; therefore, 32 different isothermal test results were completed in total.

Table 4.2. Isothermal calorimetry experimental design matrix.

Test temperatures: 8, 23, 38, 60 °C			
	w/c ratio		
$CaCl_2$ BWOC	0.40	0.46	0.50
0%	X	X	X
2%	X		X
3%	X	X	X

Note: "X" denotes a tested condition for each test temperature identified

The experimental design, as summarized in Table 4.2, was deliberately selected based on the limitations and capabilities of the isothermal calorimetry testing equipment, hydration behavior of cement at various conditions and parameters, and typical conditions and specifications used in the oil and gas industry. The lowest isothermal testing temperature (8°C) was selected based on the minimum temperature at which hydration can occur. Cement hydration ceases at a temperature below 0°C (Poole 2007; Schindler et al. 2002). Initially, 5°C was selected as the lowest isothermal testing temperature; however, it was recommended that 8°C be used in order to ensure proper hydration and data collection. A maximum test temperature of 60°C was selected because hydration occurring at temperatures greater than 60°C may result in problems related to flash set and/or the formation of different hydration products (Robbins, 2007). An isothermal test temperature of 23°C was selected because it corresponds to the reference temperature commonly used for equivalent age determination and hydration development prediction (as seen in Equations (2.11)and (2.14)). As for the selected w/c ratios, a w/c ratio of 0.46 corresponds with a standard slurry density (15.6 lb/gal) commonly used within

the oil and gas industry (Salinas et al., 2005). The minimum and maximum w/c ratios were then arbitrarily selected around this standard w/c ratio. It should be noted that the duration of the results associated with the isothermal test temperature of 23°C is approximately 168 hours (7 days), which is longer than the other temperature results. This difference occurs only because samples tested at 23°C were run over a weekend, which resulted in an additional 48 hours of data collection.

4.2.1.2 Isothermal calorimetry testing protocol

A summary of the test protocol utilized for isothermal calorimetry testing is provided as follows:

(1) Anhydrous cement was pre-weighed and placed in ampoules inside the calorimeter for 24 hours prior to the start of testing to allow the material to stabilize at the appropriate testing temperature.

(2) Calcium chloride ($CaCl_2$) was dissolved in mix water to produce pre-mixed solutions when included in the slurry mixture. These solutions were stored in temperature-controlled cabinets for 24 hours prior to mixing at a temperature equivalent to the temperature in which the isothermal calorimetry testing was performed.

    a. The dissolution was completed well before testing so that the effects of the accelerating admixture could be isolated and heat produced from dissolution was not considered.

(3) At the time of mixing, the anhydrous cement sample and $CaCl_2$ solutions were removed from their respective pre-conditioning environments and the appropriate amount of solution was measured using a micropipette.

(4) The $CaCl_2$ solution was added to the unhydrated cement sample in the ampoule and mixed for 30 seconds outside of the calorimeter environment using a Vortex mixer.
    a. Note: The cement and $CaCl_2$ samples are only outside of the testing environment temperatures for approximately 45 seconds.
(5) Using an ampoule holder, the mixed sample was then transferred and placed back inside the calorimeter and raw data collection was initiated.

4.2.1.3 Data analysis and interpretation

The following sections describe the various techniques used for modifying isothermal calorimetry test data. As will be further explained, these techniques are necessary to eliminate misleading or inaccurate data and generate useful data to facilitate a correct interpretation of the isothermal calorimetry test results. After these techniques are applied, the modified test data can be used to establish the required hydration model parameters, as described in Sections 4.2 and 4.2.1.4.

Temperature equilibration period (data offset)

As explained in Section 4.2.1.2, cement samples are not directly mixed within the calorimeter. Therefore, a period of temperature equilibration occurs at the beginning of each test. For example, although unhydrated cement and $CaCl_2$ solutions are stored in a temperature-controlled environment (equivalent to the respective isothermal testing temperature), sample mixing occurs outside of the calorimeter environment. After external mixing is complete, the sample is placed inside the calorimeter and data collection begins. The temperature equilibration period (at the beginning of data collection) is caused by the temperature difference between the externally-

mixed cement sample and isothermal calorimeter testing temperature, as well as the communication that occurs between the isothermal calorimeter environment and external environment, while the cement sample is being placed inside the calorimeter. The temperature equilibration period may result in misleading or unusable data at the start of the raw data collection; therefore, it is necessary to modify the initial raw data to produce useful results to analyze.

In order to modify the initial raw data for the early-age temperature equilibration period, Robbins suggests a thirty-minute offset be applied, which essentially ignores this period of data altogether (Robbins, 2007). Due to the importance of early age hydration for this study, a new method of data modification is presented. For each test temperature (except the 8°C condition, which will be explained upon in greater detail in the Data modification (8°C data only) section), the initial raw data included negative heat rate (Power (mW/gMat)). In other words, a negative heat rate signifies that the sample of interest is at a lower temperature than the isothermal calorimeter test temperature, resulting in the calorimeter system (internal environment) adding heat to the sample, which is recorded as a negative heat flux. Therefore, in lieu of applying a thirty-minute offset to the beginning of each data set, all of the negative heat rate data is deleted and the first positive heat rate data point is treated as the start of data collection (time zero). Although this method of data modification is not capable of accounting for all of the early age hydration data, it reduces the amount of useful data deleted or not considered by applying a thirty-minute offset.

Energy integration

Once the initial negative heat rate data are deleted, the cumulative heat must be recalculated. The conversion from heat rate (power) to cumulative heat (energy) is given by Equation (4.1). Equation (4.1) is then applied to each modified data set so that the cumulative heat data can be accurately determined and used to calculate the primary parameter of interest, DoH.

$$E = P * \Delta t \tag{4.1}$$

where, E = energy or cumulative heat, J/gMat,

P = power or heat rate, mW/gMat,

Δt = time increment, hours.

Data modification (8°C data only)

As explained in the Temperature equilibration period (data offset) section, all data sets (except for those corresponding with 8°C) report negative heat rates at the start of raw data collection. When evaluating the results from the 8°C temperature tests, the opposite seems to be true, in that artificially high heat rates are reported. Similar to the explanation regarding the occurrence of negative heat rate output, these artificially high heat rates exist because the externally-mixed sample can be at a higher temperature than the isothermal testing temperature when placed back inside the calorimeter. The external temperature (ambient temperature) can also communicate with the internal isothermal calorimeter test temperature, resulting in an increase in temperature. The increase in temperature within the calorimeter is recorded as a very large, positive heat flux, which creates misleading initial data. Additionally, as reported by the researchers at CTL, isothermal calorimeters are less efficient in “cooling” or removing heat from the sample of

interest than “heating” or adding heat to the system. The atypical spike in heat evolution data (and therefore DoH) conducted at 8°C is illustrated in Figure 4.6 and Figure 4.7 below. The legend keys provided in these figures simply indicate the isothermal calorimetry testing temperatures.

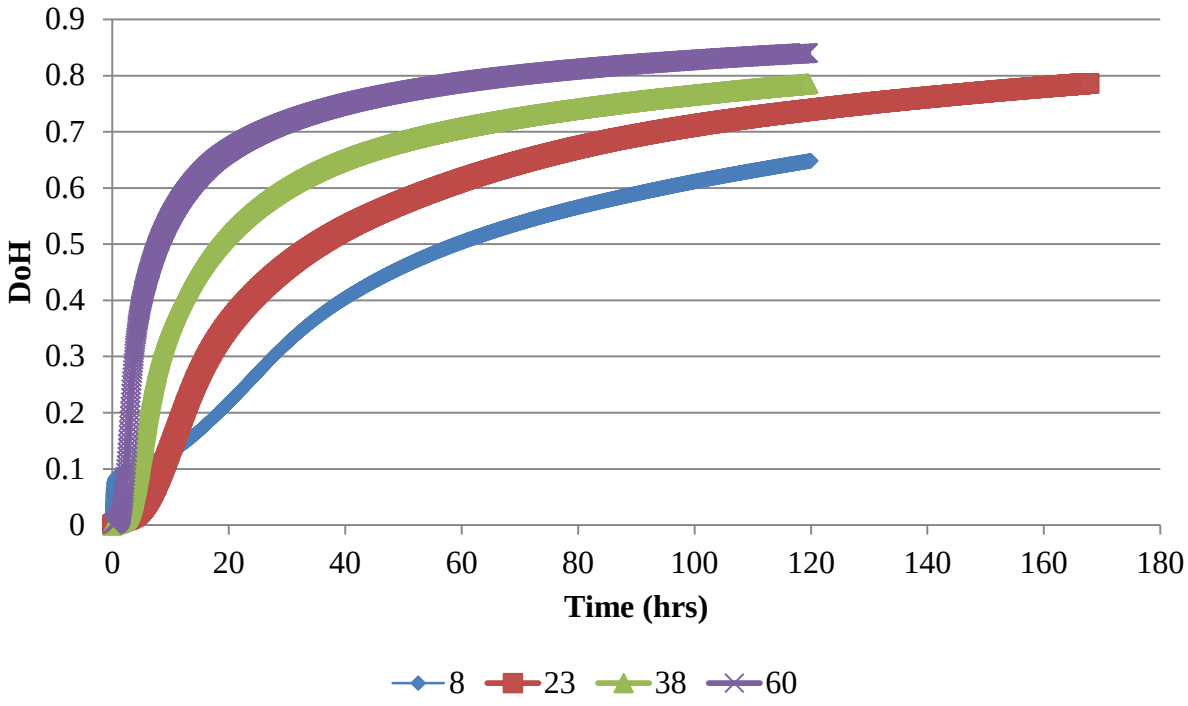

Figure 4.6. DoH vs. time: neat Class A OWC at w/c of 0.46.

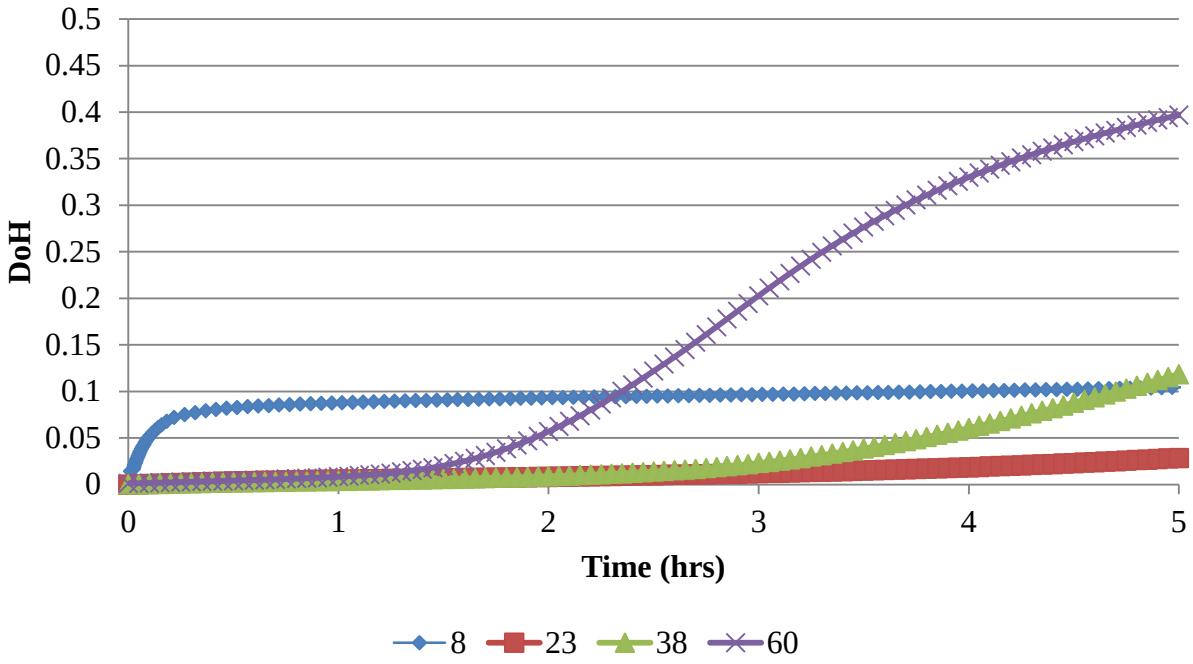

Figure 4.7. DoH vs. time (early-age only): neat Class A OWC at w/c of 0.46.

In order to modify this data for proper evaluation, two different techniques were utilized. The first technique used to modify the isothermal calorimetry data at this temperature is similar to the method used to evaluate early-age equipment calibration, as explained in the Temperature equilibration period (data offset) section. For this method, herein after referred to as the "shift" technique, the initial heat rate and evolution data points that are deemed artificially high are deleted. The duration of this artificially high heat evolution data is arbitrarily determined (approximately 0.4 hours or 24 minutes). Subsequently, a new time zero is established to be the first data point after the arbitrarily determined period of "unusable" data. Once this time is established, the heat rate (power, mW/gMat) is used to calculate a new set of cumulative heat (energy, J/gMat) using the "energy integration" procedure described in the Energy integration section. Once the modified energy is calculated, the DoH is recalculated from the new time zero

without any changes or modifications from the procedure described in Section 2.1.4. This method essentially ignores the early-age heat evolution data collected during the equipment calibration period. The results modified using the "shift" technique are illustrated in Figure 4.8. Figure 4.8 represents modified isothermal calorimetry test data conducted at a temperature of 8°C and a w/c ratio of 0.40. By using the "shift" technique, as described above, the atypical spike in heat evolution (and corresponding DoH) is eliminated.

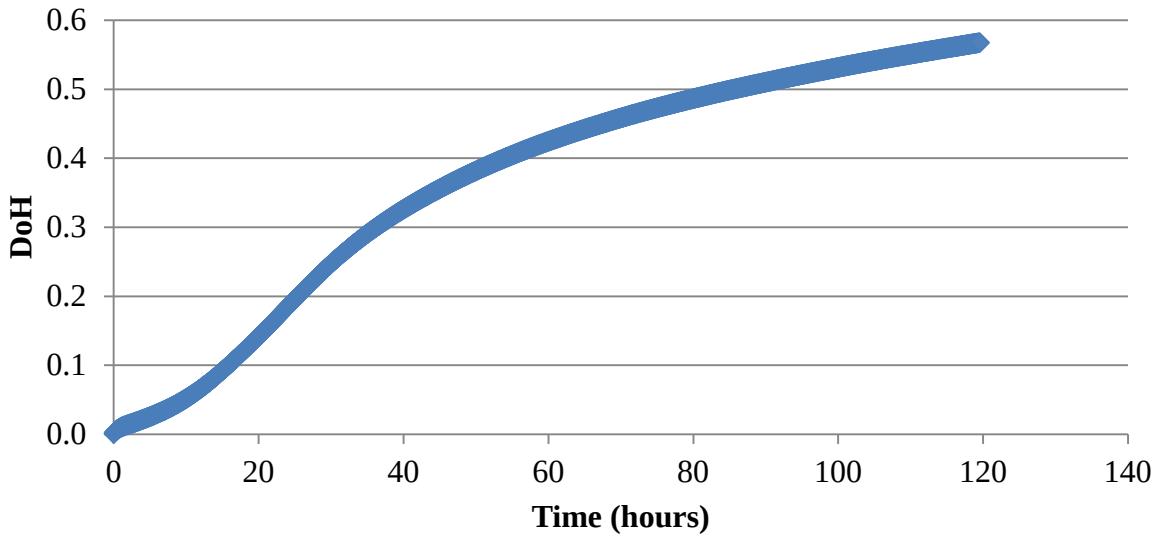

Figure 4.8. DoH vs. time – "shift" technique.

The second technique used to modify the isothermal calorimetry data at this temperature is herein referred to as the "fill-in" technique. Unlike the "shift" technique described above, this technique does not ignore the early-age heat evolution data; instead, the initial period of artificially high heat rate and evolution data is modified. The modified results using the "fill-in" technique are illustrated in Figure 4.9. Similar to Figure 4.8, the results represent the modified isothermal calorimetry testing data conducted at a temperature of 8°C and a w/c ratio of 0.40.

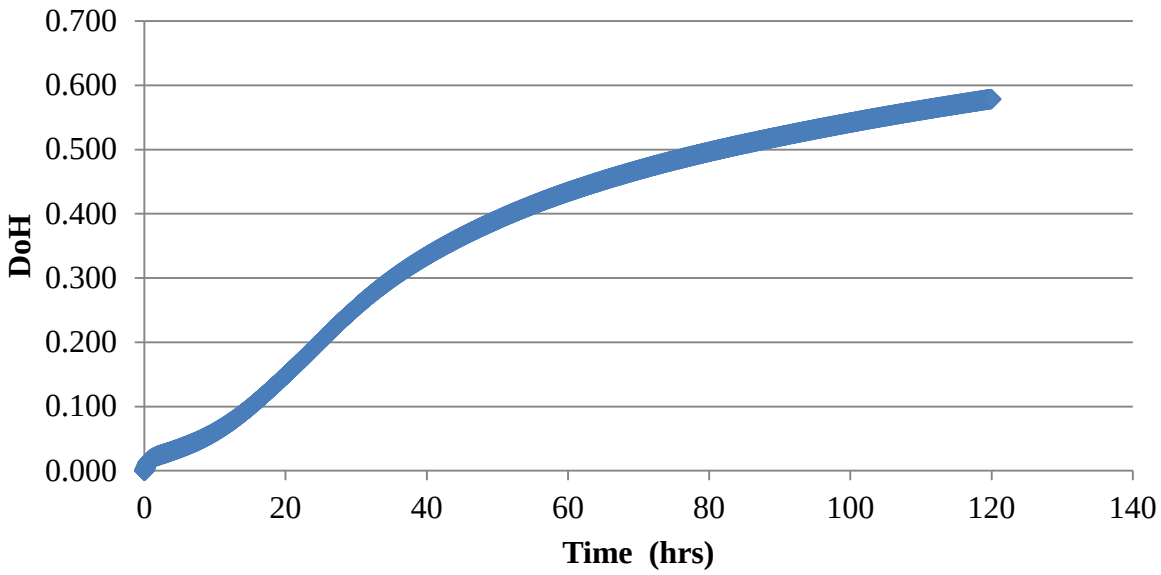

Figure 4.9. DoH vs. time – “fill-in” technique.

The first heat rate data point recorded after this initial period of artificially high heat evolution data (same point as the new time zero determined from the “shift” technique above) is assigned to the entire duration of the aforementioned “unusable” data. This heat rate is significantly lower than the unmodified raw data reported because, at that point in time (new time zero), the calorimeter has undergone proper temperature equilibration and the initially high heat flux recorded as a result of sample introduction is no longer present. Similar to the “shift” technique, this method is also arbitrary in terms of the determination of the duration of the initial artificially high heat evolution data. Figure 4.10 presents heat rate versus time for the unmodified data. As seen from the order of magnitude of the initial heat rate compared to the remaining portion of the data in this figure, the initial hydration rate curve is artificially high before equilibrating and exhibiting expected behavior.

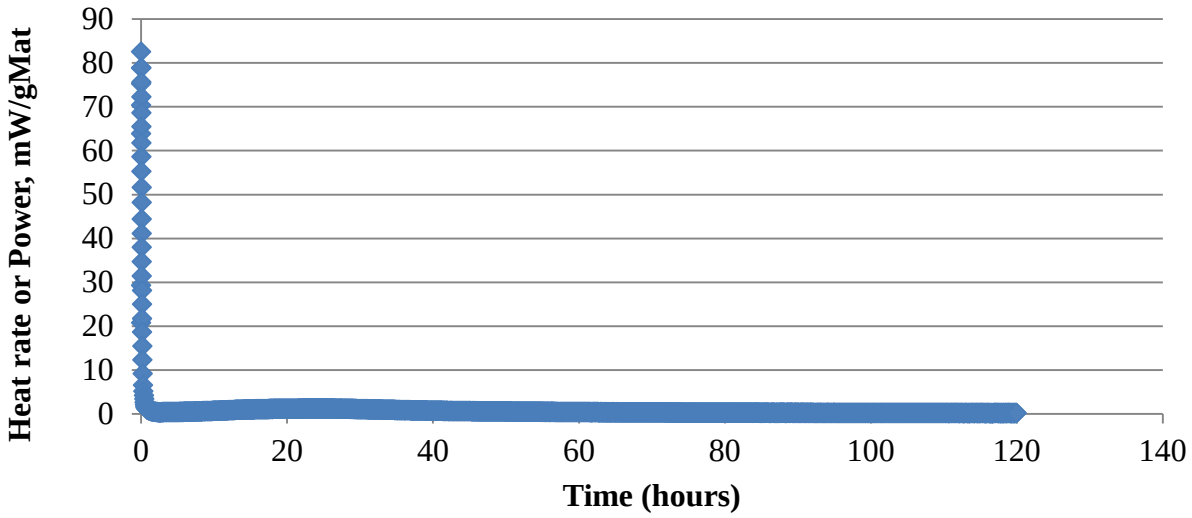

Figure 4.10. Heat rate (power) vs. time – raw (unmodified) data.

The following Figure 4.11 illustrates how the heat rate data changes by applying each of the data modification techniques described above. As seen from this figure, the data exhibits an expected behavior or shape of typical hydration kinetics curve consisting of the five primary hydration stages, similar to Figure 2.2.

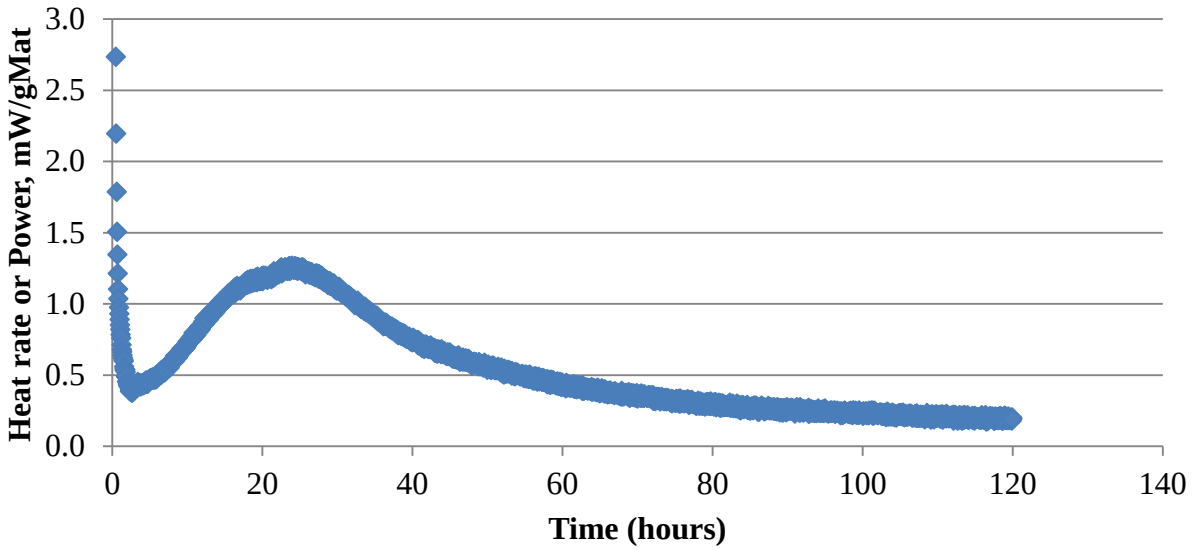

Figure 4.11. Heat rate (power) vs. time – modified data.

A comparison of the raw (unmodified) data with the two different data modification techniques is presented in Figure 4.12 below. As seen from this figure, the initial spike is removed in both data modification techniques.

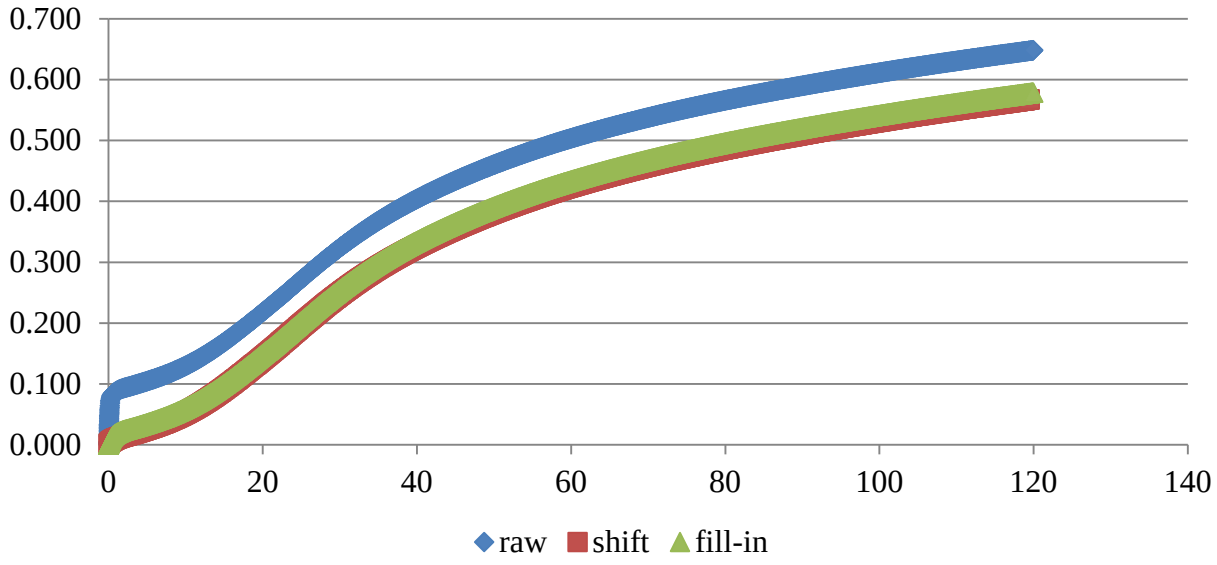

Figure 4.12. DoH vs. time: comparison between data modification methods.

4.2.1.4 Establishing hydration parameters using experimental data

The previous sections provide details on isothermal calorimetry testing and how the test results were modified to generate useful data for establishing the hydration model parameters. As described in Section 2.4.1.1, the DoH results are fit to the three parameter exponential hydration model (Equation (2.14)) to solve for α_u, τ, and β using a least squares fit. Table 4.3 presents a summary of these experimentally determined hydration parameters at each isothermal test temperature, w/c ratio, and admixture dosage level. As discussed in Section 4.2.1.1, results were not obtained for Class A OWC slurry samples with a w/c ratio of 0.46 and $CaCl_2$ dosage level of 2% due to the limitations of the eight-channel isothermal calorimeter. It should be noted that α_u is greater than 1.0 for various isothermal calorimetry results corresponding with $CaCl_2$ dosage levels of 2% and 3%. This is theoretically impossible, as complete DoH occurs at a maximum value of 1.0. These unrealistic results suggest that Equations (2.5) and (2.6) do not account for the additional heat potential due to the use of $CaCl_2$.

Table 4.3. Experimentally determined hydration parameters.

Temp, °C			8	23	38	60
Temp, K			281.15	296.15	311.15	333.15
$CaCl_2$ = 0%	w/c=.40	α_u	0.7597	0.8213	0.7605	0.7862
		τ	37.61	19.89	9.286	4.343
		β	0.8119	0.8353	0.9109	0.8393
	w/c=.46	α_u	0.835	0.8768	0.7794	0.8277
		τ	41.6	21.46	9.522	4.531
		β	0.7575	0.7803	0.9411	0.7934
	w/c=.50	α_u	0.8771	0.8832	0.7919	0.8408
		τ	45.11	21.7	9.68	4.619
		β	0.74	0.7746	0.902	0.7702

Table 4.3 (continued)

$CaCl_2$ = 2%	w/c=.40	α_u	1.134	0.8252	0.7719	0.8157
		τ	38.58	9.259	4.881	2.59
		β	0.4725	0.6468	0.6882	0.5634
	w/c=.46	α_u	N/A	N/A	N/A	N/A
		τ	N/A	N/A	N/A	N/A
		β	N/A	N/A	N/A	N/A
	w/c=.50	α_u	0.9281	0.9635	0.7919	0.8568
		τ	26.02	12.01	9.68	2.917
		β	0.6387	0.6095	0.902	0.6092
$CaCl_2$ = 3%	w/c=.40	α_u	1.64	0.9114	0.7848	0.8307
		τ	82.96	8.811	4.153	2.374
		β	0.3563	0.5213	0.5924	0.4359
	w/c=.46	α_u	2.048	0.9867	0.8558	0.9176
		τ	143.6	10.52	4.675	2.78
		β	0.3103	0.5152	0.602	0.4328
	w/c=.50	α_u	1.421	1.033	0.8705	0.9276
		τ	57.94	11.7	5.017	2.884
		β	0.4183	0.5158	0.6174	0.4498

These established hydration parameters can be used as inputs for the hydration prediction model. In addition to the experimentally determined activation energy, described in Section 2.4.1.1, these hydration parameters may be used to accurately predict DoH of Class A OWC slurry at corresponding conditions (i.e. temperature, w/c ratio, $CaCl_2$ dosage). However, in order to use the established hydration parameters for predicting the DoH of the hydrating cement slurry within the WSC, a variable temperature profile must be taken into consideration. As discussed by Poole (2007), α_u and β are considered to be independent of temperature. Also, given the small ranges of measured curing temperatures within the WSC for various tests (at most 5°C), the effect of temperature on α_u and β is even less significant. However, as seen from Table 4.3, temperature does have a significant effect on τ. This observation is logical, as τ corresponds with

the initiation of the acceleration stage (Stage 3) of the hydration curve (see Figure 2.2). This point of initiation will vary significantly with temperature because temperature is directly related to the rate of hydration. Therefore, the effect of temperature on τ and the effect of τ as a function of temperature on the DoH prediction is investigated. Figure 4.13 graphically illustrates the effect of temperature on τ for each corresponding set of test conditions (w/c ratio and $CaCl_2$ dosage level).

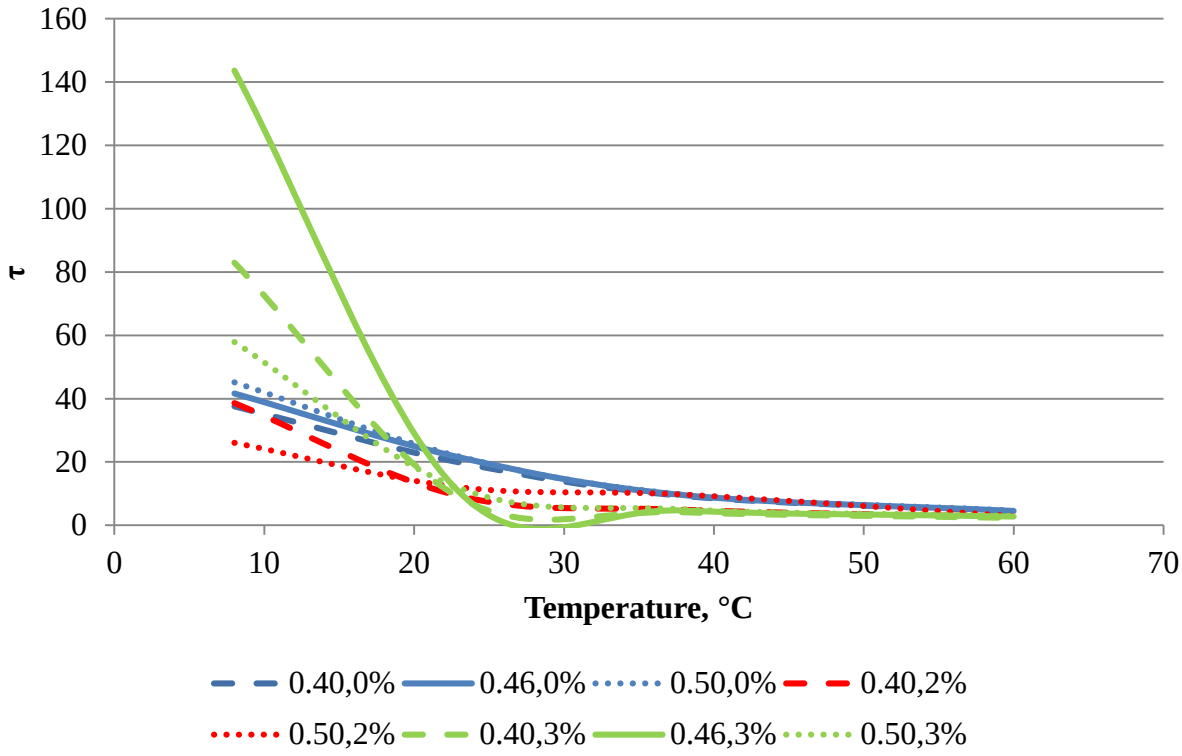

Figure 4.13. Hydration time parameter as a function of temperature.

In general, τ decreases as temperature increases, which results in a leftward shift (or earlier initiation of the acceleration stage) of the DoH prediction results. However, the degree of variability as a function of temperature is significantly different when the $CaCl_2$ dosage levels vary. Therefore, Figure 4.14 presents a subset of the results from Figure 4.13. Similarly, this

figure graphically illustrates the effect of temperature on τ, but only for $CaCl_2$ dosage levels of 0%.

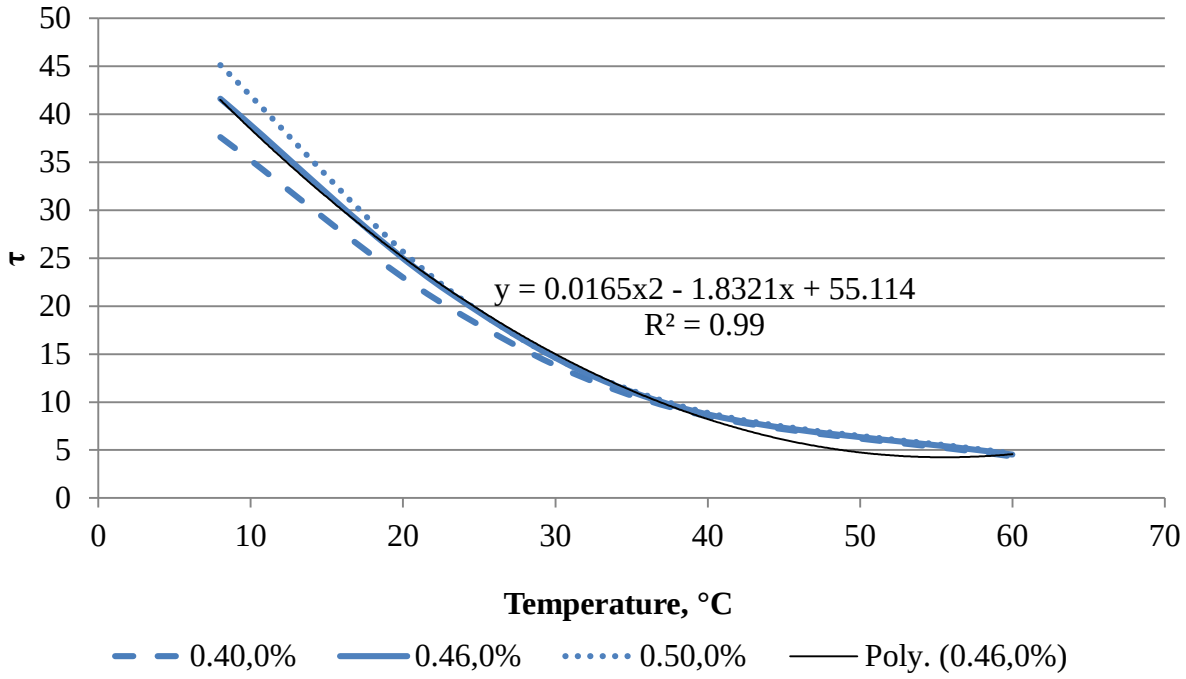

Figure 4.14. Hydration time parameter as a function of temperature (0% $CaCl_2$ only).

A similar trend is observed in Figure 4.14, where τ decreases as temperature increases; however, the range of values for τ is much smaller as compared to results associated with the Class A OWC slurries containing 2% or 3% $CaCl_2$. In order to evaluate the effect of τ as a function of temperature on the DoH prediction of WSC test results, a polynomial was fit to the data and is included in Figure 4.14 for Class A OWC at a w/c ratio of 0.46. The equation defining this polynomial is given as a function of temperature. It is used along with the temperature measurements from the WSC testing so that τ can be defined as a function of temperature throughout the duration of the test. A comparison of the DoH predicted using a constant and adjusted value for τ is presented in Figure 4.15.

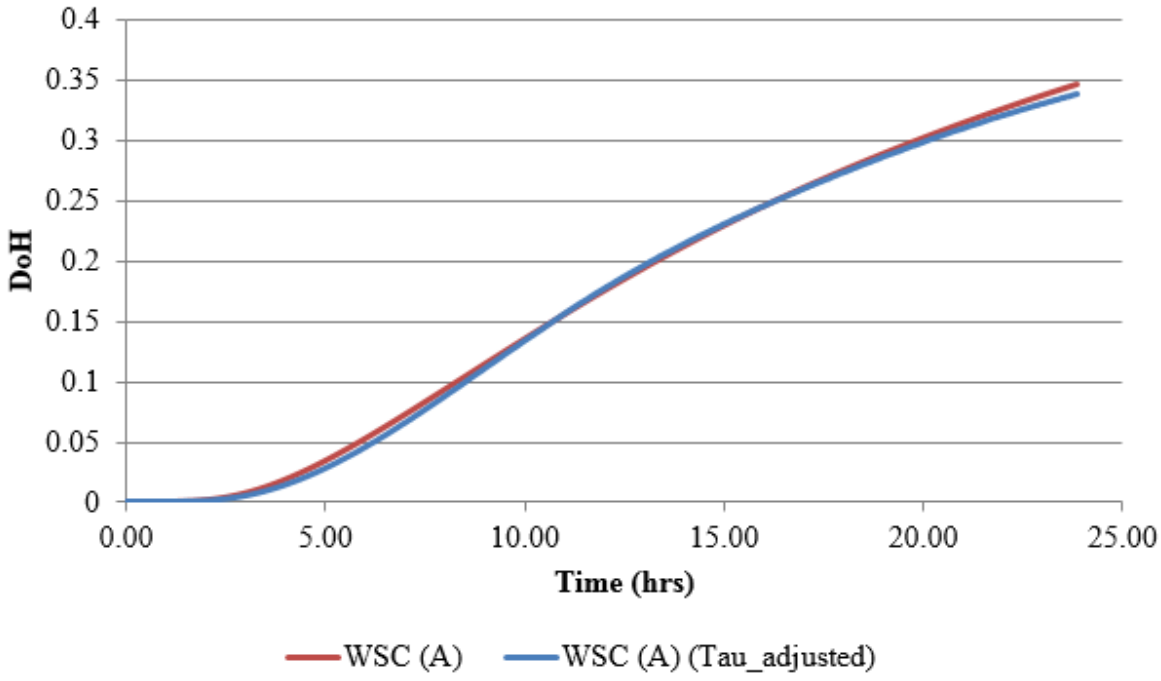

Figure 4.15. Effect of adjusted hydration time parameter on DoH for Class A OWC at a w/c ratio of 0.46.

From Figure 4.15, it can be concluded that varying τ as a function of temperature does not significantly affect the DoH prediction for Class A OWC slurry at a w/c ratio of 0.46 and 0% $CaCl_2$.

4.2.2 SGS evaluation using DoH

Similar to Section 4.1, the following section provides further evaluation of standard SGS criteria in defining the TT, and, in turn, the potential for gas migration. However, this section relates SGS test results to WSC test results by using the concept of DoH in lieu of equivalent age. Figure 4.16 presents pressure data, obtained from WSC testing using a Class A OWC and a w/c

ratio of 0.46 and 0% $CaCl_2$, as a function of DoH. Additionally, given the constant temperature profile of hydrating cement slurry during SGS testing hydration parameters established experimentally, SGS results were also plotted as a function of DoH. From this plot, the standard SGS criteria (100lb/100ft^2 and 500lb/100ft^2) were seen to correspond with DoH values of 0.000079 and 0.0027, respectively. These corresponding DoH values are indicated in Figure 4.16 to evaluate the adequacy of SGS in accurately characterizing gas migration potential. From Figure 4.16, it can be concluded that the standard SGS criteria do not accurately define the TT, as the initiation of pressure reduction does not occur this early in the hydration process. These results verify the results and conclusions presented in Section 4.1.

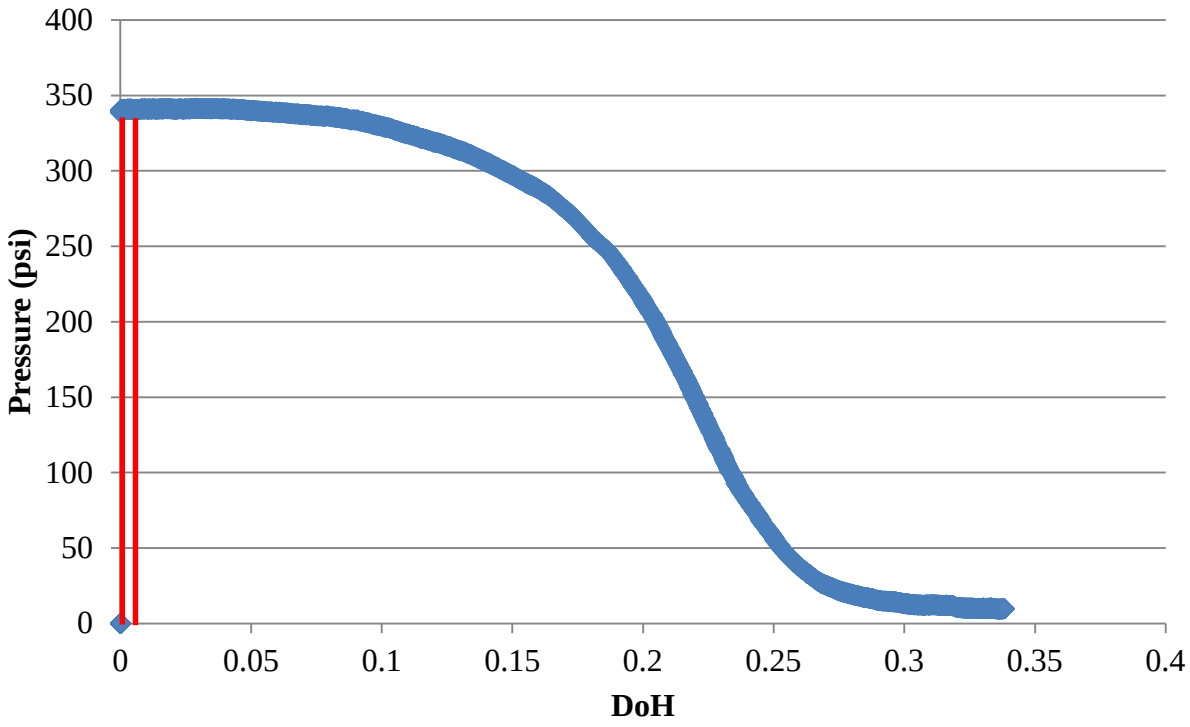

Figure 4.16. SGS criteria evaluation using DoH.

4.2.3 Experimental vs. empirical

The following section presents results of DoH as a function of time, with a focus on comparing the DoH prediction using model parameters established from isothermal calorimetry data with those established using the empirical relationships developed by Poole. Although an evaluation of the inference space used in Poole's hydration parameter development is provided in Section 2.4.1, this section explicitly illustrates how the hydration parameters (Equations (2.18), (2.19), and (2.20)) and activation energy expressions developed by Poole (Equation (2.21)) are not as accurate when predicting hydration development for the Class A OWC analyzed.

Figures 4.17, 4.18, 4.19, and 4.20 present a comparison of results between the DoH determined using the empirical estimation of the parameters in the hydration model and those established using isothermal calorimetry test results for each of the four temperatures considered in the isothermal calorimetry testing. As seen from the legend keys in these figures, a dashed line represents the predicted DoH using the hydration parameters predicted using the empirical relationships developed by Poole (Equations (2.18), (2.19), and (2.20)). A solid line indicates measured DoH data obtained by using experimentally determined hydration parameters from isothermal calorimetry results established based on (see Section 4.2.1.4). As seen from the general form of the hydration model, DoH prediction is a function of equivalent age, which requires discrete measurements of the curing temperature and an appropriate value for activation energy. Therefore, in order to properly compare the DoH prediction using empirical hydration parameters and experimental hydration parameters (from isothermal calorimetry data), each respective isothermal calorimeter test temperature (i.e. 8, 23, 38, and 60°C) was assumed to be the curing temperature necessary for the equivalent age calculation. It should be noted that the

reference temperature required for the equivalent age calculation is still assumed to be 22.8°C, which is consistent throughout the work. In addition to curing temperature, activation energy is required for establishing the equivalent age. To remain consistent (while comparing DoH using the Poole equations to that using the experimental results), the activation energy model (Equation (2.21)) developed by Poole using a non-linear regression analysis was used for predicting DoH with empirical hydration parameters. Experimental activation energy, as determined in Section 2.4.1.1, was used for predicting DoH with experimentally established hydration parameters.

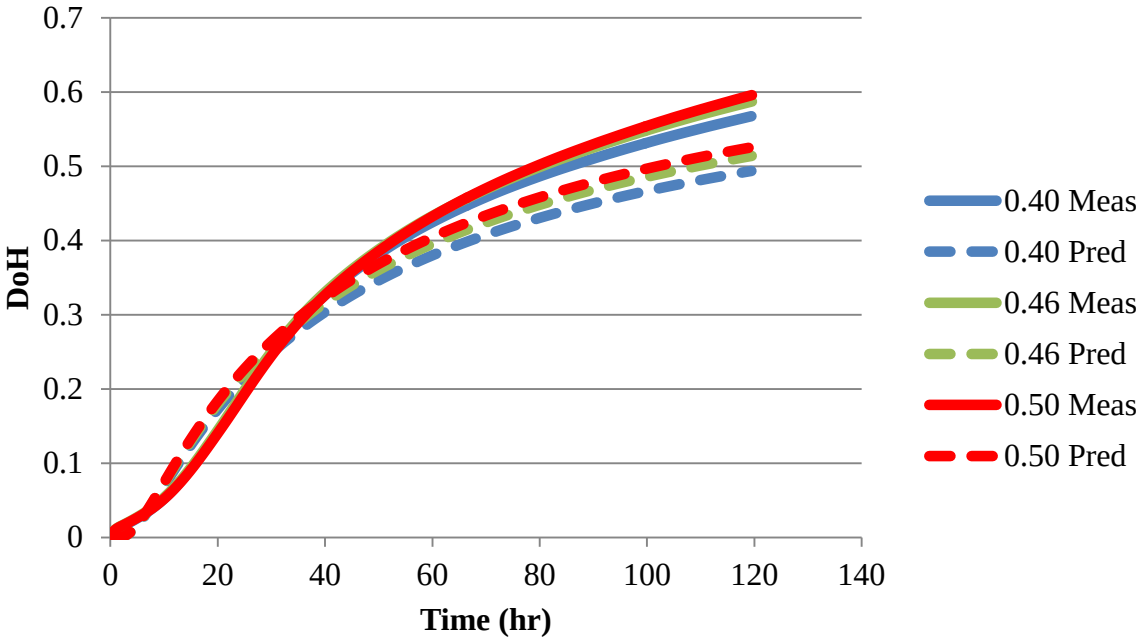

Figure 4.17. DoH vs. time (8°C - Shift).

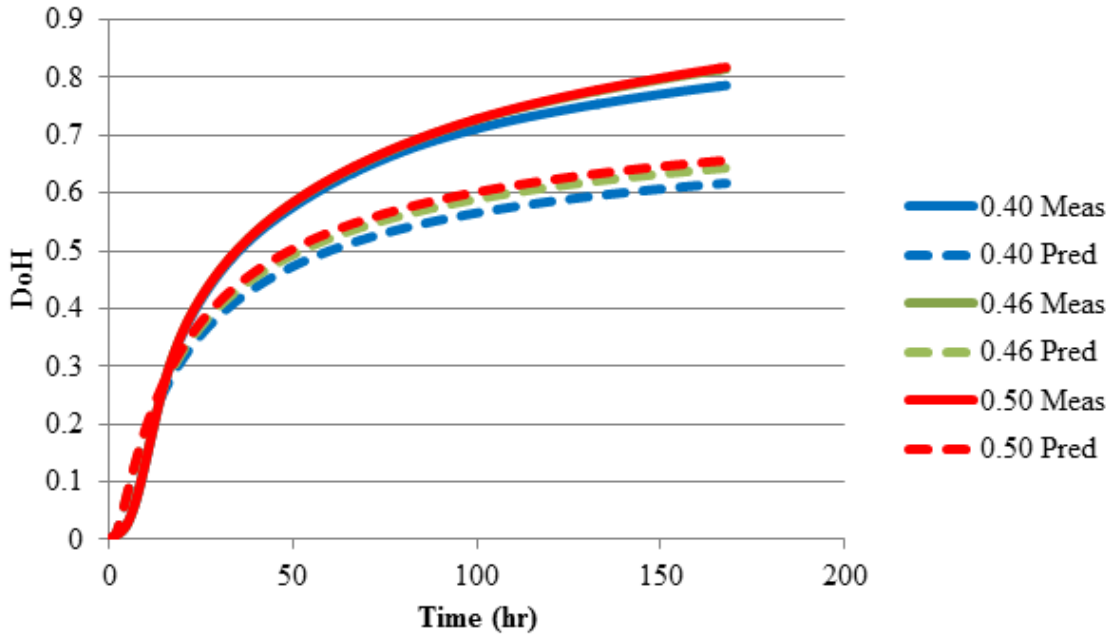

Figure 4.18. DoH vs. time (23°C).

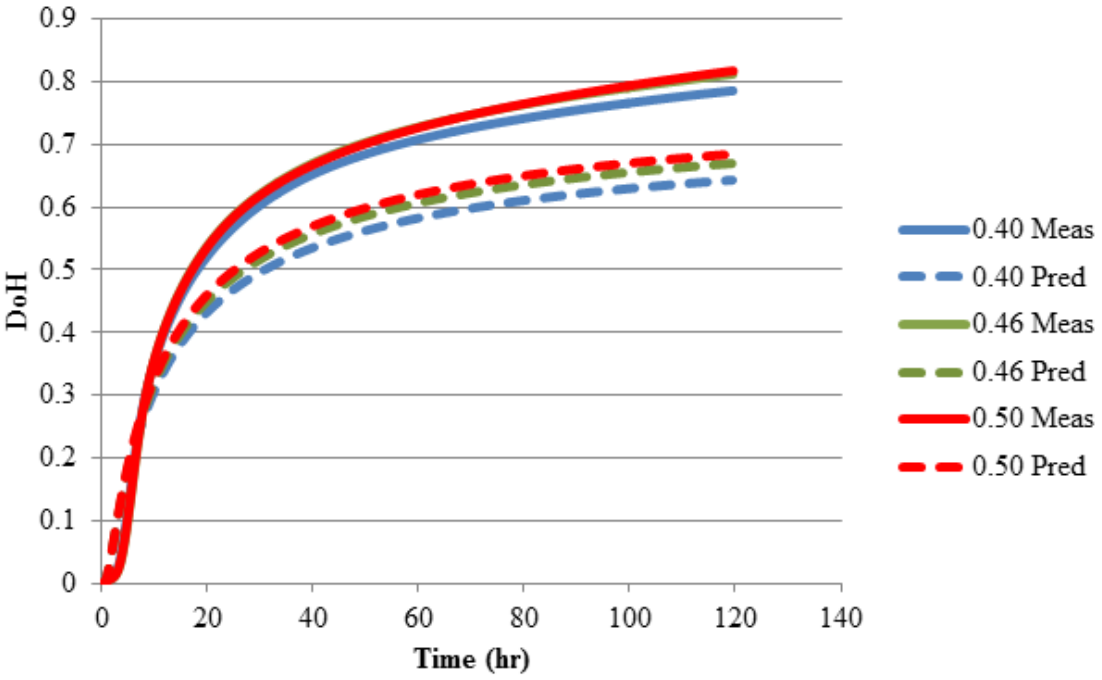

Figure 4.19. DoH vs. time (38°C).

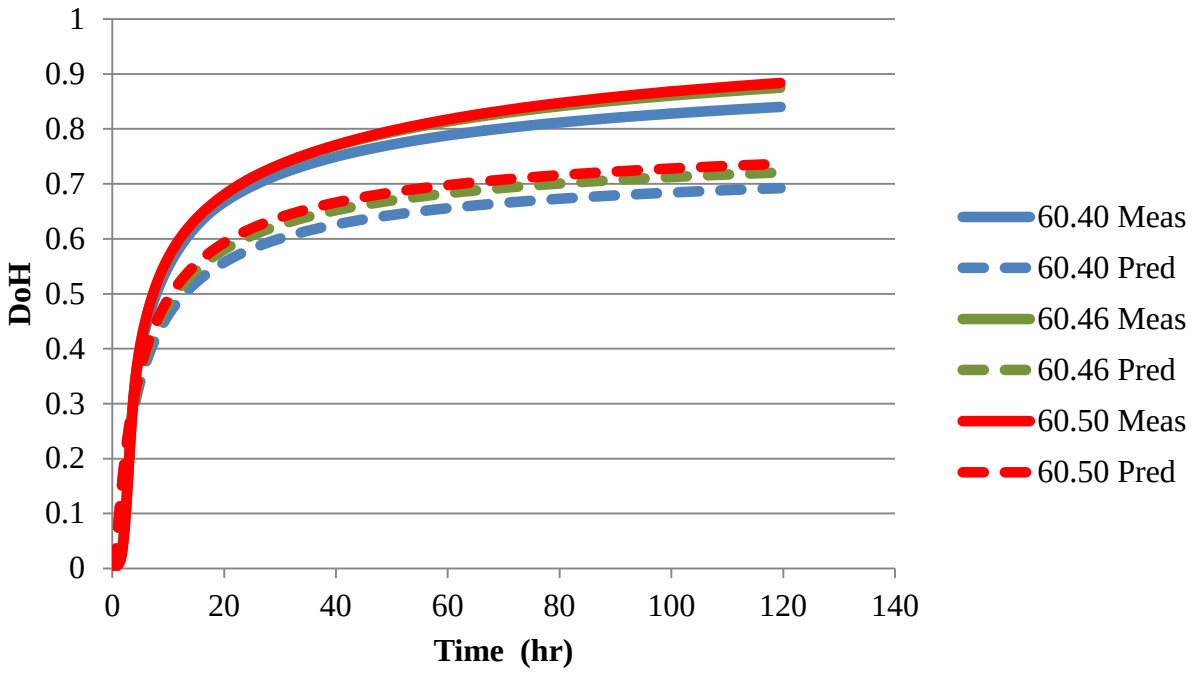

Figure 4.20. DoH vs. time (60°C).

As stated previously, the results presented in Figures 4.17, 4.18, 4.19, and 4.20 confirm that the exponential hydration prediction model presented by Poole is inadequate in accurately predicting the hydration development for the Class A OWC included in this study. In addition to the large difference at later ages (>24 hours), where the hydration prediction model is seen to underestimate the actual hydration development, a smaller, less noticeable difference exists at early ages (<24 hours), where the model overestimates hydration development as compared to experimental results. These differences between empirical and experimental hydration data are consistent for all temperatures. This difference suggests that the parameter relationships developed by Poole (as a function of cement chemistry and mixture characteristics) are only applicable to the specific cement types listed in the inference space (Table 2.8) and cement types deemed to have a similar composition.

4.2.4 WSC test results

DoH is introduced to characterize the process of cement hydration. By analyzing the temperature history of hydrating cement, the evolution of cement hydration may be characterized using the concept of DoH for slurry designs cured at different hydration rates. The following section attempts to relate pressure data obtained from successful WSC tests with predicted DoH for different levels of w/c ratio, curing temperature, and $CaCl_2$ dosage. The goal of this section is to investigate the WSC pressure data for trends with hydration development and to evaluate the feasibility of relating bulk material properties (i.e. hydrostatic pressure drop) to fundamental material properties (i.e. DoH, capillary porosity, etc.). It should be noted that a limited number of WSC tests were successfully completed, which is why minimal results are presented and compared in this section.

4.2.4.1 W/c ratio

To obtain results illustrated in Figure 4.21 and Figure 4.22, Class A OWC was blended at two different w/c ratios (0.4 and 0.46) without the addition of $CaCl_2$ accelerator to evaluate the effects of w/c ratio on pressure reduction. Cement slurries were prepared and then tested in the WSC at approximately 22.8ºC. An overburden pressure of 350 psi was applied throughout the duration of the tests, which corresponds to a simulated depth of approximately 430 feet. Only low permeability formations that do not allow gas invasion into the cement slurry were used in this study because the analysis focuses on hydrostatic pressure reduction, and not the occurrence of gas invasion or migration. Therefore, the saturated formations used for testing simulate a sealed condition, where fluid loss does not occur. It should also be noted that the pressure data

reported in this section refers to the “slurry pore pressure” sensor, which is located midway along the vertical depth and radial direction of the annulus. The legend keys in Figure 4.21 and Figure 4.22 are defined as follows: (cement type, w/c ratio, dosage of $CaCl_2$, pressure level).

Before the pressure data is reported in terms of predicted DoH, Figure 4.21 illustrates a comparison of pressure over time between Class A OWC at two different w/c ratios. As seen from this figure, the initiation of pressure drop occurs earlier as the w/c ratio decreases. It may be concluded that the w/c ratio affects the microstructural development (or percolation) of the cement matrix, and therefore, the evolution of slurry pore pressure. For example, when the w/c ratio is relatively high, the cement particles are suspended in more water and have little contact with surrounding particles. As the distance between particles increases (i.e. increase in w/c), the interactions between particles decreases and highly fluid behavior is observed. Therefore, a relatively high w/c ratio mixture design needs to achieve a higher DoH to fill the larger amount of void space between cement particles and develop a similar microstructure or level of connectivity, as compared to that of a lower w/c ratio mixture design. This effect is shown in the schematic provided in Figure 2.4.

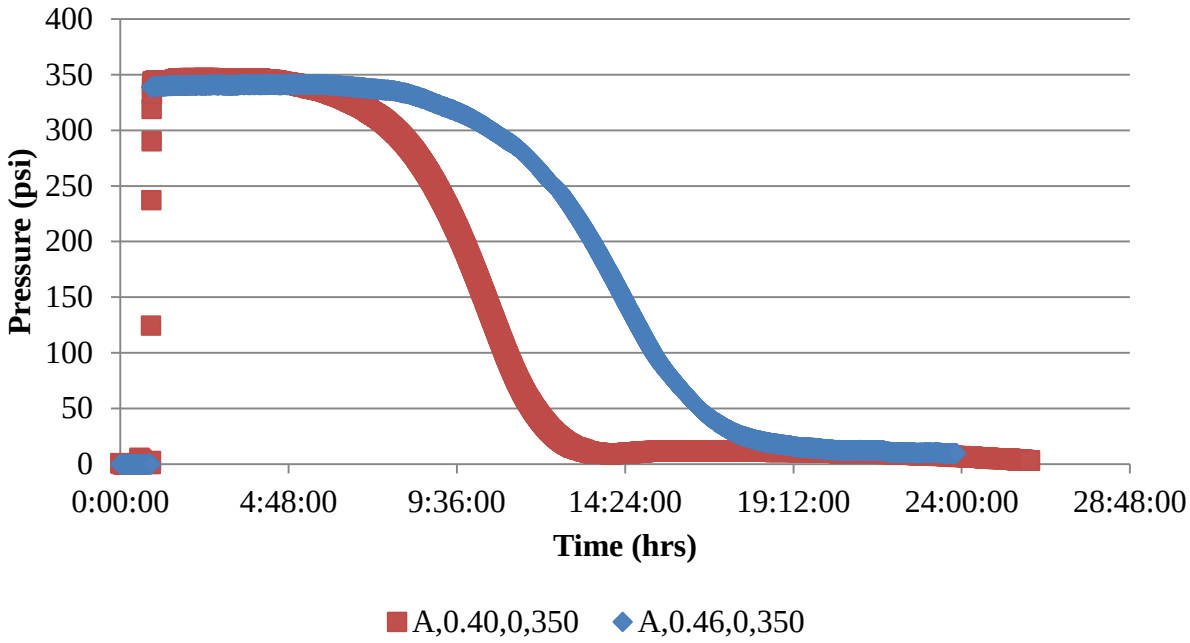

Figure 4.21. Pressure vs. time: different w/c ratios.

As discussed in Section 2.1.4, DoH is a fundamental property that can be used to characterize the hydration and microstructural development of a given cement. To predict the DoH of the in-situ cementitious slurry, the temperature profile obtained from thermocouples is required. Due to the specified mixing protocol, sample conditioning, and equipment configuration involved in WSC testing, a given cementitious slurry must be transferred from a blender to a pre-conditioning mixer to the annulus of the formation specimen within the WSC before overburden pressure may be applied and data acquisition begins. Due to this pre-testing process of sample transfer, multiple thermocouples are required, assumptions must be made, and temperature data is combined to generate reliable results. For example, the first minute of temperature data is extracted from the thermocouple placed on the blender. Then, the following 20 minutes of temperature data is collected using the thermocouple placed on the pre-

conditioning mixing bowl. The next reliable temperature data point occurs 50 minutes after mixing, which is the approximate time between mixing of the cement slurry and placement for encasing a surface casing string. Therefore, reliable temperature data is not available from the time the cementitious slurry is removed from the pre-conditioning mixing bowl (21 minutes) until the thermocouple located inside the WSC is connected (typically 50 minutes). In order to obtain a representative temperature profile, temperature data during this unknown time period is estimated via linear interpolation. The final temperature data point recorded from the pre-conditioning mixing bowl thermocouple and the first reliable temperature data point recorded from the WSC thermocouple are required. This unknown temperature data is generated using linear interpolation between these two temperatures.

From this combined set of temperature data, the exponential hydration prediction model (Equation (2.14)) is used to incrementally estimate the development of hydration. In order to do this, all required model parameters (i.e. hydration parameters, activation energy) must be determined. Due to the inadequacy of the hydration parameter relationships developed by Poole (Equations (2.18), (2.19), and (2.20)) for use with Class A OWC, as explained in Section 4.2.1, the three hydration parameters ($\alpha_{ult}, \tau, \beta$) are determined from fitting the exponential hydration prediction model to isothermal calorimetry results at the nearest testing temperature (23°C in this case). It should be noted that, unlike isothermal calorimetry testing, the temperature profile of the cementitious slurry in the WSC fluctuates as hydration proceeds. However, the minimum, maximum, and average cement curing temperatures are 20.9°C, 24.3°C, and 21.8°C for the cement slurry with a w/c ratio of 0.40 and 20.6°C, 24.7°C, and 22.6°C for cement slurry with a w/c ratio of 0.46. Therefore, it was assumed that the temperature profile was sufficiently close to

the isothermal calorimeter testing temperature to allow for the use of the fitted hydration parameters at 23°C.

Additionally, the exponential hydration prediction model is a function of equivalent age, which requires knowledge of the activation energy of the cementitious materials being hydrated (as seen in Equation (2.11)). Unlike Section 4.1, where the activation energy model developed by Poole was considered, the modified ASTM C1074 graphical method (described in Section 2.4.1.1) was utilized to obtain the most accurate value for the Class A OWC being considered. Once all required inputs for the exponential hydration prediction model were determined, the DoH of the cementitious slurry within the WSC is estimated. Figure 4.22 presents pressure data as a function of the predicted hydration development from the measured temperature profiles for different hydrating cementitious slurries.

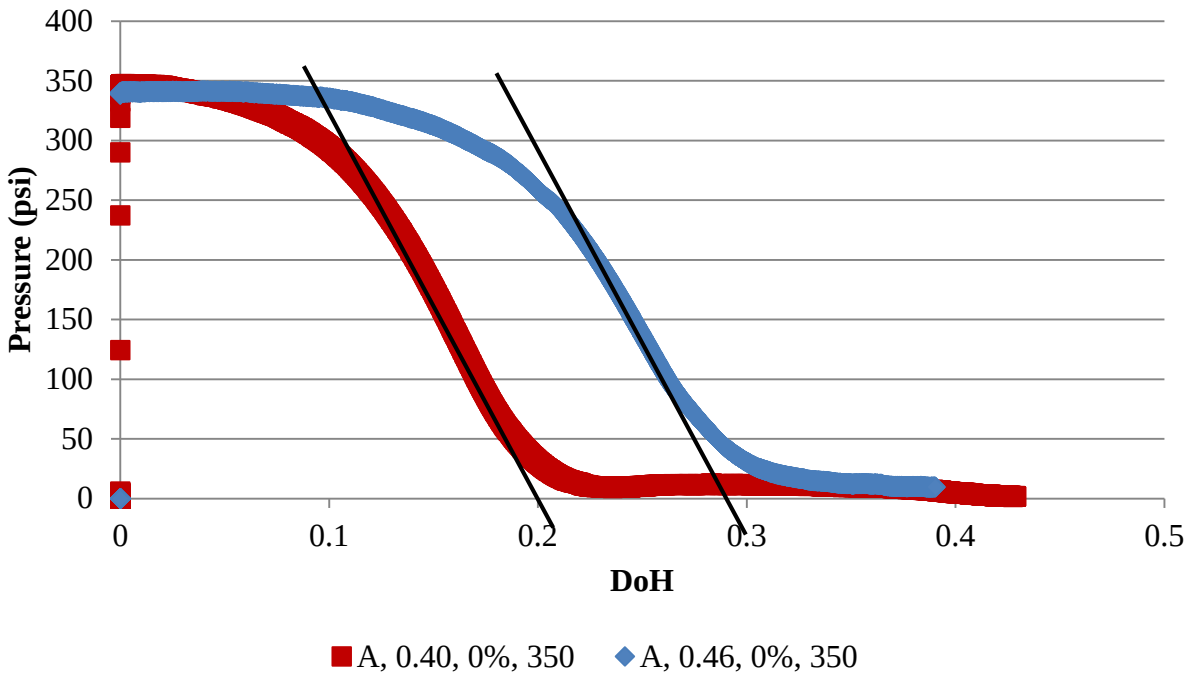

Figure 4.22. Pressure vs. DoH: different w/c ratios.

As seen from Figure 4.22, both pressure curves are very similar in shape (i.e. similar rates of pressure reduction) with the primary difference being the initiation of hydrostatic pressure drop. For a given mixture design, the effects of certain borehole conditions (i.e. temperature) can be distinguished by employing DoH to describe the cement hydration better than SGS. Similar to the pressure evolution results in terms of time, as provided in Figure 4.21, a relatively low w/c mixture design will experience pressure reduction at a lower DoH, as compared to a higher w/c mixture design. This observation is logical, in that, at a given DoH, a cementitious mixture with a lower w/c ratio will exhibit more connectivity (percolation) of hydration products than that for a greater w/c because less void space exists between cement particles. It is important to understand this observation, as it may be concluded that DoH alone is insufficient in characterizing the effects of mixture design (i.e. w/c, cement type and composition, fineness, etc.) on pressure evolution. This limitation of DoH characterization is the primary reason behind the impetus to couple DoH development with an additional material property that may normalize the pressure evolution over time of different cementitious mixture designs.

4.2.4.2 Curing temperature

In addition to investigating the ability of DoH to characterize cement hydration and hydrostatic pressure reduction between Class A OWC at different w/c ratios, WSC tests performed at different temperatures are also considered. Before the WSC pressure data is reported in terms of predicted DoH, Figure 4.23 illustrates a comparison of pressure results in terms of time between Class A OWC at two different curing temperatures. As seen from this figure, both the initiation and rate of pressure drop varies between the two temperature conditions. This result is expected, as an increase in curing temperature results in an increased rate of hydration.

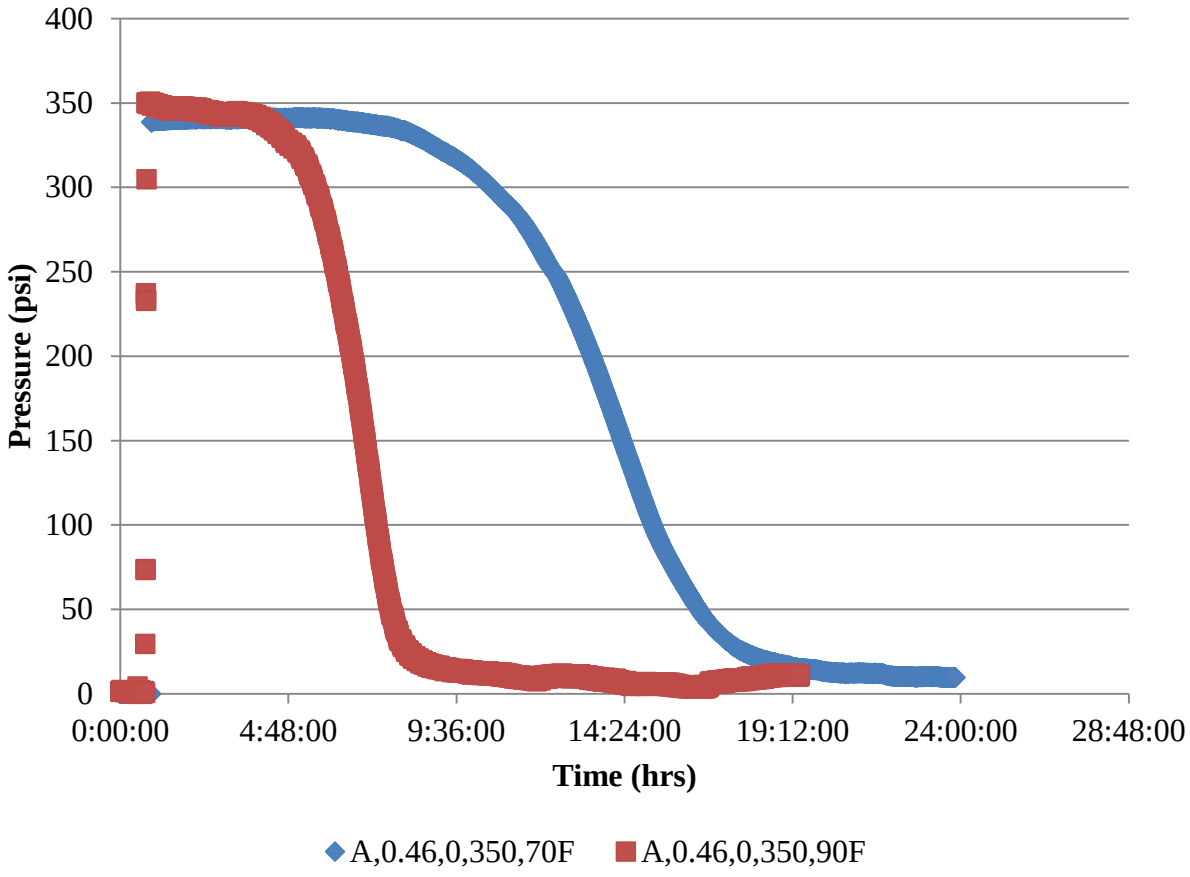

Figure 4.23. Pressure vs. time: different curing temperatures.

Similar to Figure 4.22, the exponential hydration prediction model (Equation (2.14)) is used to incrementally estimate the development of hydration. Figure 4.24 presents WSC test results as a function of predicted DoH for cements curing at different temperatures. From this figure, the hydrostatic pressure reduction between the two temperatures is improved; however, a slight difference exists between the curves. This difference may be attributed to the fitted hydration parameters used for the DoH prediction for Class A OWC at 32.2°C, in that, isothermal calorimetry testing was conducted at approximately 37.8°C. Therefore, the hydration

parameters obtained from the isothermal calorimetry results do not directly correspond with the WSC test conditions. However, it may be concluded that DoH is effective in characterizing hydrostatic pressure reduction for Class A OWC used for WSC pressure testing at different curing temperatures.

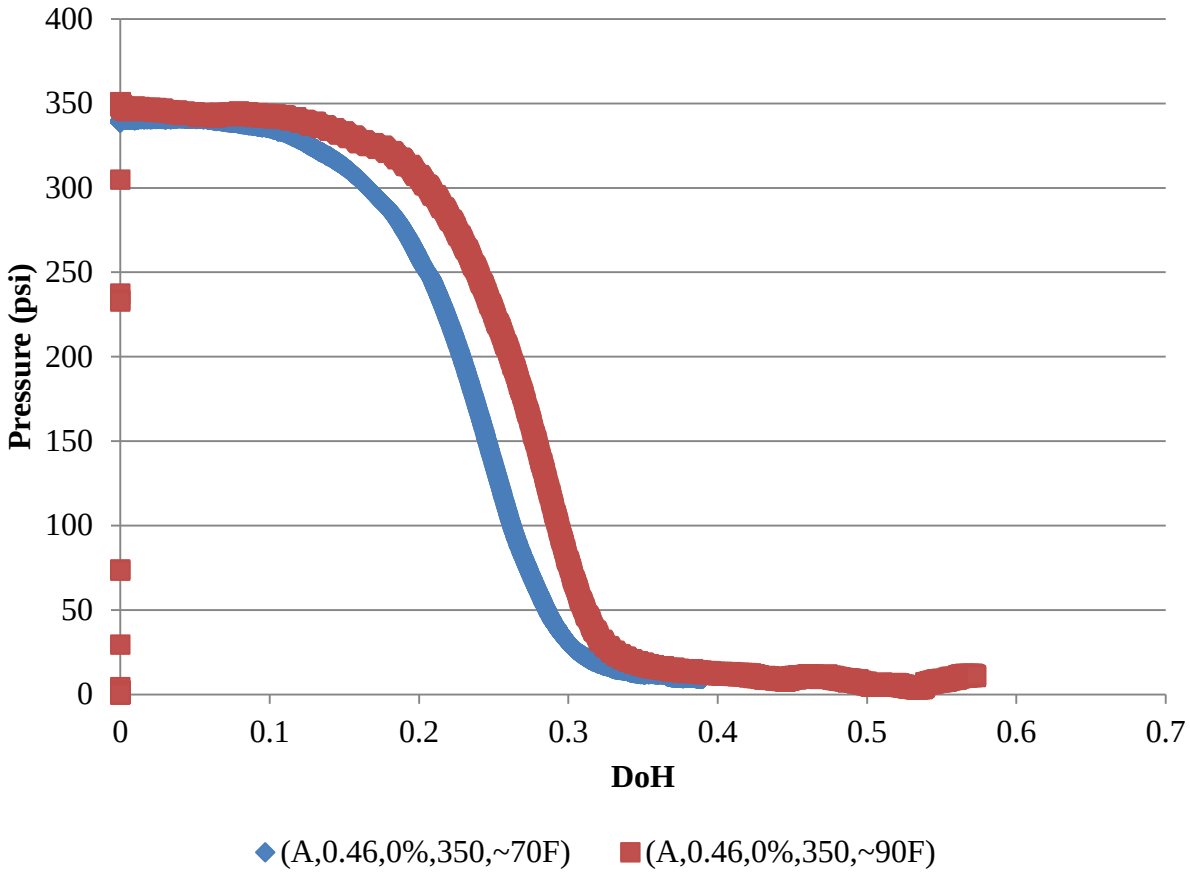

Figure 4.24. Pressure vs. DoH: different curing temperatures.

4.2.4.3 $CaCl_2$ admixture

In addition to investigating the ability of DoH to characterize cement hydration and hydrostatic pressure reduction between Class A OWC at different curing temperatures, WSC tests performed

at different $CaCl_2$ dosages are also considered. Before the WSC pressure data is reported in terms of predicted DoH, Figure 4.25 illustrates a comparison of pressure results in terms of time between Class A OWC at two different curing temperatures. As seen from this figure, both the initiation and rate of pressure drop varies between the different $CaCl_2$ dosage levels. This result is expected, as an increase in $CaCl_2$ dosage results in an increased rate of hydration.

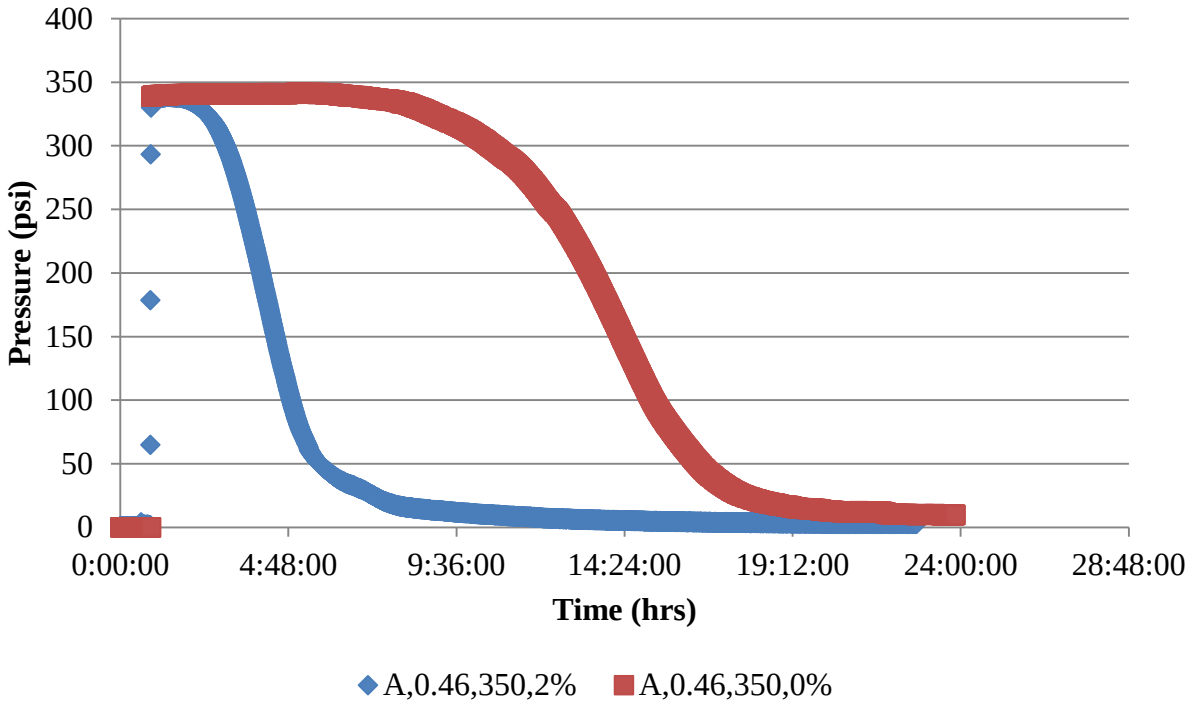

Figure 4.25. Pressure vs. time: different $CaCl_2$ dosage levels.

Similar to Figure 4.22 and Figure 4.24, the exponential hydration prediction model (Equation (2.14)) is used to incrementally estimate the development of hydration. As seen in Table 4.2 and Table 4.3, isothermal calorimetry testing was not conducted for a Class A OWC slurry with a w/c ratio of 0.46 and 2% $CaCl_2$. Therefore, in order to obtain the hydration

parameters necessary for predicting DoH, a linear regression analysis was performed on the available established hydration parameters from isothermal calorimetry testing performed at 23°C. From this analysis, regression equations as a function of $CaCl_2$ dosage and w/c ratio were developed (Equations (4.2), (4.3), and (4.4)). These regression equations have an R^2 of 0.90, 0.93, and 0.99, respectively.

$$\alpha_u = 0.358 + 0.03670 * CaCl_2 + 1.093 * w/c \quad (4.2)$$

$$\tau = 8.69 - 3.73 * CaCl_2 + 26 * w/c \quad (4.3)$$

$$\beta = 0.9624 - 0.09221 * CaCl_2 - 0.36 * w/c \quad (4.4)$$

Using these regression equations, hydration parameters for Class A OWC slurry with a w/c ratio of 0.46 and 2% $CaCl_2$ are established. Table 4.4 presents the complete list of hydration parameters established from isothermal calorimetry testing, including the hydration parameters established using the regression equations.

Table 4.4. Hydration parameters for Class A OWC with a w/c ratio of 0.46 and 2% $CaCl_2$.

Temp, °C			8	23	38	60
Temp, K			281.15	296.15	311.15	333.15
$CaCl_2$ = 0%	w/c=.40	α_u	0.7597	0.8213	0.7605	0.7862
		τ	37.61	19.89	9.286	4.343
		β	0.8119	0.8353	0.9109	0.8393
	w/c=.46	α_u	0.835	0.8768	0.7794	0.8277
		τ	41.6	21.46	9.522	4.531
		β	0.7575	0.7803	0.9411	0.7934
	w/c=.50	α_u	0.8771	0.8832	0.7919	0.8408
		τ	45.11	21.7	9.68	4.619
		β	0.74	0.7746	0.902	0.7702
$CaCl_2$ = 2%	w/c=.40	α_u	1.134	0.8252	0.7719	0.8157
		τ	38.58	9.259	4.881	2.59
		β	0.4725	0.6468	0.6882	0.5634
	w/c=.46	α_u	N/A	***0.93418***	N/A	N/A
		τ	N/A	***13.19***	N/A	N/A
		β	N/A	***0.61238***	N/A	N/A
	w/c=.50	α_u	0.9281	0.9635	0.7919	0.8568
		τ	26.02	12.01	9.68	2.917
		β	0.6387	0.6095	0.902	0.6092
$CaCl_2$ = 3%	w/c=.40	α_u	1.64	0.9114	0.7848	0.8307
		τ	82.96	8.811	4.153	2.374
		β	0.3563	0.5213	0.5924	0.4359
	w/c=.46	α_u	2.048	0.9867	0.8558	0.9176
		τ	143.6	10.52	4.675	2.78
		β	0.3103	0.5152	0.602	0.4328
	w/c=.50	α_u	1.421	1.033	0.8705	0.9276
		τ	57.94	11.7	5.017	2.884
		β	0.4183	0.5158	0.6174	0.4498

Figure 4.26 presents WSC test results as a function of predicted DoH for different levels of $CaCl_2$ dosage. From this figure, the hydrostatic pressure reduction between the two admixture

dosage levels is improved. Both pressure curves are very similar in shape (i.e. similar rates of pressure reduction) with the primary difference being the initiation of hydrostatic pressure drop. Hydrostatic pressure reduction initiation occurs at a lower DoH for a Class A OWC slurry with 2% $CaCl_2$ as compared to a neat slurry. It may be concluded that DoH is ineffective in characterizing hydrostatic pressure reduction for Class A OWC used for WSC pressure testing at different $CaCl_2$ dosage levels.

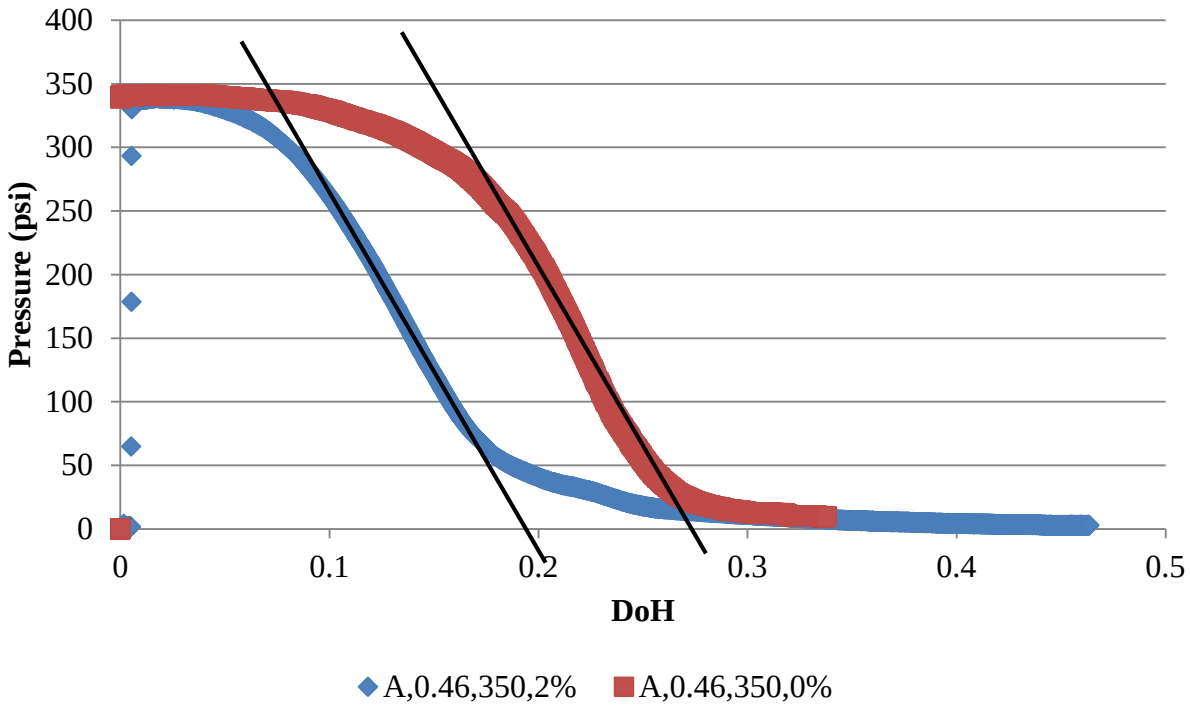

Figure 4.26. Pressure vs. DoH: different $CaCl_2$ dosage levels.

4.3 CAPILLARY POROSITY

As stated previously, one of the primary objectives of this study is to use fundamental properties of cement hydration to characterize the bulk property (specifically hydrostatic pressure reduction) of cement slurries within a given borehole. As seen from the results presented in Section 4.2.4, comparisons between the performances of cementitious mixtures (defined by the initiation and rate of hydrostatic pressure reduction) with different w/c ratios show that DoH is unable to normalize the pressure evolution. Therefore, the characterization of the evolution of volumetric fraction of solids (hydration products) and microstructural development should be introduced to broaden the applicability of this analysis approach to slurry designs with different w/c ratios. The following section attempts to relate hydrostatic pressure reduction with a different material property, namely, capillary porosity.

Capillary porosity is a function of DoH and initial w/c ratio and may be used to analyze the void volume of a given hydrating cement microstructure. More specifically, capillary porosity is defined as the ratio of capillary pore volume to original volume of the cement slurry, as given by the Equation (4.5) (Mindess et al. 2003). By using Equation (4.5) and the results presented in Figure 4.22, it is possible to obtain pressure evolution results in terms of capillary porosity, as seen in Figure 4.27.

$$P_c(\alpha) = \frac{V_c}{V_p} = \frac{w/c - 0.36 \cdot \alpha}{w/c + 0.32} \tag{4.5}$$

where, $P_c(\alpha)$ = capillary porosity at degree of hydration (α) ;

V_c= capillary pore volume;

V_p = original volume of cement slurry.

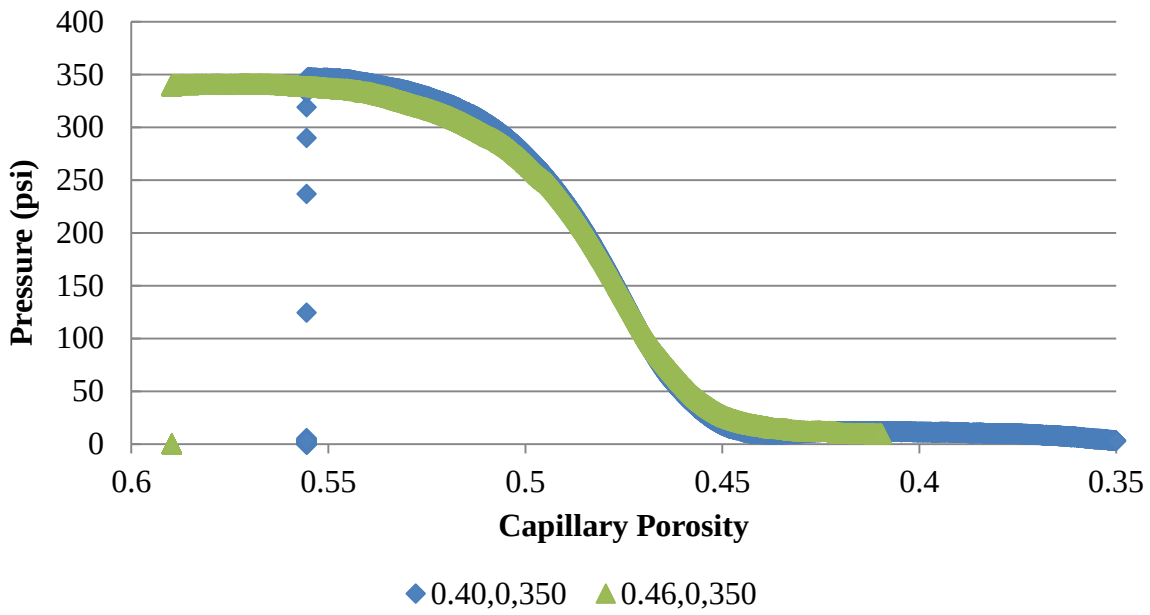

Figure 4.27. Pressure vs. capillary porosity: different w/c ratios.

As seen from Figure 4.27, the concept of capillary porosity is effective in normalizing the pressure evolution of cementitious mixtures with different w/c ratios. For example, at a given slurry pore pressure of 175 psi, the capillary porosity for each Class A OWC slurry tested (0.40 and 0.46 w/c ratio) is calculated as 48.1% and 48.0%, respectively. From this, it can be seen that the solid fraction (hydration products) in the cement matrix is nearly identical for an equivalent reduction in hydrostatic pressure between mixtures with the same cement but different w/c ratios. Therefore, it can be concluded that capillary porosity is capable of describing microstructural development and how it relates to the evolution of hydrostatic pressure reduction for cementitious mixtures of identical compositions with different w/c ratios.

4.3.1 Limitations of capillary porosity

Although Figure 4.27 illustrates the effectiveness of capillary porosity in normalizing the hydrostatic pressure reduction results to account for the effects of different w/c ratios, it is necessary to investigate the ability of this parameter to do so between various cement types with different cement chemistries and compositions. Therefore, additional WSC testing was conducted on different cement types to compare the hydrostatic pressure evolution as a function of capillary porosity. Figure 4.28 illustrates a comparison of WSC testing results between three different cement types. In addition to the previously reported WSC test results of Class A OWC (at w/c ratios 0.40 and 0.46), results for Type I and Type II/V cement types are also reported. It should be noted that capillary porosity is also unable to normalize hydrostatic pressure reduction results between different levels of $CaCl_2$ dosages because capillary porosity is a function of DoH, as seen from Equation (4.5). Table A.5.1 provides a comparison of the oxide analyses for these three cement types.

As discussed previously, Equation (4.5) requires an accurate DoH prediction for the given cement type used for WSC testing. As done for results generated in Section 4.2, DoH prediction for Class A OWC used fitted values from isothermal calorimetry data for the hydration parameters, as explained in section 4.2.1, and the experimentally determined activation energy, as explained in Section 2.4.1.1. As for DoH prediction for Type I cement, the hydration parameter relationships (Equations (2.18), (2.19), and (2.20)) and activation energy prediction model (Equation (2.21)) developed by Poole were used. These relationships were deemed appropriate because of the similarity between the Type I cement composition used for WSC testing and the composition of the cement types used for their development, as shown in the

inference space defined in Table 2.8. Finally, the DoH prediction for the Type II/V cement also used the hydration parameter relationships and activation energy prediction model developed by Poole. Isothermal calorimetry testing was not conducted on this cement type; therefore, the exponential hydration model (Equation (2.14)) could not be fit to heat evolution data to obtain representative values for the hydration parameters necessary for an accurate DoH prediction. Instead, the hydration parameter relationships and activation energy prediction model developed by Poole were used with the Type II/V cement composition, as seen in Table A.5.1. It should be noted that the DoH prediction for Type II/V cement, and in turn, capillary porosity results, are not as reliable because Type II/V cement is further outside the inference space given in Table 2.8.

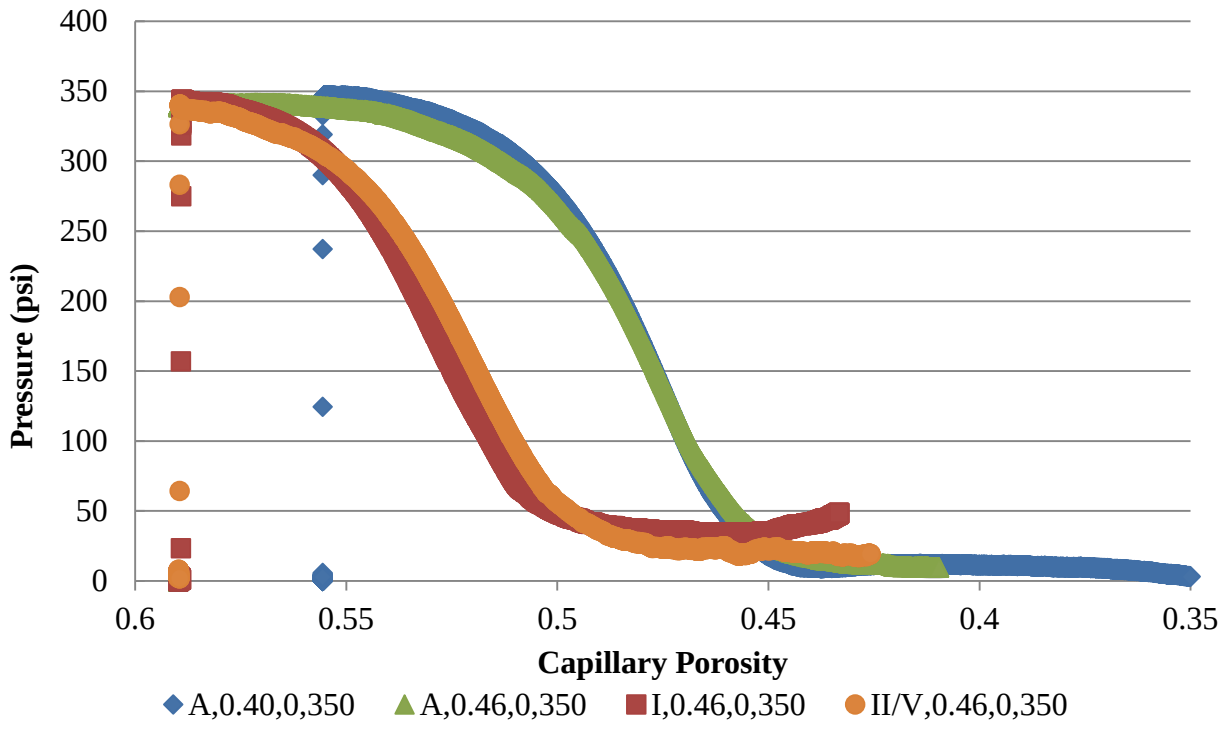

Figure 4.28. Pressure vs. capillary porosity: different cement types.

As seen from Figure 4.28, the capillary porosity parameter, as calculated from Equation (4.5), is unable to effectively normalize the hydrostatic pressure reduction results between the three cement types tested. When analyzing the results further, it is observed that both the Type I and Type II/V cements initiate hydrostatic pressure reduction at a larger value of capillary porosity than the Class A OWC. Therefore, the initiation of hydrostatic pressure reduction is not simply a function of the volumetric fraction of solids (hydration products), as indicated by the capillary porosity parameter. However, due to the effectiveness of the capillary porosity parameter in normalizing the WSC pressure results between cements of identical composition (i.e. Class A OWC at different w/c ratios), as presented in Figure 4.27, a relationship between hydrostatic pressure reduction and the formation of hydration products or microstructural development must exist. Therefore, it is suggested that hydrostatic pressure reduction may be related to the *type* of hydration products formed, in addition to the *amount* or fraction of solids (hydration products) formed, as described with the capillary porosity parameter.

To evaluate this assertion, a comparison of the type of hydration products formed between the three cement types tested is required. When comparing the compositions of all three cement types tested (Table A.5.1), an interesting difference can be identified. The C_3A content varies between all three cement types, with Type I cement having the largest percentage of C_3A content, followed by Type II/V cement and Class A OWC in decreasing order. From this observation, it is suggested that the hydration reaction of C_3A (Equation (2.3)), which involves the formation of ettringite as a primary hydration product, is influential in the evolution of hydrostatic pressure reduction. As seen from Table 2.4, ettringite has significantly different properties and characteristics as compared to the primary hydration products of CSH and CH. Although the hydrostatic pressure reduction of Type II/V cement, presented in Figure 4.28, does

not necessarily exhibit an expected trend of initiation between that of Type I cement and Class A OWC, as may be suggested based on the relative C_3A content, additional research should be conducted to further investigate the relationship between hydrostatic pressure reduction and *type* of hydration products formed.

4.4 HYDRATION PRODUCTS

As stated in the previous section, capillary porosity (Equation (4.5)) is unable to accurately characterize hydrostatic pressure reduction between different cement types. Therefore, instead of focusing on total hydration products formed, the composition or proportioning of individual hydration products (i.e. CSH, ettringite, etc.) is examined. Section 2.4.2 presents a brief overview of the technical basis and capabilities of VCCTL. The following sections present results obtained from VCCTL simulations of cements with similar compositions to those used for WSC pressure testing.

4.4.1 Validation of VCCTL results

Before VCCTL simulations are performed and used to predict individual hydration product development of cement used for WSC tests, the compositions of available VCCTL cements must be evaluated. After evaluating the VCCTL cement compositions, selections are made based on similarity to the compositions of the cement used in WSC tests. As discussed in Section 2.4.2, VCCTL contains a database of standard cement types (CCRL). It should be noted that the

amount of material property information varies significantly between VCCTL cements included in the CCRL. Using the Bogue equations and available (limited) oxide analysis data, composition of all database cement types were investigated. A detailed summary and comparison of all cement compositions is provided in Appendix A.

Unfortunately, with the limited amount of oxide analysis data in the CCRL, a VCCTL cement with a similar composition to the Class A OWC used for this study was not found. Therefore, isothermal calorimetry test results cannot be used to verify VCCTL simulation results because Class A OWC was the only cement type tested. Instead, a VCCTL cement with a similar composition to Type I cement was found and used to evaluate the accuracy and reliability of simulation results. To do this, many VCCTL simulations were performed in an attempt to replicate the exact conditions of the WSC testing for the Type I cement (i.e. semi-adiabatic thermal conditions, sealed moisture condition, etc.). Figure 4.29 presents the various VCCTL simulations performed attempting to replicate the DoH prediction for the Type I cement used in the WSC testing.

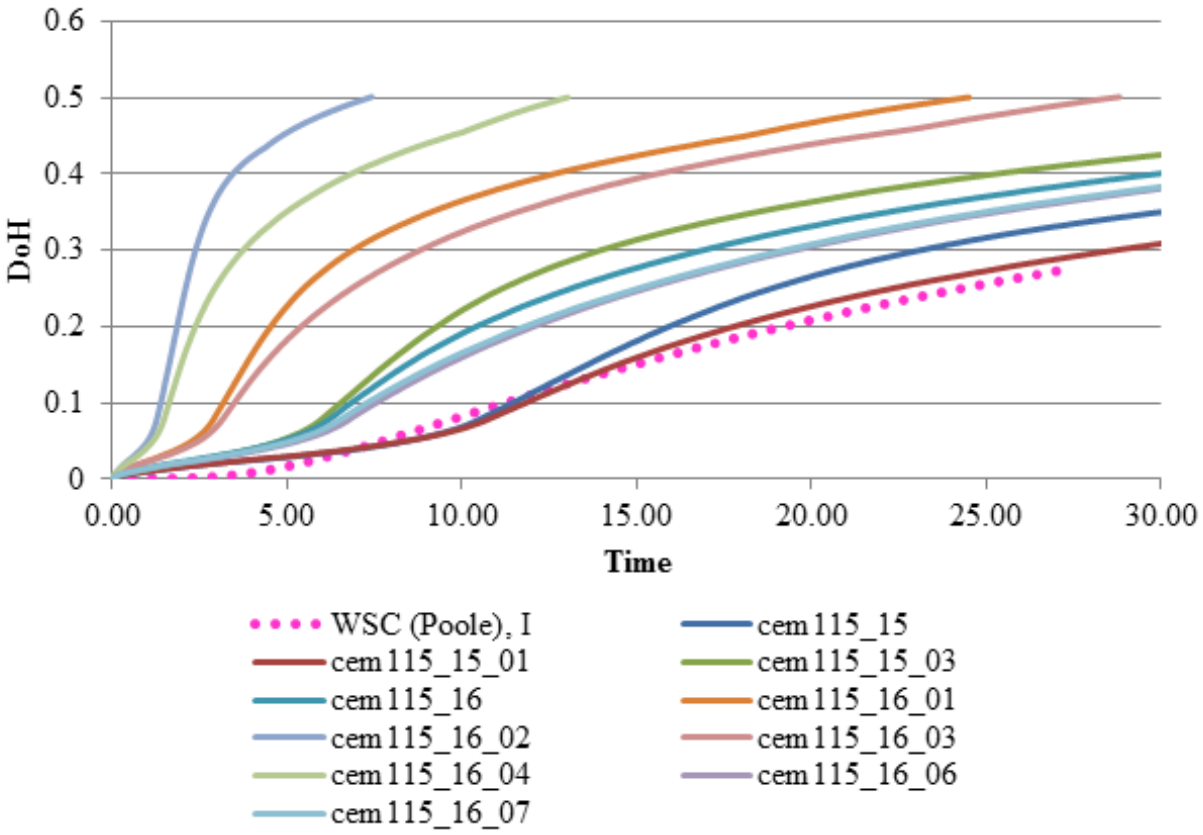

Figure 4.29. Various VCCTL simulations compared with DoH prediction of Type I cement.

From these results, an adequate fit or replication of the DoH prediction for the Type I cement was not achieved. A number of factors and reasons could be attributed to these observed differences in the DoH prediction. For example, as stated previously, VCCTL cement types do not have identical composition to that of the Type I cement used in WSC testing. Additionally, without any isothermal calorimetry test data, the cycle conversion factor used to establish aging conditions was varied. Ideally, it would be best to modify the available VCCTL cement data files to replicate the composition and characteristics of the cement used for WSC testing. However, without detailed particle size distribution (PSD) data, modifying or creating a new cement data file is not possible.

4.4.2 Example of material property results

Although VCCTL simulation results could not be verified with experimental data, Figure 4.30 presents an example of various volume fractions of individual hydration products formed for VCCTL cem115. These results are plotted as a function of DoH. The vertical line in the figure indicates the initiation of hydrostatic pressure reduction observed for Type I cement used for WSC tests. Ideally, if VCCTL results can be verified, simulations can be performed on similar database cements. From these results, the proportioning of individual hydration products can be analyzed and compared between cement types. If a significant difference in individual hydration product formation exists between cement types, the previous suggestion that the *type* of hydration products influence microstructural development may be further evaluated.

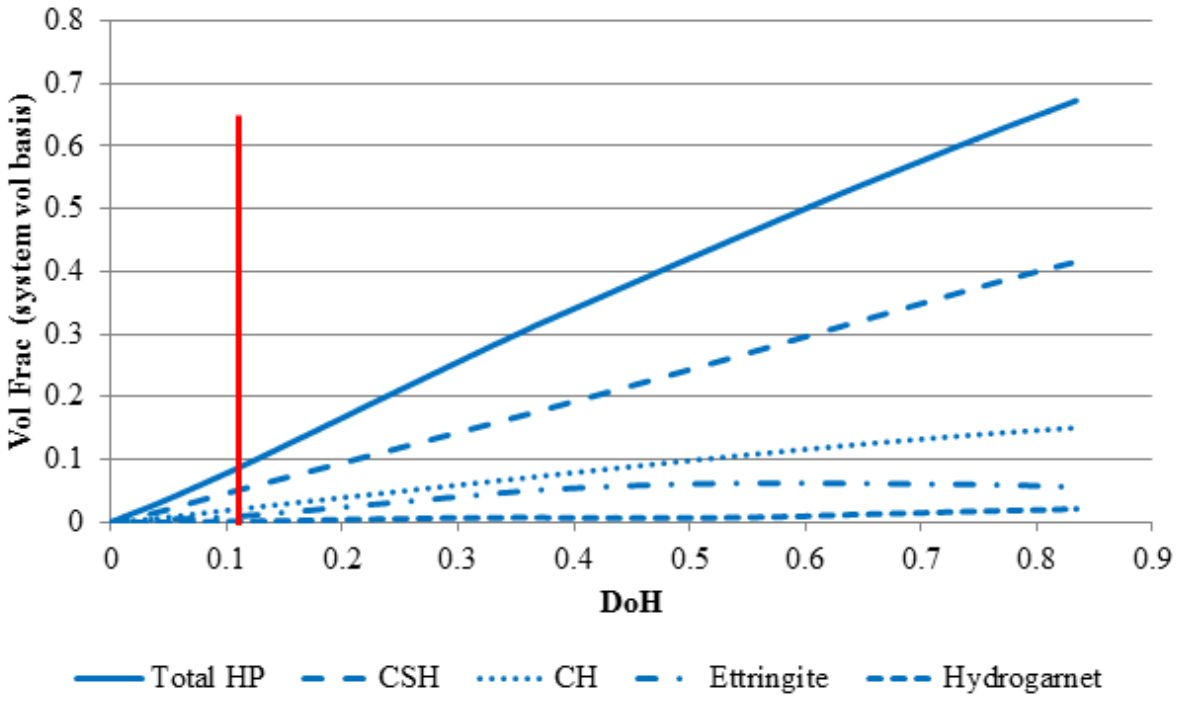

Figure 4.30. Example VCCTL results for similar Type I cement.

5.0 CONCLUSIONS AND RECOMMENDATIONS

5.1 CONCLUSIONS

(1) The current practice of using SGS to define TT for assessing the risk of gas migration is inadequate. Standard SGS criteria (100lb/100ft^2 and 500lb/100ft^2) were evaluated for a Class A OWC in the WSC. The standard SGS criteria did not accurately indicate the period of time where the cement slurry would be susceptible to stray gas invasion and migration through the annulus.

(2) Degree of hydration is introduced to improve upon the current approach of SGS by providing a means for characterizing cement hydration using a more fundamental parameter. It was concluded that DoH is effective in characterizing the effects of curing temperature on hydrostatic pressure reduction for a specific mixture design. Although the rates of cement hydration are different, hydrostatic pressure reduction results are identical with respect to DoH. This verifies that shortening the critical hydration period does not prevent the occurrence of gas migration.

(3) DoH was found to be ineffective in characterizing hydrostatic pressure reduction for cement slurries with different w/c ratios or cement compositions. A cement slurry with a low w/c ratio tested in the WSC resulted in a hydrostatic pressure reduction initiation at a lower DoH, as compared to that of a higher w/c ratio. This observation

is logical, as a slurry design with a relatively high w/c ratio must achieve a higher DoH to develop the same volumetric fraction of solids (hydration product) as compared to that of a design with a low w/c ratio. Therefore, DoH criteria can be used to establish the period of time where the cement slurry would be susceptible to stray gas invasion for a specific cement slurry. The DoH criteria must be established for the specific cement type and mixture design to be used in the cement job.

(4) DoH was found to be ineffective in characterizing hydrostatic pressure reduction for cement slurries with different $CaCl_2$ dosage levels. A cement slurry with a high $CaCl_2$ dosage resulted in hydrostatic pressure reduction initiation at a lower DoH as compared to that of a neat slurry. This observation is logical, as the use of $CaCl_2$ results in an increase in hydration rate and change in type of hydration products formed. It may be concluded that DoH is ineffective in characterizing hydrostatic pressure reduction for Class A OWC used for WSC pressure testing at different $CaCl_2$ dosage levels.

(5) Capillary porosity was identified as a parameter capable of describing the microstructural development for slurries with different w/c ratios at any given DoH. This parameter was shown to be effective in characterizing hydrostatic pressure reduction between cement slurry designs for different w/c ratios when the cement composition was the same.

(6) Capillary porosity was found to be ineffective in characterizing hydrostatic pressure reduction of cement slurries with different compositions. WSC pressure testing was conducted on Class A OWC, Type I cement, and Type II/V cement. From the results, it was observed that both the Type I and Type II/V cements initiate

hydrostatic pressure reduction at a larger value of capillary porosity as compared to Class A OWC. Therefore, it may be concluded that the initiation of hydrostatic pressure reduction is not simply a function of the volumetric fraction of hydration products, as indicated by the capillary porosity parameter.

(7) By analyzing the WSC pressure results as a function of capillary porosity and the corresponding cement compositions, it was suggested that the *type* of hydration products formed is important to consider, in addition to the *amount* or fraction of hydration products formed. It was observed that both the Type I and Type II/V cements initiate hydrostatic pressure reduction at a larger capillary porosity as compared to Class A OWC. When analyzing the comparison of cement compositions, it was observed that the C_3A content varies between all three cement types, with Type I cement having the largest percentage of C_3A content, followed by Type II/V cement and Class A OWC in decreasing order. From this observation, it was suggested that the hydration reaction of C_3A (Equation (2.3)), which involves the formation of ettringite as a primary hydration product, is influential on the evolution of hydrostatic pressure reduction. Ettringite has significantly different properties and characteristics as compared to the primary hydration products of CSH and CH. One primary difference is that CH and CSH will only form in unoccupied space but ettringite will form by forcing adjacent hydration product out of the region in which it will expand into. This characteristic might be beneficial in preventing gas from entering in the cement annulus as the cement transforms from a liquid to a solid.

(8) An attempt was made to perform VCCTL simulations on cement types representative of those used in performing the WSC testing in an attempt to obtain representative material properties (i.e. volume fraction of each type of hydration product, DoH, capillary porosity, etc.). Valid VCCTL results could not be obtained for the cements used to perform the WSC testing because the CCRL did not contain representative cements and insufficient test data was available for the actual cements used.

5.2 RECOMMENDATIONS FOR FUTURE RESEARCH

Although useful conclusions were drawn and various objectives identified in Chapter 1 were met from the completion of this work, this section provides recommendations on additional research needed to further investigate and better understand the occurrence of stray gas migration occurring during the reduction of hydrostatic pressure reduction within the cement annulus during cement completion. As evidenced by Equations (2.4) and (2.5), the method of DoH calculation utilized for this work is indirect, in that it is based on heat evolution of hydrating cement. Although this method is acceptable and has been documented in literature, it may be possible to improve this calculation by more accurately quantifying the total heat potential (Equation (2.5)) of various cement types and materials. For example, the current equation only accounts for the heat evolution of individual cement clinker phases. In the future, it may be beneficial to perform work to allow for the incorporation of Blaine fineness, interactions between

individual clinker phases, and additional heat contributions due to commonly used SCMs and/or admixtures (such as $CaCl_2$), to name a few.

As stated in Section 4.2.1, isothermal calorimetry is the most direct and accurate measurement of heat evolution; however, limitations still exist with this method. As briefly explained in Section 4.2.1.3, various data modification and evaluation techniques were developed in order to compensate for limitations of the isothermal calorimetry equipment, namely, early-age temperature equilibration. Although these data modifications and evaluation techniques developed and utilized in this work are adequate in obtaining useful data, additional assumptions and uncertainties are introduced. Also, these assumptions and uncertainties are magnified due to the importance of accurately characterizing early-age cement hydration as it relates to hydrostatic pressure reduction. Additionally, the ability to account for and characterize slower reactions, such as those that occur with C_2S and pozzolanic materials, or tests conducted at low temperatures (i.e. where cement hydration begins to cease) may be less accurate, because the signal-to-noise ratio decreases with time (Poole 2007).

This work also compares the heat and hydration evolution of different cement types with significantly different compositions. As mentioned in Section 2.1.1, the data utilized for these comparisons are entirely based on Bogue equations. Although these equations are commonly used and reported in literature, it is known that Rietveld analysis is more accurate in determining the exact composition of cement. By incorporating Rietveld analysis into future research, the reliability of cement compositions will be enhanced.

VCCTL simulations were performed on cement types in the CCRL similar to that used for WSC testing so representative material properties could be established (i.e. DoH, capillary porosity, etc.). These results were unable to be validated using isothermal calorimetry testing

results since the CCRL did not include a cement similar to the Class A OWC tested. In order to improve the accuracy of the VCCTL results, CCRL cement data files should be modified (in terms of cement composition) to simulate the cement type used for WSC testing. Particle size distribution (PSD) data is required to accurately modify the volume and surface area fractions of individual cement compounds. Also, additional isothermal calorimetry testing should be performed on Type I and Type II/V cement to obtain experimental data that may be used to validate VCCTL results for simulations of these cement types.

This study serves as part of the foundation for developing a comprehensive cement evaluation tool, in order to predict the behavior of hydrating cement slurry at any time and depth along the wellbore. These material properties are related to the susceptibility of gas migration occurrence. Additional WSC testing should be conducted using high-permeability formations to directly test for and observe whether the gas migration actually does occur under various borehole conditions. By combining the findings and conclusions derived from the work of this study with additional high-permeability WSC testing, a better understanding of the gas migration mechanism of hydrostatic pressure reduction may be achieved.

APPENDIX A

CEMENT MATERIAL INFORMATION

A.1 MILL SHEET INFORMATION

Mill sheet data and physical properties of cements used in this project are presented in Table A.1.

Table A.1. Mill sheet data for cement types used for WSC testing.

Cement type			API Class A	ASTM Type I	ASTM Type II/V
Standard chemical requirements (ASTM C114)	Silicon Dioxide (SiO_2), %		21.2	19.1	20.41
	Aluminum Oxide (Al_2O_3), %		3.7	4.7	4.04
	Ferric Oxide (Fe_2O_3), %		4	3.1	3.71
	Calcium Oxide (CaO), %		63.6	62	63.07
	Magnesium Oxide (MgO), %		2.7	4.3	4.62
	Sulfur Trioxide (SO_3), % A		2.7	3.2	2.85
	Loss on Ignition (LOI), %		1.03	2.1	1.39
	Insoluble Residue, %		0.08	0.31	0.40
	Alkalies (Na_2O equivalent), %		0.37	0.82	0.53
	Tricalcium Silicate (C_3S), % (Bogue)		59.52	62.11	61.07
	Dicalcium Silicate (C_2S), % (Bogue)		15.88	7.91	12.45
	Tricalcium Aluminate (C_3A), % (Bogue)		3.04	7.21	4.43
	Tetracalcium Aluminoferrite (C_4AF), % (Bogue)		12.17	9.43	11.29
Physical requirements	(ASTM C 204) Blaine Fineness, m^2/kg		362	399	325
	(ASTM C 191) Time of Setting (Vicat), minutes	Initial Set		91	
		Final Set		186	
	(ASTM C 185) Air Content, %			7	
	(ASTM C 151) Autoclave Expansion, %			0.23	
	(ASTM C 1038) Expansion in Water, %			0.01	
	(ASTM C 187) Normal Consistency, %			26	
	(ASTM C 109) Compressive Strength, psi	1 Day		2842	
		3 Day		4133	
		7 Day		4857	
		28 Day		5786	
	API Compressive Strength (slurry cubes), psi	8 Hour, 100 ºF	813		
		24 Hour, 100 ºF	2944		

A.2 CCRL CEMENT TYPE COMPARISON

The following tables present mill sheet data available for various CCRL cement types and the corresponding cement composition estimated using the Bogue equations.

Table A.2. CCRL Cement 115.

SiO2 (S)	21.48%
Al2O3 (A)	4.48%
Fe2O3 (F)	3.47%
CaO '(C)	65.07%
MgO (M)	0.96%
SO3 (S_bar)	2.67%
Loss on ignition	1.04%
Free Lime (XRD)	0.50%
Insol. Residue	0.28%
Blaine	363
Bogue Calculations (by wt)	
C3S	58.98%
C2S	17.09%
C3A	6.00%
C4AF	10.56%

Table A.3. CCRL Cement 116.

SiO2 (S)	20.57%
Al2O3 (A)	5.40%
Fe2O3 (F)	1.99%
CaO '(C)	64.96%
MgO (M)	1.28%
SO3 (S_bar)	2.91%
Loss on ignition	1.53%
Free Lime (XRD)	0.99%
Insol. Residue	0.12%
Blaine	365
Bogue Calculations (by wt)	
C3S	60.70%
C2S	13.18%
C3A	10.94%
C4AF	6.06%

Table A.4. CCRL Cement 133.

SiO2 (S)	20.60%
Al2O3 (A)	5.60%
Fe2O3 (F)	2.49%
CaO '(C)	65.04%
MgO (M)	1.49%
SO3 (S_bar)	2.31%
Loss on ignition	1.27%
Free Lime (XRD)	0.44%
Insol. Residue	0.22%
Blaine	350
Bogue Calculations (by wt)	
C3S	60.45%
C2S	13.46%
C3A	10.63%
C4AF	7.58%

Table A.5. CCRL Cement 135.

SiO2 (S)	21.45%
Al2O3 (A)	4.45%
Fe2O3 (F)	3.07%
CaO '(C)	63.81%
MgO (M)	2.42%
SO3 (S_bar)	2.46%
Loss on ignition	0.81%
Free Lime (XRD)	0.64%
Insol. Residue	0.16%
Blaine	394
Bogue Calculations (by wt)	
C3S	55.43%
C2S	19.68%
C3A	6.60%
C4AF	9.34%

Table A.6. CCRL Cement 136.

SiO2 (S)	20.86%
Al2O3 (A)	5.34%
Fe2O3 (F)	3.58%
CaO '(C)	63.91%
MgO (M)	1.51%
SO3 (S_bar)	2.36%
Loss on ignition	1.66%
Free Lime (XRD)	0.58%
Insol. Residue	0.25%
Blaine	390
Bogue Calculations (by wt)	
C3S	53.95%
C2S	19.10%
C3A	8.09%
C4AF	10.88%

Table A.7. CCRL Cement 141.

SiO2 (S)	18.96%
Al2O3 (A)	5.72%
Fe2O3 (F)	2.47%
CaO '(C)	61.46%
MgO (M)	2.63%
SO3 (S_bar)	4.71%
Loss on ignition	1.87%
Free Lime (XRD)	0.41%
Insol. Residue	0.22%
Blaine	397
Bogue Calculations (by wt)	
C3S	50.70%
C2S	16.12%
C3A	10.98%
C4AF	7.52%

BIBLIOGRAPHY

AB, T. (2004). Thermometric 3114/3236 TAM Air Isothermal Calorimeter (Product Manual). Cheshire: R.L. Taylor and Associates.

Al-buraik, K., Al-abdulqader, K., Aramco, S., Bsaibes, R., & Dowell, S. (1998). IADC / SPE 47775 Prevention of Shallow Gas Migration Through Cement.

American Petroleum Institute. (2005). *API 10A: Specification for Cements and Materials for Well Cementing*.

American Petroleum Institute. (2010). *API 65-2: Isolating Potential Flow Zones During Well Construction*. Retrieved from www.shalegas.energy.gov/resources/65-2_e2.pdf?

American Society of Testing Materials. (2014a). *ASTM C1074: Standard Practice for Estimating Concrete Strength by the Maturity Method*.

American Society of Testing Materials. (2014b). ASTM C150: Standard Specification for Portland Cement, 1–9. http://doi.org/10.1520/C0150

Belrute, R. M., & Cheung, P. R. (1990). A Method for Selection of Cement Recipes to Control Fluid Invasion After Cementing, (November), 433–440.

Bentz, D. P. (2005). CEMHYD3D : A Three-Dimensional Cement Hydration and Microstructure Development Modeling Package Version 3.0.

Bonett, A., & Pafitis, D. (1996). Getting to the Root of Gas Migration. *Oilfield Review*, 36–49. Retrieved from http://www.slb.com/~/media/Files/resources/oilfield_review/ors96/spr96/ors96_gas_p36_49.pdf

Bullard, J. W. (2009). Virtual Cement and Concrete Testing Laboratory.

Byfors, J. (1980). *Plain Concrete at Early Ages*. Swedish Cement and Concrete Research Institute.

Carino, N. J., & Lew, H. S. (2001). THE MATURITY METHOD: FROM THEORY TO APPLICATION. In *Structures Congress & Exposition*.

Carter, G., Services, H., & Slagle, K. (1960). A Study of Completion Practices TO Minimize Gas Communication.

Dusseault, M., Jackson, R., & Macdonald, D. (2014). *Towards a Road Map for Mitigating the Rates and Occurrences of Long-Term Wellbore Leakage*.

Geiker, M., Walter, A., Gutteridge, A., Killoh, D., & Parrott, L. J. (1990). Monitoring Portland Cement Hydration: Comparison of Methods. *Cement and Concrete Research*, *20*(1), 919–926.

Glasstone, S., Laidler, K. J., & Erving, H. (1941). *The Theory of Rate Processes: The Kinetics of Chemical Reactions, Viscosity, Diffusion, and Electrochemical Phenomena*. New York: McGraw-Hill Book Company, Inc.

Haijin, Z., Guangming, L., Aiping, L., Chengbin, X., & Shaohui, A. (2012). IADC / SPE 155923 Research on a New Method to Evaluate the Hydrostatic Pressure of Cement Slurries. *IADE/SPE Asia Pacific Drilling Technology Conference and Exhibition*.

Kada-Benameur, H., Wirquin, E., & Duthoit, B. (2000). Determination of apparent activation energy of concrete by isothermal calorimetry. *Cement and Concrete Research*, *30*(2), 301–305. http://doi.org/10.1016/S0008-8846(99)00250-1

Kjellsen, K. O., & Detwiler, R. J. (1993). Later Ages Strength Prediction by a Modified Maturity Method. *ACI Materials Journal*, *90*(3), 220–227. http://doi.org/10.14359/3873

Komex International. (2002). *Evaluation of Potential Groundwater Contamination Due to Surface Casing Vent Flow/Gas Migration*.

Li, Z. (2015). *Development of Wellbore Simulator for Better Understanding of Oil Well Cement Behavior and Gas Migration During Early Gelation*. University of Pittsburgh.

Lin, F., & Meyer, C. (2009). Hydration kinetics modeling of Portland cement considering the effects of curing temperature and applied pressure. *Cement and Concrete Research*, *39*(4), 255–265. http://doi.org/10.1016/j.cemconres.2009.01.014

Malhotra, V. M., & Carino, N. J. (2004). *Handbook on Nondestructive Testing of Concrete*.

Mindess, S., Young, J. F., & Darwin. (2003). *Concrete* (2nd ed.). Pearson Education, Inc.

Mueller, D. T. (2002). OTC 14282 Redefining the Static Gel Strength Requirements for Cements Employed in SWF Mitigation. *Offshore Technology Conference*, (1), 1–6. Retrieved from

https://www.onepetro.org/download/conference-paper/OTC-14282-MS?id=conference-paper/OTC-14282-MS

Poole, J. L. (2007). *Modeling Temperature Sensitivity and Heat Evolution of Concrete*.

Princigallo, A., Lura, P., van Breugel, K., & Levita, G. (2003). Early development of properties in a cement paste: A numerical and experimental study. *Cement and Concrete Research*, *33*(7), 1013–1020. http://doi.org/10.1016/S0008-8846(03)00002-4

Robbins, M. E. (2007). *Predicting the Early Age Temperature Response of Concrete Using Isothermal Calorimetry*. *Portland Cement Association*.

Sabins, F., Tinsley, J., & Sutton, D. (1982). Transition Time of Cement Slurries Between the Fluid and Set States. *Society of Petroleum Engineers Journal*, *22*(6). http://doi.org/10.2118/9285-PA

Salinas, V., Flores, R., Kruse, D., Co, H. E., Primeaux, K., & Corp, E. P. (2005). Effectively Controlling Gas Migration When Lost Circulation Is Encountered in South Texas. *International Petroleum Technology Conference*.

Schindler, A. K. (2004). Effect of Temperature on Hydration of Cementitious Materials. *ACI Materials Journal*, *101*.

Schindler, A. K., Dossey, T., & McCullough, B. (2002). *Temperature Control During Construction to Improve the Long Term Performance of Portland Cement Concrete Pavements*.

Schindler, A. K., & Folliard, K. J. (2005). Heat of Hydration Models for Cementitious Materials. *ACI Materials Journal*, *102*.

SPE International. (2015). Cement composition and classification. Retrieved October 10, 2014, from http://petrowiki.org/Cement_composition_and_classification

Stark, J. (2011). Recent advances in the field of cement hydration and microstructure analysis. *Cement and Concrete Research*, *41*(7), 666–678. http://doi.org/10.1016/j.cemconres.2011.03.028

Sutton, D. L., Sabins, F., & Faul, R. (1984a). Annular gas flow theory and prevention methods described. *Oil and Gas Journal*, *82*.

Sutton, D. L., Sabins, F., & Faul, R. (1984b). New evaluation for annular gas-flow potential. *Oil and Gas Journal*, *82*.

TA Instruments. (2014). TAM Air isothermal calorimeter brochure.

Williams, H., Keese, R., Roy-delage, S. Le, Roye, J., Leach, D., Rottler, P., & Porcherie, O. (2012). Flexible Technology. *Oilfield Review*, (July).

Zhang, J., Weissinger, E. a., Peethamparan, S., & Scherer, G. W. (2010). Early hydration and setting of oil well cement. *Cement and Concrete Research*, *40*(7), 1023–1033. http://doi.org/10.1016/j.cemconres.2010.03.014

Zhou, D., & Wojtanowicz, A. K. (2011). Annular Pressure Reduction During Primary Cementing. *Journal of Energy Resources Technology*, *133*(3), 031003. http://doi.org/10.1115/1.4004809